Concrete Dams:
Seismic Analysis, Design and Retrifitting

M. Ghaemian

April 2, 2000

Contents

List of Figures

Chapter 1

INTRODUCTION

People from the beginning of recorded history have constructed barriers across rivers and other water courses to store or divert water. The earliest of these dams were used to water farms. For example, the ancient Egyptians built earth dams that raised the river level and diverted water into canals to irrigate fields above the river. Behind the dam, waters pile up to form an artificial lake which sometime can be very long. The artificial lake backed up by a dam is called a reservoir.

Dams are built primarily for irrigation, water supply, flood control, electric power, recreation, and improvement of navigation. Many modern dams are multipurpose. Irrigation dams store water to equalize the water supply for crops throughout the year. Water supply dams collect water for domestic, industrial, and municipal uses for cities without suitable lakes or rivers nearby for a water supply. Flood control dams impound floodwaters of rivers and release them under control to the river below the dam. Hydroelectric power dams are built to generate electric power by directing water in penstocks through turbines, wheels with curved blades as spokes. The falling water spins the blades of the turbines connected to generators. Power dams are expected to generate power to repay the cost of construction. The output depends, first, upon the head of water, or height of stored water above the turbines. The higher the water the more weight and pressure bear upon the turbine blades. A second factor is the volume of water throughout the year. The minimum flow in dry months fixes the amount of firm power which customers can rely upon to receive regularly. Sometimes extra power, or run-of-stream power, generated in flood seasons can be sold, usually at lower rates.

Dams also provide benefits other than those mentioned above. Their reservoirs provide recreation, such as fishing and swimming. They become refuges for fish and birds. Dams conserve soil by preventing erosion. They slow down streams so that the water does not carry away soil. Dams can also create problems. Their reservoirs may cover towns or historic and scenic places. Dams may impair fishing. Another problem of dams is silting. Some rivers pick up clay and sand and deposit them behind the dam, thereby lessening its usefulness.

1.1 TYPES OF DAMS

Dams range in size and complexity of construction from low earth embankment constructed to impound or divert water in small streams to massive earth or concrete dams built across major rivers to store water. The type of dam that is built and its size are a complex function of a demonstrated necessity for water storage or diversion, the amount of water available, topography, geology, and kinds and amount of local materials for construction. Although large embankment dams do not posses the graceful and architecturally attractive configurations of many concrete dams, they commonly require an equal amount of engineering skill in planning, design, and construction. The world's largest dams, as measured by the volumes of materials used in their construction, are embankment dams. In contrast, many of the world's highest dams are built of concrete, and many of them are 180 m (600 ft) or more high.

There are several basic types of dams. Differences depend on their geometric configurations and the material of which they are constructed. Under special circumstances, feature of the basic types are combined within a particular dam to meet unusual design requirement. The followings are the main types of dams:

1. Embankment dams.
   a. Homogenous dams, constructed entirely from a more or less uniform natural material.
   b. Zoned dams, containing materials of distinctly different properties in various portions of dams.
2. Concrete arch and dome dams.
   a. Single arch and dome dams.
   b. Multiple-arch and multiple-dome dams.

3. Concrete gravity and gravity-arch dams.
4. Concrete slab and buttress dams.
5. Dams combining two or more basic characteristics of the above basic types.

1.1.1 Embankment Dams

A broad spectrum of natural and fabricated materials have been used in the construction of embankment dams. Embankment dams are made by building an embankment of gravel, sand, and clay across a river. To prevent leakage, often a core, or inner wall, of concrete or other watertight materials is used. In a rolled-fill dam, earth is hauled by vehicles onto the dam and rolled tight with heavy machinery. In the hydraulic fill dam, earth is carried to the dam by water in pipes or flumes and also deposited by the water. The placing of the earth is so controlled that the finer, watertight materials form the core. In the semihydraulic fill dam, trucks bring the earth to the dam and jets of water distribute the materials. Rock dams are made by dumping rocks across the river. A wall of rocks is then laid on the upstream side and over this is built a waterproof facing of reinforced concrete, timber, or steel.

Controlling factors in choosing this type of dam are the amounts and types of materials locally available for construction and the size and configuration of the dam. Many small embankment dams are built entirely of a single type of material such as stream alluvium, weathered bedrock, or glacial till. Larger embankment dams generally are zoned and constructed of a variety of materials, either extracted from different local sources, or prepared by mechanical or hydraulic separation of a source material into fractions with different properties. Where rock is used extensively, it may be obtained by separation from bowldery stream deposits, glacial till, side-rock accumulations, or by quarrying.

Construction of an embankment dam requires prior investigation of foundation geology and an inventory and soil-mechanics study of materials available for emplacement in the embankment. An important element in a zoned dam is an impermeable blanket or core which usually consists of clayey materials, obtained locally. In the absence of such materials, the dam is built of quarried rock or unsorted pebbly or bowldery deposits, and the impermeable core is constructed of ordinary concrete or asphaltic concrete. Alternatively, in locations where natural impermeable materials are unavailable, embankment dams are built of rock or earth-rock aggregates and impermeable layers

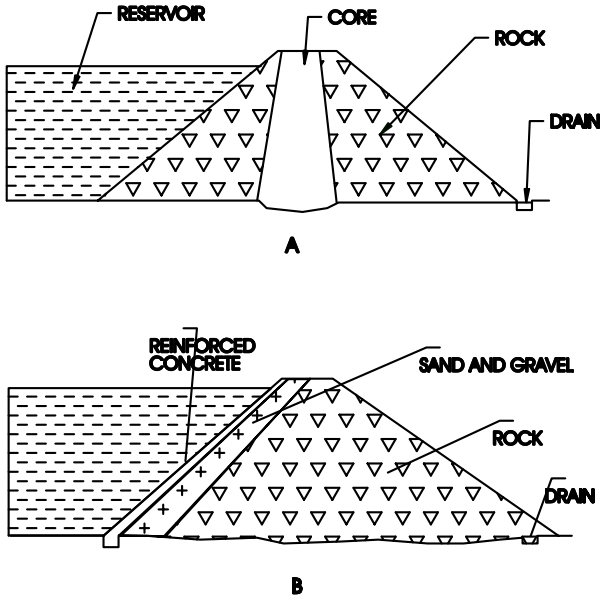

Figure 1.1: Idealized section of embankment dams a) Rock-fill dam with symmetrical clay core b) Rock and gravel dam with reinforced concrete slab

of reinforced concrete, asphaltic concrete, or riveted sheet steel are placed on the upstream face of the dam. Control of seepage through the dam or under it commonly requires installation of porous materials within or immediately beneath the dam.

Embankment dams have been built on a great variety of foundations, ranging from weak, unconsolidated stream or glacial deposits to high-strength sedimentary rocks and crystalline igneous and metamorphic rocks. A particular advantage of an embankment dam, as compared with a concrete dam, is that the bearing-strength requirements of the foundation are much less. Minor settlement of an embankment dam owing to load stresses during and after construction generally is not a serious matter because of the ability of the embankment to adjust to small dislocations without failure. Cross-sections of selected examples of embankment dams are shown in figure 1.1.

1.1.2 Concrete Arch and Dome Dams

The ultimate complexity of design and analysis of stresses is attained in arch and dome dams. These dams are thin, curved structures commonly containing reinforcing, either steel rods or prestressed steel cables. Volume requirements for aggregate for manufacture of concrete are much less than in gravity and gravity-arch dams, but the competency of bedrock in foundations and abutment to sustain or resist loads must be of a high order. Arch dams usually are built in narrow, deep gorges in mountainous regions where access and availability of construction materials pose especially acute problems. At sites where abutments are not entirely satisfactory rock may be excavated and replaced with concrete to form artificial abutments. Their height can be as high as 272 m (905 ft).

Arch dams are of two kinds. Constant-radius arch dams commonly have a vertical upstream face with a constant radius of curvature. Variable-radius dams have upstream and downstream curves (extrados and intrados curves) of systematically decreasing radii with depth below the crest When a dam is also doubly curved, that is, it is curved in both horizontal and vertical planes, it is sometimes called a "dome" dam. Curves that have been used in construction of arch or dome dams are arcs or sectors of circles, ellipses, or parabola. Some dams are constructed with two or several contiguous arches or domes, and are then described as multiple arch or multiple-dome dams. Figure 1.2 shows Cross-section of several varieties of arch dams.

Engineering analysis of arch and dome dams assumes that two major types of deflections or dislocations affect the dam and its abutments. Pressure of water on the upstream face of the dam and, in some instances, uplift pressures from seepage beneath the dam, tend to rotate the dam about its base by cantilever action. In addition, the pressure of reservoir water tends to flatten the arch and push it downstream, so that stresses are created which act horizontally within the dam toward the abutments. That portion of the bedrock abutment which receives the thrust from the load of reservoir water either by a tendency for downstream movement of the dam or flattening of the arch is called the thrust block and must be sufficiently strong to resist the forces acting on it without failure or appreciable, dislocation. Simply stated, an arch dam utilizes the strength of an arch to resist the loads placed upon it by the familiar "arch action". It is clear that the foundation and abutments must be competent not only to support the dead weight of the dam on the foundation but also the forces that are directed into the abutments because of

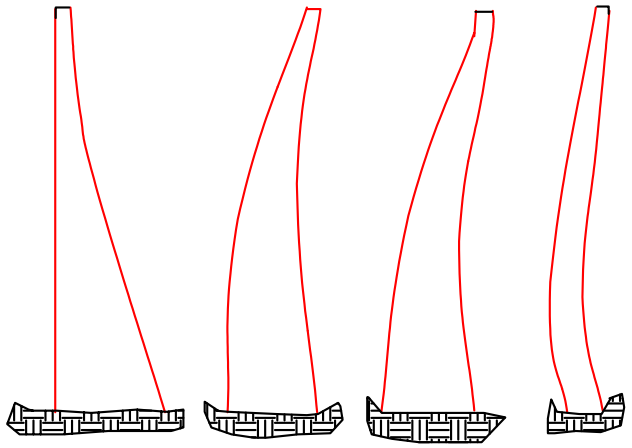

Figure 1.2: Cross-sections of several arch dams

arch action in response to loads created by impounded reservoir water, and, in areas of cold climates, pressures exerted by ice forming on the reservoir surface. In regions of seismic activity consideration must also be given to the interaction of the dam and pulses of energy associated with earthquakes.

1.1.3 Concrete Gravity and Gravity-Arch Dams

A concrete gravity dam has a cross-section such that, with a flat bottom, the dam is free-standing; that is, the dam has a center of gravity low enough that the dam will not topple if unsupported at the abutments. Gravity dams require maximum amounts of concrete for their construction as compared with other types of concrete dams, and resist dislocation by the hydrostatic pressure of reservoir water by sheer weight. Concrete gravity dams have been constructed up to 285 m (950 ft)high. Properly constructed gravity dams with adequate foundation probably are among the safest of all dams and least susceptible to failure with time. They withstand the pressure or push of water by their weight. In cross section, they are like a triangle, broad at the base and narrow at the crest. They are built in this shape because water pressure becomes greater with the depth of water. A typical gravity dam is shown in figure 1.3.

Final selection of the site for a gravity or gravity-arch dam is made only after comprehensive investigation of hydrologic, topographic, and, especially,

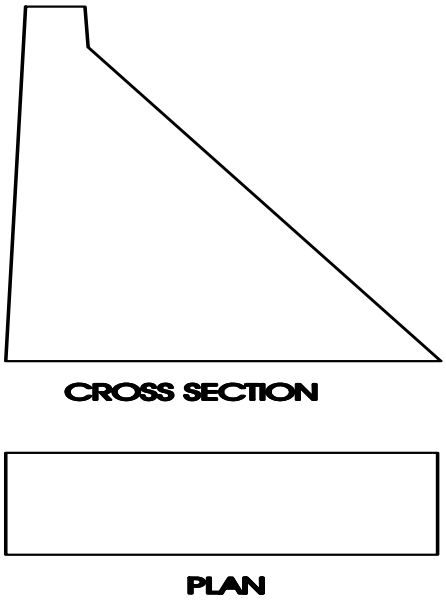

Figure 1.3: Cross-section of typical concrete gravity dam

subsurface geologic conditions. A favorable site usually is one in a constriction in a valley where sound bedrock is reasonably close to the surface both in the floor and abutments of the dam.

An important consideration in construction of a concrete gravity or gravity-arch dam is the availability, within a reasonable hauling distance, of adequate deposit of aggregate suitable for manufacture of concrete, whether the aggregate is obtained from unconsolidated deposits or is quarried.

The simplest form of a gravity dam is one in which the top or crest is straight. depending on the topographic configuration of a valley and the foundation geology, it may be possible to construct a gravity-arch dam which incorporates the advantages of mass weight and low center of gravity of a gravity dam with those inherent in an arch dam. in gravity-arch dams the requirements for sound rock in abutments are somewhat more stringent than in simple gravity dams.

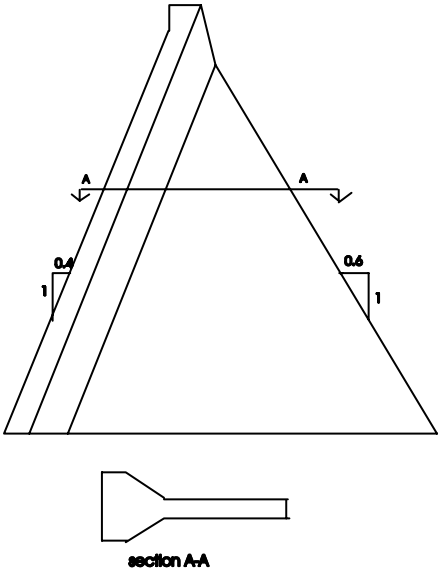

Figure 1.4: Cross-section of a concrete buttress dam

1.1.4 Concrete Slab and Buttress Dams

In locations where aggregate for concrete or for earthfill is in limited supply and the foundation rocks are moderately to highly competent, buttress dams provide a possible alternative to other kinds of dams. They are up to 130 m (430 ft) high. In cross-section, buttress dams resemble gravity dams, but with flatter upstream slopes. In a buttress dam a slab of reinforced concrete upstream rest on a succession of upright buttress which have thicknesses and a spacing sufficient to support the concrete slab and the load of the water in the reservoir that exert on the slab. A cross-section of a typical buttress dam is shown in figure 1.4

1.2 APPURTENANT FEATURES OF DAMS

Appurtenances are structures and equipment on a project site, other than the dam itself. They include, but are not limited to, such facilities as intake towers, powerhouse structures, tunnels, canals, penstocks, low-level outlets, surge tanks and towers, gate hoist mechanisms and their supporting struc-

tures, and all critical water control and release facilities. Also included are mechanical and electrical control and standby power supply equipment located in the powerhouse or in the remote control centres.

In previous sections of this chapter the characteristics and configurations of basic types of dams have been outlined, but no consideration was given to the various appurtenant features that enable use of a dam and the reservoir behind it for their intended purposes. In this section mention is made of various features that are incorporated into the designs of dams for control of flow of water impounded in the reservoir through or outside of a dam. Design of many of these features requires intensive prior investigations of hydrology, topography, and subsurface geology of the dam site. Following is a tabulation and description of several kinds of appurtenant features included in the construction of dams.

Coffer dams usually are temporary structures built upstream from a dam to divert stream flow around the excavation for a dam. In valleys of steep profile diversion commonly is accomplished by a **tunnel** or tunnels in the walls of the valley. Commonly the diversion tunnels are put to further use to control flow from reservoir either for drainage of the reservoir or for flow under pressure into a hydroelectric generating plant. In valleys of low profile diversion is by tunnels, canals, or by **conduits** which subsequently are buried by the dam. It is not unusual in embankment dams to incorporate the coffer dam into the larger embankment structure comprising the designed dam.

Tunnels in bedrock outside of dams serve a variety of purposes. Flow through them is controlled by valves external to the dam or in valve chambers or vaults within the dam or in bedrock outside of the dam. Tunnels for control of the water level in the reservoir are commonly called gravity tunnel and serve a principal function in diverting water to some point downstream from the dam. Tunnels that transmit water under pressure to elevate the water to a higher level than the intake of the tunnel or to generate hydroelectric power are called pressure tunnel and usually require considerable competency in the rock through which they are constructed . Valves control the flow of water through tunnels and penstocks. In many large dams the valves are installed in underground vaults or chambers to which access is gained downstream from the dam.

Many dams are constructed to generate hydroelectric power. The **powerhouse** is located at, or in the vicinity of, the toe of a dam or at some distance downstream. Flow of water into the power house is controlled by

valves upstream from the dam, within the dam downstream, or in valve vaults excavated in rock outside of the dam.

A **sluice** is a passage through the dam itself for lowering the water level of the reservoir. Pipes for conducting water to the power turbines are called **penstocks**. The flow of water from intake towers through spillways, sluices, and penstocks is regulated by **control gates**.

A **Spillway** is designed to contain and control overflow of reservoir water when the reservoir is full. Spillways are, or should be, designed to accommodate flows during maximum flood stage so as to prevent damage to the dam and appurtenant features. Their size and location with respect to the dam is determined by the size and type of dam, local topography geology and a careful review of the history of stream flow at the site of the dam. Water may pass over the crest of the dam itself, or near the dam in chutes, tunnels, or shafts. Overflow of embankment dams outside of a spillway can have especially disastrous consequences so that safety usually requires a spillway capable of containing at least a hundred-year flood. Spillways are located within or on the downstream face of a dam outside of the dam on one side or the other, or within the reservoir, where water spills into a "**glory hole**" and passes through a shaft and tunnel or tunnels in the abutment of the dam.

Gates are devices installed in the tops of spillways to control the flow of water over the spillway.

Levees are artificial riverbanks constructed high enough to prevent flooding. A dam across a river intended to permit flow, once a certain depth of water has been reached, may be called a **barrage**. A small dam that forms a millpond or fishpond is called a **weir**.

1.3 SAFETY OF DAMS AND RESERVOIRS

There are Several types of reservoirs as defined by their locations. The common type is a reservoir behind a dam in a valley. Increasing use is being made of tidal-storage reservoir for power generation along coast lines and excavated reservoirs for water storage for municipal or other use. In the latter type the excavated material commonly is employed to construct an embankment on one or all sides of the reservoir.

Reservoirs and their associated dams serve many purposes including electric power generation, storage and diversion of irrigation water, storage of industrial and municipal water supplies, recreation, and flood control. Less

frequent uses of reservoirs include storage and control of stream water for navigation, and storage of sewage and waste products from mining or manufacturing operations. In some stances fuel powered and thermonuclear power plants require large volumes of cooling water, and reservoirs are constructed for this purpose. Whether a dam backs up water for a long or a short distance is not important from the structural point of view. Pressure depends not upon how far water is backed upstream but upon its depth at the dam. But the length of the reservoir and its capacity may change the risk associated in the case of failure.

There are no accurate records of the number of dams that have failed throughout the history of their construction. However, ruins of dams built through a long span of history in both ancient and more recent times indicates that the number must be high, probably in the thousands, if dams of all heights are included in the count. The magnitude of floods generated by dam failure or by collapse of the walls of a reservoir are not related to the height of a dam. More pertinent is the volume of water stored in the reservoir behind the dam, and the configuration of the valley below it, wether the dam is low or high.

The cost in human life, goods, and property damage of a flood generated by breaching of a dam or collapse of reservoir wall depends to a large extent on the magnitude of flood and what lies in the pathway of the flood. With an expanding population in many part of the world and an increasing occupation of floodplains by dwellings, commercials and industrial facilities , and highways, dam built long ago and dam built in recent times present a growing potential for massive destruction of life and property. the cause of floods associated with failure of dams and reservoir are numerous. In embankment dams a common cause of breaching is overtopping of existing spillways or waterlevel control facilities, although some failures have been attributed to slope failure, foundation subsidence, or earthquake damage. Failure of concrete dams usually is attribute to imperfect design or construction, to use of inferior materials in the dam, or to failure of foundation and/or abutment rocks. Construction of a dam and reservoir imposes new loads on foundation materials. Initial adjustment in the dam and foundation occurs as the dam is being built and as the load on the foundation is increased to a final load equal to the weight of the dam. Filling of the reservoir impose additional loads not only on the floor and wall of the reservoir but also on the upstream face of the dam. As the reservoir level is decreased and increased these loads fluctuate , and a cycle dynamic system of changing loads is superimposed on the static

load of the dam on its foundation. Seepage of water through or beneath the dam may produce slow deterioration that may promote eventual failure. The responsibility for the safety of dams and reservoirs no longer belongs only to the designer and builder but must be shared by those who have knowledge and understanding, however imperfect they may be, of the expected behavior of natural materials under the condition superimposed by the loads of dams and reservoirs. Modern technology and social responsibility require that safe construction and maintenance of dams and reservoir shall be the shared responsibility of engineers, geologists, and rock mechanical expert.

Recognition of the need for worldwide surveillance of dams and reservoirs with emphasis on their safety has resulted in the formation of the International Commission on Large Dams (lCOLD) a unit of the World Power Conference within individual countries increasing efforts are being made to regulate and maintain continued safety of dams and reservoirs through the close cooperation of engineering organizations and government agencies. In spite of these good works, dams continue to fail, and intensification of efforts to assure the safety of existing dams and reservoirs and those that will be in the future is an increasingly urgent necessity.

1.4 HOW DAMS ARE BUILT

The methods of building dams can be envisioned by following the construction of Hoover Dam, built between 1930 and 1935. The engineers constructed a concrete arch-gravity dam at an approved cost of $174,000,000. It is as tall as a 60-story skyscraper. Its crest is 45 feet (14 meters) thick and its base, 660 feet (201 meters). It stores the entire flow of the Colorado River for two years. Much preliminary work had to be done. The engineers made geologic and topographic surveys to select the site. They made maps of 70 locations, bored holes to test the rock for a sound foundation, and studied the river's speed, high water level, and silting. Once the location was chosen, designers made their plans. They then made models to test their design. Where once had been burning desert, engineers built Boulder City to house about 5,000 workers. Construction gangs built railroads and highways for transporting great quantities of equipment and materials. Workmen strung cables across the canyon from pairs of towers, which travel on tracks along opposite sides of the site. Each of the five cableways could carry 25 tons (22,680 kilograms). Two of them had spans of nearly half a mile. Construction crews also built

a great gravel screening plant and two huge concrete mixing plants.

On each side of the river two tunnels, each 50 feet (15 meters) in diameter, were drilled and blasted from the rock of the canyon walls. These tunnels were used to divert the river around the site. When construction was completed the tunnels served as spillway outlets and penstocks for the power plant. Next, cofferdams of earth and rock were built upstream and downstream from the dam site to block the river. "High scalers" stripped tons of loose and projecting rock from canyon walls. The overburden, or loose rock and muck, was dug out to expose the bedrock. Grout, a thin mortar of cement and water, was next forced into the foundation to fill seams and holes. Forms were made. These would be used for building the dam in enormous blocks. Concrete was poured into the forms from eight-cubic-yard buckets traveling on the cableways. As each block of concrete dried, grout was pumped between the blocks, making the dam into one solid piece. Allowing so gigantic a structure to cool naturally would have taken a century because of the heat given off by the setting cement. In addition the concrete would have shrunk and cracked. Cold water circulating through 528 miles (850 kilometers) of one-inch (25-mm) pipes embedded in the concrete carried off the heat. Refrigerating pipes were also used to freeze landslides of wet earth at Grand Coulee Dam. Another problem was the freezing of control gates in winter. A huge electrical heating apparatus was installed in the spillway and gates.

1.5 FAMOUS DAMS OF THE WORLD

Rogun and Nurek, in Tajikistan, are among the world's highest dams. They rise to a height of more than 1,000 feet (300 meters) each. Some of the world's other major dams are Grande Dixence and Mauvoisin, in Switzerland; Chicoasen, in Mexico; Inguri, in Georgia; Sayano-Shushensk, in Russia; Mica, in Canada; and Guavio, in Colombia. Three of the foreign dams that are constructed of the largest volume of materials are Tarbela, in Pakistan; Lower Usuma, in Nigeria; and Guri, in Venezuela. Dams that form the largest reservoirs in capacity are Owen Falls (Lake Victoria), in Uganda; Bratsk, in Russia; Kariba Gorge, bordering Zambia and Zimbabwe; and Aswan High, in Egypt. One of the oldest great dams is Egypt's Aswan for irrigation on the Nile, finished in 1902. The Dnepr, completed in 1932, was one of the earliest major Soviet dams. Another historical dam is Mettur, on the Cauvery River

in India. The world's first dam to furnish hydroelectric power from ocean tides was completed in 1966. It is located on the Rance River, near St-Malo, in France.

The following tables show some of the famous dams of the world with their specifications. In the tables the followings notation was used for simplicity.

H-Height (ft);

L-Length (ft);

M-material in dam (cu yd);

RC-Reservoir Capacity (billions of gal)

A–Arch;

B–Slab and buttress;

C–Concrete;

E–Rolled earth fill;

G–Gravity;

H–Hydraulic earth fill;

M–Multiple arch;

R–Rock fill;

S–Stone masonry;

FC–Flood control;

I–Irrigation;

M–Mining;

N–Navigation; P–Power;

RP–Recreation purposes;

RR–River regulation;

WS–Water supply;

UC–Under construction.

Table 1.1 *Highest dams of the world*

Name	Location	Type	Purpose	Year	H	L	M	R
Rogun	Tajikistan	E	P-I	1987	1,066	2,506	81,096,000	3,091
Nurek	Turkmenistan	E	P-I	1980	1,040	2,390	75,864,000	2,745
Grande Dixence	Switzerland	C-G	P	1962	935	2,280	7,792,000	106
Inguri	Russia	A	P-I-FC	1980	892	2,513	4,967,000	261
Vaiont	Italy	A	-	1961	858	624	460,000	-
Tehri	India	E-R	-	UC	856	-	-	935,271
Guavio	Colombia	E-R	-	1989	807	1,280	23,223,000	269
Mica	Canada	E-R	P-FC	1974	794	2,600	42,000,000	6,517
Sayano-Shushenshaya	Russia	A	P-N	1980	794	3,504	11,916,000	8,261
Chicoasen	Mexico	E-R	P	1981	787	1,568	15,700,000	439
Chivor	Colombia	E-R	P	1977	778	919	14,126,000	215
Mauvoisin	Switzerland	C-A	P	1957	777	1,706	2,655,000	48
Oroville	California	E	P-I-FC-WS	1968	770	6,920	78,008,000	1,153
Chirkeyskaya	Russia	A	P-I-FC-WS	1975	764	1,109	1,602,000	734
Bhakra	India	C-G	P-I	1963	742	1,700	5,400,000	2,607
Hoover	USA	C-A-G	P-I-FC-RR	1936	726	1,244	4,400,000	9,696
Contra	Switzerland	A	P	1965	722	1,246	861,000	23
Mratinje	Yugoslavia	A	P	1975	722	879	971,000	232
Dworshak	Idaho	G	P-FC-RP	1972	717	3,287	6,500,000	1,125
Glen canyon	USA	C-A-G	P	1964	710	1,560	4,901,000	8,798
Toktogul	Kyrgyzstan	A	P-I	1977	705	1,476	4,186,000	5,148
Daniel Johnson	Canada	C-M	P	1968	703	4,311	2,950,000	37,473
Luzzone	Switzerland	C-A	P	1963	682	1,738	1,739,000	23
Keban	Turkey	E-R-G	P	1974	679	3,881	20,900,000	8,182
Dez	Iran	C-A	P-I	1963	666	696	647,000	882
Almendra	Spain	A-G	P	1970	662	1,860	2,188,000	700
Kolnbrein	Austria	A	P	1978	656	2,054	1,995,000	53
Karun	Iran	A	P-I	1975	656	1,247	1,570,000	766
New Bullard's Bar	USA	A	P-I-FC-RP	1970	637	2,200	2,700,000	557
New Melones	USA	E-R	P-I-FC-RP	1975	625	1,600	15,970,000	782

Table 1.2 *Largest dams of the world*

Name	Location	Type	Purpose	Year	H	L	M	R.
New Cornelia Tailings	USA	E	M	1973	98	36,500	274,026,000	6
TarbelaName	Pakistan	E-R	P-I	1976	470	9,000	159,200,000	3,617
Fort Peck	USA	H	P-I-FC-N	1940	250	21,026	125,612,000	6,234
Lower Usuma	Nigeria	E	-	1990	528	14,531	121,640,000	26
Ataturk	Turkey	E-R	-	1990	604	5,971	110,522,000	-
Guri	Venezuela	E-R-G	P	1986	531	30,853	101,819,000	36,720
Yacyreta-Apipe	Argentina-Paraguay	E-G	P-I-WS-RP	UC	108	164,000	95,063,000	4,464
Oahe	USA	E	P-I-FC-N	1963	245	9,300	92,008,000	7,687
Mangla	Pakistan	E	P-I	1967	380	11,000	85,872,000	1,678
Gardiner	Canada	E	P-I-WS	1968	223	16,700	85,743,000	2,607
Afsluitdijk	The Netherland	E	FC-WS	1932	62	10,500	82,927,000	1,585
Rogun	Tajikistan	E	P-I	1987	1,066	2,506	81,096,000	3,091
Oroville	USA	E	P-I-FC-WS	1968	770	6,920	78,008,000	1,153
San Luis	USA	E	P-I	1967	382	18,600	77,666,000	664
Nurek	Turkmenistan	E	P-I	1980	1,040	2,390	75,864,000	2,745
Garrison	USA	E	P-I-FC-N	1956	203	11,300	66,506,000	7,925
Oosterschelde	The Netherland	E-G	FC-WS	1986	164	29,528	65,397,000	-
Cochiti	USA	E	FC-RP	1957	253	26,891	64,631,000	167
Tabka	Syria	E	P-I-FC	1975	197	14,764	60,168,000	3,698
Kiev	Ukraine	E-G	P-N	1964	72	177,448	57,552,000	984
Aswan High	Egypt	E-R	P-I-RP	1970	364	12,565	57,203,000	44,642
Bennett	Canada	E	P	1967	600	6,700	57,203,000	18,575
Tucurui	Brazil	E-G	P-N-WS	1984	282	13,779	56,244,000	8,982
Mission Trailing #2	USA	E	-	1973	128	-	52,435	15
Fort Randall	USA	E	P-I-FC-N	1956	165	10,700	50,205,000	1,858
Kanev	Ukraine	E	P	1974	82	52,950	49,520,000	692
Itumbiara	Brazil	E-G	-	1980	328	21,981	47,088,000	4,499

Table 1.3 *Dams with greatest reservoir*

Name	Location	Type	Purpose	Year	H	L	M	R
Owen Falls	Uganda	C-G	P-I	1954	100	2,725	-	54,091
Bratsk	Russia	E-C-G	P-N-WS	1964	410	16,864	18,283,000	44,713
Aswan High	Egypt	E-R	P-I-RP	1970	364	12,565	57,203,000	44,642
Kariba Gorge	Zambia-Zimbabwe	C-A	P	1959	420	2,025	1,350,000	42,361
Akosombo	Ghana	R	P	1965	463	2,100	10,400,000	39,102
Daniel Johnson	Canada	C-M	P	1968	703	4,311	2,950,000	37,473
Guri	Venezuela	E–RG	P	1986	531	30,853	101,819,000	36,720
Krasnoyarsk	Russia	C-G	P-FC-N	1972	407	3,493	5,685,000	19,364
Bennet	Canada	E	P	1967	600	6,700	57,203,000	18,575
Zeyskaya	Russia	B	P-I-FC	1975	369	2,343	3,139,000	18,069

1.6 POWER GENERATOR, FLOOD CONTROL AND IRRIGATION DAMS

1.6.1 Power Generator Dams

Most electric power is generated in large plants that use coal, gas, oil, or nuclear energy. Electric energy may also be obtained from waterpower. The roar of a waterfall suggests the power of water. Rampaging floodwaters can uproot strong trees and twist railroad tracks. When the power of water is harnessed, however, it can do useful work for man. Since ancient times man has put to work the energy in the flow of water. He first made water work for him with the waterwheel–a wheel with paddles around its rim. Flowing water rotated the waterwheel, which in turn ran machinery that was linked to it. Today, new kinds of waterwheels spin generators that produce electricity. Electricity from water-turned generators is called hydroelectric power.

Waterpower produces about 8 percent of the electricity used in the United States. It accounts, however, for only a fraction of the total energy used for mechanical power, heat, light, and refrigeration. Coal, petroleum, and natural gas supply most of the rest. Among water's virtues as a source of power is the fact that it can be used again after it supplies energy, while other energy sources are destroyed when they are used. Hydroelectric installations also supply added benefits to a region. For example, a dam built to provide a head for water turbines usually creates a reservoir that can supply water for irrigation and drinking. Water passes downward through a hydraulic

turbine that is connected to a generator. Large plants, which depend on large volumes of water dammed upstream, can generate more than 2,000 MW. There are many small plants on rivers, some generating only a few hundred kilowatts. Among the largest plants in the United States are Hoover Dam and the Grand Coulee Dam. Hoover Dam has an installed capacity of 1,244 MW. Grand Coulee has an installed capacity of 2,025 MW. It is part of the Columbia River Basin project, which has a planned capacity of 9,770 MW.

The power produced by water depends upon the water's weight and head (height of fall). Each cubic meter of water weighs 1000 kilograms. For example, a column of water that is one meter square and one meter high would contain one cubic meter of water. It would press upon each square meter of turbine blade with a force of 1000 (1 x 1000) kilograms. Engineers measure waterpower in terms of watts (kilowatts or megawatts). One watt is the force it takes to raise one kilogram one meter in one second. The power potential of a waterfall is found by multiplying its flow, measured in cubic meter per second, by its height, measured in meter. Then the product is multiplied by 980, which is 1000 (the number of kilogram in a cubic meter of water) multiplied by 9.81(gravitational acceleration). For example, a 100-meter high waterfall with a flow of 10 cubic meter per second would develop 100 x 10 x 980, or 980,000, watts. The output of a hydroelectric plant is usually measured in kilowatts or megawatts of electricity.

1.6.2 Flood Control Dams

One way to avoid floods is to take the obvious precaution of living where there is no danger of high waters. It has always been convenient and often necessary to build homes and factories on the floodplains along rivers and streams and on the seacoasts. American pioneer settlers depended upon the streams for drinking water, transportation, and power to run their mills and factories. Floodplains, deep with the silt laid down by overflowing rivers, are fertile farmlands. The earliest towns and farms, therefore, were established along the riverfronts, and large portions of them were built on land that was subject to periodic flooding. While the communities were small, the damages suffered from floods were limited. With the great population and industrial growth of the cities, flood damage has become a serious national problem. One of the basic approaches to flood control is to minimize the extent of flooding by building dams, reservoirs, levees, and other engineering works.

Engineers in ancient times built earthen mounds to keep back floodwater. Such artificial embankments, called levees, held Chinese rivers in check for centuries. This method was followed in colonial America.

Because a levee at one point confines the water there and raises the peak of flood waters upstream and downstream, levees once started usually have to be built at all the low points of a river system. Furthermore, a system of levees is only as strong as its weakest spot. Thus uniform height and strength are required. Only a government which controls the river from end to end can safely supervise levee building. Floodways and spillways divert excess water from the main river channel and carry it off by a different route.

Dams and the reservoirs behind them help control floods. By emptying a dam before a flood is expected, storage space is obtained in which the flood waters can be impounded for gradual release later. Even if the reservoir is nearly full, it acts like a safety valve. The amount of water which would add 3 meter to the height of a river 30 meter wide would add only one meter to a reservoir or lake 90 meter wide. Moreover, evaporation from the broad surface of a reservoir or lake is far greater than evaporation from the narrow surface of a river. Thus less water flows on to swell floods downstream. Flood-control dams are built to create big storage capacity and are planned for rapid filling and emptying. During excessive rains, water collects in the storage reservoirs and is released in controlled amounts to the channel below the dams. The water carries with it large quantities of the richest topsoil, which muddies the rivers and is ultimately lost in the ocean. American rivers, for example, carry off an estimated 280 million cubic meters of solid matter each year. Agricultural experts propose to return the steepest hills along the headwaters of American rivers to forest. By means of terracing, contour plowing, and a wise choice of plants, runoff and erosion are checked on gentler slopes. By damming gullies, runoff is slowed, and silt from above slowly rebuilds the eroded spots. Thus flood prevention and erosion control go hand in hand. Preventing soil erosion also aids flood control by slowing the rate at which silt fills the reservoirs behind flood-control dams. Steps to lessen the effects of drought also aid in flood control. Some lakes, swamps, and marshes that were once drained to make farm lands are being restored to preserve the level of underground water in time of drought. This program also reduces floods by increasing evaporation and by the safety-valve action of wide lakes or swamps on narrow rivers. Thus the prevention and control of floods are tied with drought measures as well as with waterpower, navigation, soil conservation, and land use.

1.6.3 Irrigation Dams

Irrigation is the artificial supply of water to agricultural land. It is practiced by more than half the farmers in the world because they need more water for their crops than is available from rainfall. Irrigation projects must also allow for removal of excess water.

Generally the need for irrigation water is highest in the dry season when river flows are lowest. To ensure continuous supply, water must be stored on a seasonal and sometimes annual basis. By erecting a dam, an artificial lake, or reservoir, is created from which water can be released as required. Some reservoirs are capable of storing billions of gallons of water. Large dams and the associated reservoirs are often built for multipurpose use–irrigation, flood control, hydroelectric power generation, municipal and industrial water supply, and recreation. Systems of dams and reservoirs along a river and its tributaries are developed with the purpose of providing comprehensive and integrated water resources management in an entire basin.

1.7 INSTRUMENTATIONS AND SURVEILLANCE OF DAMS

1.7.1 Surveillance

External and internal examination of dams are required during their life time. Long term surveillance program can ensure dams owner of their safe operation. Long term surveillance requires instrument installation and monitoring to assess the performance of structures with respect to design parameters. Design of monitoring installations is to measure displacement, settlement, strain, stress, piezometric pressures, seepage, uplift, flow velocity and water levels, and alarm systems as required for a particular impoundment. Compilation of results on a computerized data base is done and results are interpreted and reported in the form of recommendations outlining appropriate action need to be taken, when it is necessary.

1.7.2 Instrumentation

Instruments are used to characterize dam site condition as well as dam structure conditions. Instruments can be used for verifying design verification,

safety assessment, performance assessment.

Design Verification Instruments are used to verify design assumptions and to check that performance is as predicted. Instrument data from the initial phase of a project may reveal the need (or the opportunity) to modify the design in later phases.

Safety Instruments can provide early warning of impending failures, allowing time for safe evacuation of the area and time to implement remedial action. Safety monitoring requires quick retrieval, processing, and presentation of data, so that decisions can be made promptly.

Performance Instruments are used to monitor the in-service performance of a structure. For example, monitoring parameters such as leakage, pore water pressure, and deformation can provide an indication of the performance of a dam.

The Choice of Instruments depends on critical parameters of each project. The designer must identify those parameters and then select instruments to measure them. What information is required for the initial design? What information is required for evaluating performance during and after construction? When the parameters are identified, the specification for instruments should include the required range, resolution, and precision of measurements.

In some cases It may be necessary to have complementary parameters and redundant measurements. In some cases, it may be sufficient to monitor only one parameters but when the problem is more complex, it is useful to measure a number of parameters and to look for correlation between the measurements. Thus it is common practice to choose instruments that provide complementary measurements. For example, inclinometer data indicating increased rate of movement may be correlated with piezometer data that shows increased pore pressures. Another benefit of selecting instruments to monitor complementary parameters is that at least some data will always be available, even if one instrument fails.

Instrument performance is specified by range, resolution, accuracy, and precision. The economical designer will specify minimum performance requirements, since the cost of an instrument increases with resolution, accuracy, and precision. **Range** is defined by the highest and lowest readings the instrument is expected to produce. The designer typically specifies the highest values required. **Resolution** is the smallest change that can be displayed on a readout device. Resolution typically decreases as range increases. Sometimes the term accuracy is mistakenly substituted for resolution. Resolution is usually many times better than accuracy and is never expressed

as a ± value. Accuracy is the degree to which readings match an absolute value. Accuracy is expressed as a ± value, such as ±1mm, ±1% of reading, or ±1% of full scale. Precision or repeatability is often more important than accuracy, since what is usually of interest is a change rather than an absolute value. Every time a reading is repeated, the value returned by the instrument is slightly different. Precision is expressed as a ± value representing how close repeated readings approach a mean reading. The difference in cost between a high-quality instrument and a lesser-quality instrument is generally insignificant when compared to the total cost of installing and monitoring an instrument. For example, the cost of drilling and backfilling a borehole is typically 10 to 20 times greater than the cost of the piezometer that goes in it. It is false economy to install a cheaper, less reliable instrument. It is expensive and sometimes impossible to replace a failed instrument. Even when it is possible to replace the instrument, the original baseline data is no longer useful. Some instruments are excellent for short-term applications, but may exhibit excessive drift over the long term. Temperature and humidity also affect instrument choice. Instruments such as hydraulic piezometers and liquid settlement gauges have limited use in freezing weather. In tropical heat and humidity, simple mechanical devices may be more reliable than electrical instruments.

Consider the personnel and resources at the site when choosing instruments. Do technicians have the skills required to install and read a particular type of instrument? Are adequate support facilities available for maintenance and calibration of the instrument?

An automatic data acquisition system may be required when:

(1) there is a need for real-time monitoring and automatic alarms;

(2) sensors are located at a remote site or in a location that prevents easy access;

(3) there are too many sensors for timely manual readings; or

(4) qualified technicians are not available.

If a data acquisition system is required, the choice of instruments should be narrowed to those that can be connected to the system easily and inexpensively.

1.7.3 Instruments

In the following section, Some instruments used in monitoring of dams are briefly described.

Piezometers measure pore-water pressure and ground water levels. Piezometer measurements help engineers to Monitor water levels, Predict slope stability, Design and build for lateral earth pressures, Design and build for uplift pressures and buoyancy, Monitor seepage and verify models of flow.

Inclinometers may be installed to check that actual movements of a structure correlate to those predicted during the design phase. Inclinometers are installed to monitor the magnitude, direction, and Corrective Measures rate of movement. This information helps engineers determine the need for corrective measures. Inclinometers are installed for long term monitoring to detect Long-Term Performance changes in ground conditions or in the structure itself. Inclinometers, particularly in-place inclinometers that are monitored continuously, can provide early warning of catastrophic failure. Horizontal inclinometers are used to monitor settlement in foundations and embankments. Inclinometers monitor movement, a direct measure of stability, so they are often used in site investigations. Installed at the proposed site for a dam, an inclinometer might detect movement at a sub-surface shear plane. The shear plane could cause problems later when the reservoir behind the dam is filled and pore-water pressure along the shear plane increases.

Beam sensors are used for monitoring settlement, heave, lateral deformation, or convergence. Two version of beam sensors are horizontal version for monitoring settlement and heave and vertical version for monitoring lateral displacement and convergence.

Tiltmeter is used for monitoring changes in inclination. It is used for monitoring the rotation of concrete dams.

Beam sensors differ from tiltmeters in two important respects: First, the beam sensor has a defined gauge length, typically 1 to 3 meters, so changes in tilt can be converted simply and accurately to millimeters of movement (settlement, heave, convergence, or lateral displacement). Second, beam sensors can be linked end-to- end to monitor differential movements and provide absolute displacement and settlement profiles.

Tiltmeters typically have a more limited function, that of monitoring rotation. A tiltmeter can be used with a large number of tilt plates to detect differential movement in a structure, but the resulting data cannot provide absolute displacement and settlement profiles. In general, however, both types of sensors can be used to evaluate the performance of dams under load. They Provide early warning of threatening deformations, allowing time for corrective action to be taken or, if necessary, for safe evacuation of the area.

Borehole Extensometers are used to monitor settlement, heave, convergence, and lateral deformation in soil and rock. Typical applications include monitoring settlement or heave in excavations, foundations, and embankments. Data from the extensometer indicate the depths at which settlement has occurred as well as total amount of settlement.

Pneumatic settlement cells provide a single-point measurement of settlement. They can be read from a central location and are particularly useful where access is difficult. They are used to monitor consolidation in the foundation during construction and monitor long-term settlement in the foundation and fill.

Surface Extensometers (Tape Extensometer) is used to determine changes in the distance between reference points anchored in walls or structures of an excavation, precision measure of convergence.

Load cells are used to proof-test and measure loads in tie- backs, rock bolts, ground anchors, and struts. They are also used for monitoring the performance of anchor systems.

Total Pressure Cells measure the combined pressure of effective stress and pore-water pressure. In general, they are used to verify design assumptions and to warn of soil pressures in excess of those a structure is designed to withstand. Total pressure cells are installed within fills to determine the distribution , magnitude and directions of total stresses. They can also be installed with one surface against a structure to measure total stresses acting on upstream face of the dam, retaining walls, against piles, and pipes. In Embankment Dam Total pressure cells used to confirm design assumptions and An array of cells provides data to determine distribution, size, and direction of total stresses within the clay core.

Soil strainmeters are used for monitoring horizontal strain in embankments and monitoring tension cracks in earth structures.

Embeded jointmeters are used for monitoring movement at joints in mass concrete structures. It is used in mass concrete structures such as dams, abutments, foundations to monitor movement at joints.

Surface-mount jointmeters are used to monitor movement at joints and cracks in concrete structures under harsh environments and submersion. Typical application include monitoring movement at submerged construction joints in concrete dams and monitoring joints or cracks in tunnels and tanks.

Strain gauge is used for monitoring strain in steel structural members, reinforced and mass concrete.

1.8 ECOLOGICAL/ENVIRONMENTAL CONSIDERATION OF DAM OPERATION

The following observations are generalized from the literature at large. Whether any particular concern applies to any particular dam is a function of a suite of factors that might include the dam's type (e.g. concrete or earth), its purpose (e.g. hydrologic regulation, hydroelectric generation, tailings impoundment), its size, location and operating protocol (e.g. timing of drawdowns, epilimnetic versus hypolimnetic draw, peaking versus base load generation, etc.). Finally, The observations are derived from an ecocentric rather than any anthropocentric ethical premise, that is a rather uncompromising ecological view of the relationship between nature and humans.

The ecosystem approach can work for dam owners/operators to a greater extent than they may perceive it to be working against them. Here, the Physicochemical effects (physical or chemical factors) have separated from biological effects. Generally changes in the biological community are driven by changes in the physical or chemical (physicochemical) dimensions of the habitat (niche).

Impacts are also organized spatially as those that occur: (a) downstream of the dam,(b)within the water column of the reservoir/impoundment, (c) at the sediment/water interface (which may or may not feed into the water column) and (d) a category for impacts that act outside the immediate dam/reservoir system. These latter impacts might be viewed as externalities with less relevance for operators. In any event, the evidence for external impacts is substantially weaker than that for a-c.

Downstream impacts could include changes in **Physicochemical factors** and **Community structure.** The physicochemical factors are: temperature, oxygen content, water chemistry, particulate loading, transparency, discharge patterns, flow rates/shear and channel simplification. The community structures are: environmental conditions exceed tolerance limits of original community members, species richness, genetic diversity, productivity and feedback.

Water column impacts could include changes in Physicochemical parameters and Community structure. The Physicochemical parameters consists of temperature, oxygen content, water chemistry, transparency, morphometry, internal seiches and altered currents. The community structures are longer migration times, environmental conditions exceed tolerance limits of original

community members, productivity, diversity and feedback.

Sediment impacts could include changes in Physicochemical parameters and Community structure. The first one consists of temperature, oxygen content, light, remineralization, compression and sedimentation. The second one consists of environmental conditions exceed tolerance limits of original community members, species richness, productivity and feedback

Externalities could occur at a variety of scales and might include Local, Regional or Global externalities. The local externalities can cause riparian losses, hydrologic budget, habitat fragmentation. The regional externalities can cause climate change while the global externalities can cause climate change and orbit dynamics. These externalities could lead to loss of biodiversity and decreasing ecological integrity.

Dams can be operated in ways that decrease their environmental impacts. Recent examples include the installation of a selective water withdrawal system on the Hungry Horse Dam and the (initially seredipitous) drawdown at Glen Canyon. Doing so requires increased communication and trust among engineers, ecologists and other professionals in order to properly bound the problem. Engineers need to evaluate the extent to which regard for the environment is codified as good practice. There will have to be a willingness to experiment (e.g. demonstration projects) with a commitment to redefining operational technical directives as new knowledge emerges (e.g. optimal performance standards might equate ecological integrity with revenue generation).

Ecological integrity (the genetic diversity, species diversity and ecological diversity that maintains the flows of energy and materials through ecosystems) is the key mechanism for adapting to changes in environmental conditions through evolutionary change. Protecting diversity means protecting habitat, not only against loss but against fragmentation.

1.9 THE HISTORY OF DAMS DESIGN

Throughout the history, dams have been designed to fulfill a specific purpose to civilizations. The following historical outline illustrate the main dam purposes and the development of their design.

1.9.1 Irrigation Dams

A steady supply of water for irrigation is extremely important for any civilization to thrive. Heavy flooding in the wet season and long droughts in the dry season makes farming very difficult. However, if the water is contained during the wet season and released periodically through the dry season, a constant water supply will be present.

Ancient Dams

The first dam designed for irrigation purposes was the Marib dam in Yemen Capital City of Saba. The Marib was an embankment dam constructed about 510 BC. It reached a height of 20m and was about 700m long. The embankment slopes on each side were 1:1.8 with no road crest along the top. The most interesting aspect of this dam is that the fill was placed in layers parallel to the slopes, instead of the typical horizontal layer configuration. This dam also did not have any type of impermeable element in its design. On each end of the dam an outlet structure was built of excellent aslar masonry. The sills of both outlets were almost located at the same height from the riverbed. A 50m long spillway, with a sill height was also included in the dam design located in the northern section of the dam. the capacity of the Marib dam was 30 milliom m^3, about 15% of the average annual rainfall for the area. the final failure came about 1,300 years after the completion of the dam. It was not repaired and lead to immigration of about 50,000 people that depended on the water supply. Recently, a modern embankment dam with a capacity of 400 million m^3 was built in 1986, 3 km upstream of the ancient dam site.

The Kirsi dam of Iraq was built under the Assyrian king of Sennacherib about 355 km north of Baghdad. This dam was also a diversion dam, used to direct the river flow into a 15 km long canal for irrigation purposes. It was designed as a gravity dam constructed rubble masonry weirs. The upstream face was vertical with a board overflow crest and a stepped downstream face.

Romans

The Romans were highly advanced in hydraulic engineering from their many engineering feast such as aqueducts. However, they did not attempt dam construction until around 150 BC when they annexed Greece. One advantage

the Romans had, was that they already possessed fully developed construction technique based on traditional tools such as levers, picks and shovels. The Romans also used pulleys in multiple configurations to lift heavy objects vertically and horizontally. Some of the Romans advance tools included rules, squares, plumblines, and spirit levels. Traditional building materials were used in their design however, the Romans also added concrete to their dams. This allowed them to develop new shapes using formwork and concrete. They added volcanic ash or ground brick into the concrete mix to ensure that it would harden, even when submersed under water.

Medieval and Postmedieval Europe

Damming for irrigation purposes was practiced throughout this era. Irrigation was used throughout Europe, however, it was essential in the southern countries of Europe like Italy and Spain and required storage reservoirs. The dams in these southern countries were mostly of masonry, which contrast to dams built in northern Europe that were built mainly of soil embankments. The reason for dams built in Italy and Spain being masonry is most likely an inheritance from Roman civilizations who used embankments primarily for supporting elements.

The first true arch dam built in Europe since the Roman time, was built in 1632-1640 near Elche. The arch stretched across the main section of the gorge and butted into wing walls directed upstream on either side of the gorge. The arch thrust was directed downwards, since it did not have much support at the crest level. The main arch was 75m long and 9m wide at the crest and had a curve radius of 62m and a curve angle of 70°. The design of this dam was later tested using the crown-cantilever computer analysis that determined it to be satisfactory.

1.9.2 Dams Designed for Water Supply

It is impossible for a civilization to survive without a constant fresh water supply, since it is a basic need of all humans. In many parts of the world, the freshwater supply fluctuates from enormous amounts during the rainy season to long droughts during the dry season. for this reason dams were invented to store large amounts of water from the end of the rainy season until the end of the dry season, to ensure a constant supply of water.

Ancient Dams

The oldest dam in the world is the Jawa dam found 100 km northeast of Jordan capital Amman. This dam was built around 3,000 B.C. and was designed as a gravity dam. The design of this dam was quite complex considering that it was first dam to be built. It consisted of two dry masonry walls, with an earth core that acted as the water-retaining element. An impervious blanket was also provided in front of the upstream heel. A downstream embankment provided stability of the structure. The dam was later raised by 1m, using similar design methods as the original dam.

Romans

The Romans were the first civilization to use an arch dam. It is remarkable that the Roman did not use the arch dam earlier, since they had already become masters at employing it into their bridges and buildings. The first arch dam was constructed at Barcinas on Cubillas river 2km north of Granada, in southeast Spain. the arch design for this dam was not actually used to increase stability, but to lengthen the dam crest for easier passage of floodwater.

the first true arch dam was built by the Romans in the Vallon de Baume 4km south of Saint-Remy de Province in southeastern France. This dam was 12 high and 18m long, with a radius about 14m and a 73° central angle. It consisted of 1.3m upstream wall and a 1m downstream wall made out of masonry. The earth core between the two walls was about 1.6m wide, which means that the downstream wall was subjected to the entire load.

Medieval and Postmedieval Europe

The Roman standard of public fresh water supply continued throughout this period. the water supply for Istanbul in Turkey, during the beginning of the ear, was dealt with by many underground cisterns within the city. It was not until after the conquest of Istanbul in 1453 that the Ottoman Turks reconstructed some of the old Roman aqueducts. The first storage dam was built in 1560 on the remains of the Roman Belgrade dam. It was massive gravity dam, with a height of 15m and a base width of 56% of its height. The length of the dam was about 85m and had a 1.3 million m^3 reservoir capacity. This dam also included a couple of unnecessary buttresses to add stability to the structure.

1.9.3 Flood Control Dams

Since large number of natural fatalities, injuries and damage are caused by rapid flooding it is important to have flood control methods. Dams have been used for flood control since the first civilizations were formed.

Ancient dams

The Sadd-elKafara dam of Egypt was built around 2600 BC, about the same time as the beginning of the Pyramids. It stands 14m high and has a 113m crest. the lack of knowledge in hydrology and soil mechanics lead to the dam being over, designed. It had three distinct sections; the downstream shell made of rock, the upstream shell also made of rock and a centre core made out of fine silty sand and gravel. 17,000 blocks weighting 300kg each were carefully placement over the upstream and downstream walls to protect the dam against erosion. Construction problems were most likely encountered since it took longer than one dry season to built, and no evidence of any type of diversion could be found.

Romans

the Romans built the Cavdarhisar dam near Kutahya in western Turkey to protect against raging floodwater. It was designed as a gravity structure with height of 7m, wide of 8m and a length of 80m. It also contained a large bottom outlet with a clear section about $11m^2$ that shows this dam was not designed to be a reservoir, not a flood control measure.

Medieval and Postmedieval Europe

Throughout the period few dams were actually built to for flood protection, however, many dams were built to cause flooding. Controlled flooding was used for transporting wood by fluming. Originally, the dams built for fluming were made from timber, however, few of these dams have any remains. from around the end of the 17^{th} century the timber dam were replaced with masonry fluming dams. An example of a fluming dam is the Belcna dam in western Slovenia built in 1769. It was 18m high with a length of 35m, a crest width of 6.8m and a 12.4m base width. It was built of solid masonry and contained two outlets 5.1m in height and a width of 3.7m which allowed a large amount of water to rush out in a short time.

1.9.4 Power Dams

Waterpower was a technology that did not really take off until after the 11^{th} century. The invention of the dam was an essential development in the rise of waterpower because it diversified the applications of both the vertical and horizontal water wheels.

Romans

The Romans were the first civilization to harness the power of water however; they were limited to mostly grinding cereals. One of the most sophisticated dams built by the Romans was the Monte Novo dam located 15km east of Evora in southeast Portugal. It was a 5.7m high, 52m long arch dam with a radius of 19m and a central angle of 90°. The dam was built using blocks of shist laid horizontally in a lime mortar. the dam's reinforcement consisted of the fact that the curved central part at each end was embedded into the wing walls without any abutment blocks to absorb the horizontal arch thrust. The designers of this dam must have been unsure of their sophisticated design, because they also included two buttresses to increase the stability. It is thought that the water from two outlets was used to drive waterwheels further down the river, The outlets were 1.2m and 1.4m wide, with a height of 1m through the dam's base.

Medieval and Postmedieval Europe

It took several centuries for Europe to recover from impacts of Christianization and Germanization. By the end of the 8^{th} century, about 300 years after the disintegration of the western half of the roman empire technology had gain sprouted new wings. Dams were built in order to remove the waterwheels from rivers where debris, ice jams and floods played havoc with the waterwheels and their structures.

One of the interesting dam built in this period for waterpower was the Castellar dam and millhouse in southwestern Spain. The dam's reservoir capacity is very small(0.3 milliom m^3), however, the height of the dam was 19m high. This large height gave a very high potential head of the water in the reservoir, which could be transferred into waterwheel power. The millhouse was located at one end of the weir and supplied directly with water from the reservoir, a method of design that is used in modern low-head dam power plants. Another equally modern design characteristic was the location

of the millhouse, which was near the toe of the 19m high reservoir. An equal number of vertical shafts lead the water to the horizontal water wheels. The sturdy end and intermediate walls of the mill house act as buttress because the width of the dam was only 36% of its height. Many of the concepts built into this dam have direct links to modern methods, although it was built around 1500 AD.

1.9.5 The Moslem World

Arabia

Arabs quickly developed their country within one century after the impact of new Islamic religious founded by prophet Mohammed. Several irrigation dams around the new power centres of Mecca and Madina, were built. The following is a summary of 7^{th} and 8^{th}century dams in central Arabia.

Table 1.4 *Summary of* 7^{th} *and* 8^{th} *century dams in central Arabia*

Nearest City	Name	Height (m)	Length (m)
Mecca	Agrab	4.0	113
-	Ardab	5.5	315
-	Darwaish	10.0	150
-	Sammallaagi	11.0	225
Medina	Hashquq	2.0	130
-	Qusaybah	30.0	205

All of these dams were of the gravity type. They all have two outer walls of dry masonry and an earth or rubble core in between. The walls of some of these dams were vertical. Whereas, the other had inclined walls as much as 60%. Strong inclinations were applied to dams with relatively wide base, like Darwaish.

Although, most of these dams are already destroyed, one third of them like Saammallagi, are operative and more or less in their original shape.

South Western Asia

The Moslems conquered southwestern Asia in Seventh and Eighth centuries as far as the Indus river and Uzbakistan. During this time, Adhaim dam was built on the Adhaim river. This dam was located 150 km north of Baghdad. The dam was 130 meters long and 12 meters high. Adhaim Dam had an

equal width all along its length. Upstream face was vertical and downstream one was stepped to 43% average inclination.

In the 10th century, a whole series of irrigation and power dams were built on Kur river, east of Shiraz in southern of Iran. Table 1.5 shows , dimensions and the name of the dams on the Kur river.

The Amir dam is a large power dam including 30 water wheel being driven by a retained water. This dam has a trapezoidal cross section with a relatively steep down stream face and a base width of more than twice its height.

Table 1.5 *Dimensions and name of the dams on the Kur river*

Name	Height (m)	Length (m)
Amir	9	103
Feizband	7	222
Tilkan	6	162
Mawan	6	66
Djahanabad	5	50

Towards the end of the 10th century, several large gravity dams were built under Ghaznavid rule. These dams were built in countries such as Iran, Afghanistan and Uzbakestan. Table 1.6 contains some information about Ghaznavid gravity dams. Khan dam was built of granite ashlar masonry and was barely stable.

Table 1.6 *Ghaznavid Gravity Dams*

Name	Nearest city	Height (m)	Length (m)
Gishtbank	Samarkand	8	25
Khan	Saamarkand	15.2	52
Sheshtaraz	Mashhad	25	35
Soltan Mahmud	Kabul	32	220

Genghis khan from Mongolia started to conquer the world in 1205. Mongolians initiated the construction of several dams in Iran. Table 1.7 shows the summary of the data.

Table 1.7 *Mongolians Dams*

Year of completion	Name	Nearest city	Type	Height (m)	Length (m)
1285	Saveh	Tehran	Gravity	25	65
~1300	Kebar	-	Arch	26	55
~1350	Kalat	Mashhad	Gravity	26	74
1400	Abbas	Tabas	Arch	20	?
~1450	Golestan	Mashhad	Gravity	16	-

The Saveh dam was the first structure built during this time. It was a gravity dam. The design of this dam was not successful. The river crushed the dam after the first impoundment.

In 16^{th} and 17^{th} century, the construction of arch dams discontinued and only gravity dams were built. Most of the well known dams during this time, were located in northeastern Iran and Uzbakistan.

Abdullahkan dam was built in the beginning of the 16th century. This dam is 150 km northwest of samarkand. The height of this dam is 15 meters and it has a length of 85 meters. Its downstream face was stepped to an average inclination of 69%. Khajoo dam is one of the most beautiful dams not only in the Moslem, but in the entire world which is located in Isfahan of Iran.

1.9.6 Development of the Modern Dams

Unlike past periods in history, the modern dam is designed using specific principles. The largest change in the design of a modern dam compared to the earlier dams, has been the formation of engineering schools. This changed the individualistic craftsmanship of engineering into a profession based on scientific principles. Engineers were subdivided into specific disciplines, increasing the advancements of both dam principles and construction methods.

The modern embankment dam has improved greatly with the increase in research on hydrology and soil mechanics. Henri Gautier was one of the first to study slope stability of different soils. His experiments determined the natural slope response of soils. As time went on, engineers were then able to choose different soils based on their internal angle of friction, to increase the height of embankment dam designs. Studies were conducted on how soil permeability changed for different soils. In 1186 Philipp Forchheimer, professor of hydraulics in Austria, developed a graphical method of Pierre S. deLaplace's formula of how water flows in a soil. This graphical method is commonly known as a flownet. The single most important theoretical

development of soil mechanics was published in 1925 by Karl von Terzaghi. He found the explanation for why clays consolidate, by determining that the consolidation was caused by the dissipation of the water pressure in the soil pores. This finding led Terzaghi to the concept of effective stress, that is equal to the total stress minus the pore water pressure. This concept is still considered the single most important concept of modern soil mechanics. In 1980, the Nurek earth filled embankment dam in Tajikistan was completed. It stretched to a record height of 300m and had an embankment volume of 59 million m^3.

The analysis of stress in structures in their elastic condition, the concepts of the modulus of elasticity, and safety stresses was introduced in 1819 by Louis M. H. Navier. These concepts were the beginning of understanding how the force in gravity dam designs acted and helped to increase the height, without increasing the amount of materials used.

Breakthrough advancements in arch dam design came in 1880's when Hubert Visher and Luther Wagnore developed a new method of arch dam design. This new method did not merely design the arch dams as astach of individual arches but as an interdependent system of arches. It also considered the median vertical section of the dam to be a cantilever fixed at the base. The distribution of the loads resulted in a considerable relief for the lower arches, and the upper ones had to partially support the cantilever. Throughout this period, the arch dam took on many new shapes.

With the modern ear, improved mechanical construction method have caused the greatest impact on all types of modern dam designs. Scraper, bulldozers and vibrators all grew in size, resulting in the modern dams being completed in record time. New techniques for placing concrete, have played a roll in the construction and design methods for gravity dams. Roller compacted concrete is among the newest techniques implements in gravity dam construction. In the early 1950's Switzerland introduced bulldozers to spread concrete, and vibrators were attached to caterpillar tractors. In the late 1970's early 1980's vibrations rollers replaced the tractor mounted immersed vibrating system. These new construction techniques have spread throughout the world at a rapid pace, increasing both the dimensions of dams and the speed of completion.

The number of new dams being built has decreased considerably. This trend will not be able to continue as the world population continues to increase and fresh water, irrigation and flood control needs increase as well. Engineers need to constantly search for a better solution, taking all aspects

of design and the repercussions of that design into account. The past is a collection of design ideas, both good and bad, that should never be overlooked when faced with a new design challenge.

As time progress onwards, dams continue to grow in height and capacity. As they become larger, their impacts on society and the environments also increases. It is important that proper monitoring programs are setup to ensure that failure do not occur, because their effects will be devastating, One method of monitoring is a system of alarms downstream of the dam to warn of potential failures. the environment is an aspect that needs to be carefully controlled. With the growing size and capacity of modern dams, the environmental impact and awareness therefore increases as well.

1.10 BEAVERS

A mammal belonging to the order of rodents, or gnawing animals, the beaver has been recognized as a master engineer. By using teeth and paws, beavers construct dams, lodges, storehouses, and canals. The animal is also known for its aquatic life-style as well as for its beautiful fur.

The beaver has a thick body covered with a coat of long, reddish-brown outer hairs and soft, dense, brown underfur. This warm, waterproof coat allows the beaver to swim in icy water in the wintertime without discomfort. Most of the beaver's physical characteristics of the fur, toes, tail, ears, nose, and lips are so constructed that the animal is well equipped for life in the water as well as on land. The toes on the beaver's large hind feet are webbed for swimming. The second toe on each hind foot ends in a double claw with which the animal combs its fur. The front feet are small and handlike and are used for picking up and carrying various objects. The tail is shaped like a paddle, broad and flat, and is covered with scaly skin. The tail serves as a prop when the beaver sits upright and as a rudder and scull when it swims. As a danger signal to other beavers, the normally placid animal makes a loud noise by slapping its tail on the water's surface. The beaver's facial features also allow for its aquatic life-style. The short, thick head has small rounded ears and a nose which are equipped with valves that close when the animal swims underwater. A beaver may remain submerged for up to 15 minutes. The animal carries objects underwater in its mouth by closing loose lips behind prominent front teeth, thus keeping water out of its mouth. Like other rodents, the beaver has well-developed front teeth. These teeth

have a very hard layer on the front surface and a softer backing. Since this softer part wears away quickly, it leaves the thin chisel edge of the front layer exposed. The animal's teeth are always growing to make up for wear. The beaver has a total of 20 teeth.

Beavers are social animals; they live in colonies and work together. The life span of the animal may be as long as 19 years. A beaver begins its life in a litter of from two to eight young, or kits. Four is the usual number. They are born in the spring, about four months after conception. A mother will sometimes raise not only her own offspring, but also the young of another female that has died. Newborn kits weigh from 8 to 24 ounces (225 to 680 grams) and are about 15 inches (38 centimeters) long, with tails that measure 3 1/2 inches (9 centimeters). Their eyes are open at birth. They are out learning to swim when they are only a month old, and they are weaned by six months. A family usually consists of a mature pair of beavers and two sets of offspring. A female first breeds when it is by their third summer the young beavers are mature and ready to mate. They usually mate for life. A mated pair locates a fairly deep, slow-moving stream. They dig a burrow into the bank, starting below the surface of the water and slanting upward to a small room above the high-water mark. This is only a temporary residence in which the first litter will be born in the spring. Not until the following autumn does the couple set about building their permanent home–the lodge. Beavers live most of their lives in or near water. They settle along banks of streams, rivers, and lakes bordered by timberland. Large beaver populations have been credited with reducing flooding because of the dams they build across streams. On the other hand, they may also cause the flooding of roads and woodlands because of the reservoirs of water that build up behind the dams. Constant flooding can also damage valuable timber and block routes of migrating salmon. The reservoirs created by the dams are places where the beavers feel secure. It is in these artificially created ponds that beavers build their lodges and storehouses. The adult beavers select a narrow, shallow site in the water as a place to build a dam. They gnaw down a number of aspen, birch, or willow saplings. These they drag to the site and bury in mud with the butt ends pointing upstream. Into this foundation the beavers fit and pile more saplings, adding mud and stones until a strong barrier is completed. This structure allows enough seepage or overflow to keep the water in the reservoir fresh. Beaver dams come in all shapes and sizes. Normally a family of beavers can build a dam 35 feet (10 meters) long in about a week. Some dams more than 1,000 feet (300 meters) long have been found, but these are

the work of generations of beavers.

Beavers live in a structure called a lodge. The lodge is built in the riverbank or in the pond created by the dam. From a distance, the lodge resembles a heap of tree branches and mud. It consists of a platform of carefully interlaced branches held together by clay and dead leaves. When the platform has been built up a few inches above the water, the beavers fashion a dome-shaped roof over it. Before the coming of winter, the entire structure, which may enclose a room more than 5 feet (1.5 meters) high, must be plastered with mud. Entrances to the beaver lodge often open underwater, so that the animals may pass in and out below the winter ice. There are at least two, and up to five, such entrances. A steep and narrow entrance is used by the beavers for entry and exit. Another entrance is used for the transportation of wood for winter food. These underwater entrances help protect the beavers from attacks by predators which include, in North America, the wolverine, the lynx, and the wolf. Beavers move awkwardly on land; they prefer to swim. When they live in flat areas they sometimes build canals. These canals allow the beavers to more easily transport the logs that are too heavy to drag overland. A canal may measure more than 1,000 feet (300 meters) in length and from 2 to 3 feet (60 to 90 centimeters) in width.

When construction on dams, lodges, and canals is finished, the beavers gnaw whole groves of trees and sink the wood in the pond near their lodge. This collection forms the underwater winter "storehouse." Their diet consists primarily of fresh green bark and wood such as poplar, willow, and birch. In the summer they also eat water plants, berries, swampwood, and fruit. Beavers do most of their building and food gathering at night. After an autumn of toil, beavers spend the winter resting. They swim out of their warm, dry lodges only to pluck a twig or branch from the storehouse. Because the water in the pond is a meter deep or more, it does not freeze to the bottom and the beaver can swim under the ice in winter time to get sticks from the food pile accumulated the previous fall, return to the feeding chamber of the lodge and leisurely eat the food, all in a perfect safety from predators.

Beavers' dam is usually a high flat dam and having unwittingly created the lake which affords them safety and food. The dam is quite steep on the downstream side but slopes gently into the pond on the upstrean side. This result is obtained because the beaver adds material to the dam from the upstream side and, by doing so, unintentionally achieves a dam with the strongest possible configuration and therefore provides maximum security for the colony.

Although once plentiful throughout the wooded parts of the Northern Hemisphere, beavers had become an endangered species by the mid-19th century. They have been hunted for their fur, their tails, and their musk glands. Both sexes possess scent glands at the rear of the body that produce a liquid called castoreum, which is used in perfumes. It was also a popular medicine in the Middle Ages, apparently used to heal ailments ranging from headaches to dropsy. The healing ability of castoreum comes from its salicylic acid–a basic ingredient of aspirin–which the beaver acquires by eating willow bark. The beaver has in the past been hunted for its scaly tail, which was considered a culinary delicacy. Beaver flesh in general was highly esteemed during the Middle Ages. It is the quest for the beautiful pelt that has most drastically reduced the beaver population. The soft, thick underfur of the beaver, which is at its best in late winter and spring, has long been highly valued. During the 17th, 18th, and early 19th centuries, beaver skins, made into caps and capes, were a staple of the world's fur trade. In fact, much of the exploration of North America, beginning early in the 1600s and continuing through the early 19th century, was prompted by the search for beaver fur. At one time beaver pelts were a medium of exchange. Beaver populations have been diminishing for centuries, possibly because of various natural causes as well as trapping. Almost too late, conservation laws were passed throughout the world, and the beaver was saved and was resettled in some areas where it had once been common. The beaver population in Russia and in North America has recovered to the extent that bans on hunting imposed earlier in the 20th century have been slightly modified.

Chapter 2

RESERVOIR

2.1 INTRODUCTION

The first dams built by early man were low earth or rock structures designed to impound and divert water for agricultural use. Today's dams are a critical part of the nations infrastructure. They are vital for hydropower generation, drinking water, irrigation, navigation, recreation and flood control. Dams differ from other structure because of their size and their containment of water. Special attention must be taken to understand their behaviors.. The reservoir provides an extra effect of dynamic action into the dam response.

The ultimate fate of all dams and reservoirs, is deterioration and failure or filling by sedimentation. Every reservoir that impounds water behind a dam is a real or potential threat to those who live and work at the downstream side of the dam. In some locations, the effects of a sever earthquake may be dangerous to the integrity of the dam-reservoir structure and may tend to the destruction of the system. Modern technology combining the knowledge of construction and accurate design to reduce the risk that is inherent in dam and reservoir system. The capacity of the reservoir may vary depends on the shape of the valley and topography of the dam site. The more capacity of the reservoir, the more threat to the area in case of a failure.

In this chapter, we will establish reservoir's governing equation of the motion and associated boundary conditions of the dam-reservoir system.

2.2 GENERAL FORM OF RESERVOIR'S EQUATION OF MOTION

Fluids are composed of molecules in constant motion and collisions. A fluid has no structure. They are not distinguished by their microscopic (molecular) structure. To take account of each molecule in a flow, may be difficult for engineering purposes. Instead we are interested in average measuring of the molecule manifestations such as density, pressure and temperature which are their macroscopic structure. The continuum concept offers a great deal of simplification in analysis.

A fluid point (particle) represent a spatial average over some small volume V. Consider some variable as $a = \frac{1}{V}\int a' dV$, in which a' has a random characteristic(figure 2.1). The variable a can be density, ρ, velocity v, etc.. There must be a volume V such that a range of V value exist over which a is constant. Therefore for a big V we get different values of a for a range of V. However if we make V successfully smaller we get same value of a. We want $\delta \ll V^{\frac{1}{3}} \ll L$, in which δ is the largest length scale of the fluid structure (say mean free path) and L is the length scale of the domain of the problem. The restriction $V^{\frac{1}{3}} \ll L$ is for a to be measurable at a point while the criteria $\delta \ll V^{\frac{1}{3}}$is for a to be statistically significant and deterministic (always get same answer if we start from same initial condition and boundary conditions).

2.2.1 Velocity Field

In a deformable system there are an infinite number of particles. In order to define the velocity of a particle we must define the position of the particles, spatial coordinates, at the specific time. Using this, the velocity of all particles can be as $\mathbf{v}(x, y, z, t)$ which is consisted of three components of velocity v_x, v_y, v_z in x, y and z direction of coordinates, respectively. $\mathbf{v}$ is called field velocity vector. For steady flow, the value of the velocity at a position remains invariant with time, $\mathbf{v} = \mathbf{v}(x, y, z)$.

LAGRANGIAN AND EULERIAN VIEWPOINTS

In investigation of the fluid motion, two procedures may be used to study fluid particles. We can stipulate fix coordinates x_1, y_1 and $z_1$in the velocity field functions and letting time pass. we can express velocity of function

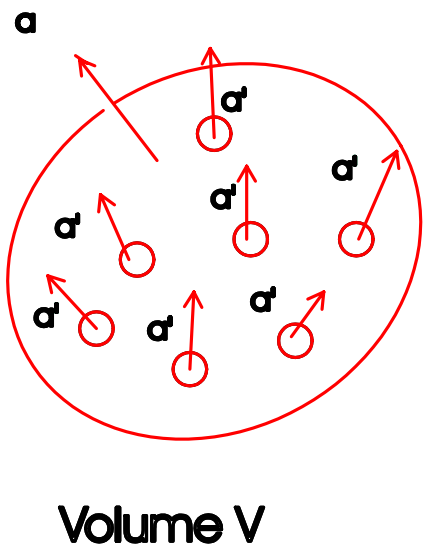

Figure 2.1: Fluid point

at any time passing this position as $\mathbf{v}(x_1, y_1, z_1, t)$. Using this approach we study the motion of a continuous string of particles which pass the fixed point. This viewpoint is called the Eulerian viewpoint.

On the other hand, we can study the motion of a single particle in the flow by following the particle in its path. This approach means continuous variation of the x, y and z to locate the particle. This approach is called the Lagrangian viewpoint where $\mathbf{v} = \mathbf{v}(x, y, z)$. The x, y and z can be expressed as a function of time $x = x(t)$, $y = y(t)$ and $z = z(t)$ (figure 2.2).

The Lagrangian viewpoint is used mainly in particle mechanics. In continuum mechanics this method requires the description of motion of an infinite number of particles and thus becomes extremely cumbersome. The Eulerian viewpoint is easier to use in continuum mechanics because it is concerned with the description of motion at a fixed position.

In the partial time derivative, from the Eulerian point of view, suppose we are standing on a bridge and note how the concentration of fish (c) just below us changes with time. In this case, the position is fixed in space, therefore by $\frac{\partial c}{\partial t}$ we mean partial of c with respect to t, holding x, y and z constant. We can also assume ourselves on a boat and moving with around the river. The change of fish concentration with respect to time reflects the motion of the boat as well as time variation. This is called total time variation and can be

written as:

$$\frac{Dc}{Dt} = \frac{\partial c}{\partial t} + \frac{\partial c}{\partial x}\frac{dx}{dt} + \frac{\partial c}{\partial y}\frac{dy}{dt} + \frac{\partial c}{\partial z}\frac{dz}{dt}$$

in which $\frac{dx}{dt}$, $\frac{dy}{dt}$ and $\frac{dz}{dt}$ are the components of the velocity of the boat. Now if we turn off the engine of the boat and float along counting fish (the lagrangian viewpoint), the velocity of the boat would be simply the velocity of the streams. The change of fish concentration in this case is called substantial time derivative and is written as follows:

$$\frac{Dc}{Dt} = \frac{\partial c}{\partial t} + v_x\frac{\partial c}{\partial x} + v_y\frac{\partial c}{\partial y} + v_z\frac{\partial c}{\partial z}$$

in which v_x, $v_y$and v_z are the components of the local fluid velocity $\mathbf{v}$.

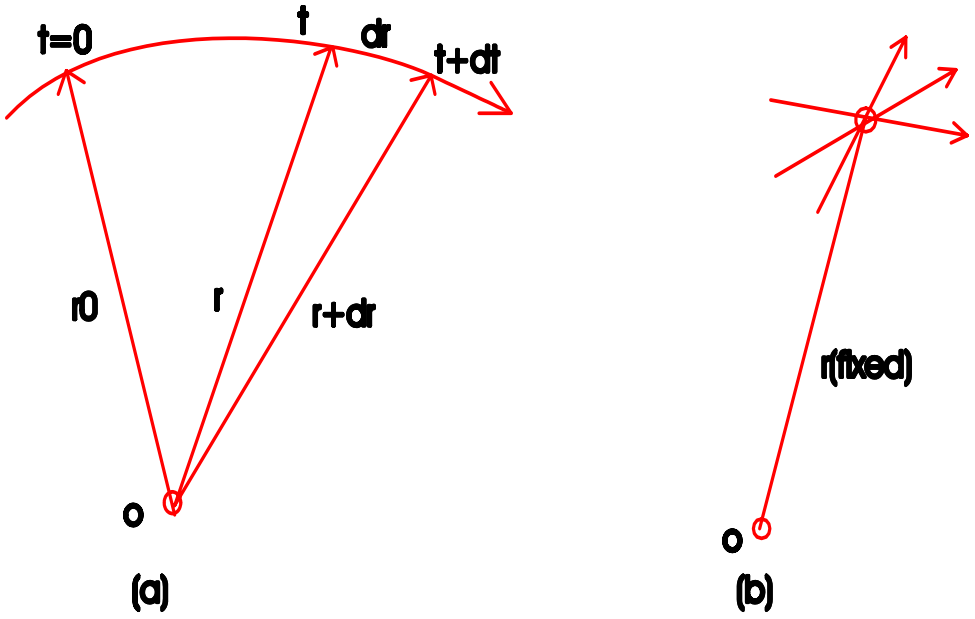

Figure 2.2: a)Lagrangian viewpoint b)Eulerian viewpoint

2.2.2 System and Control Volume

An identified quantity of matter is called system. It may undergo shape changes, position changes or temperature changes, but entailed the same

matter. On the other hand, control volume is a definite volume in space and its boundary called control surface. The amount of matter inside control volume may change but its shape is fixed. the concept of system and control volume are related to the Lagrangian and Eulerian viewpoints.

2.2.3 Reynold's Transport Equation

Consider N as properties of a substance whose measure depends on the amount of the substance presented in a system. An arbitrary flow field of $\mathbf{v} = \mathbf{v}(\mathbf{x}, \mathbf{y}, \mathbf{z}, \mathbf{t})$is observed from some reference xyz. We consider a system of fluid with finite mass at time t and $t + \Delta t$ (figure 2.3). The streamlines correspond to those at time t. The control volume is considered with system at time t and is fixed.

The distribution of N per unit mass will be given as η, such that $N = \iiint \eta\rho dV$ with dV representing an element of volume with mass density of ρ. We are trying to establish a relation between the rate of change of N in system with variation of this property inside the control volume.

The system at time t and $t+\Delta t$ can be divided into three regions. Region II is common to the system at both time t and $t + \Delta t$. Rate of change of N with respect to time for the system can be written as:

$$\left(\frac{dN}{dt}\right)_{system} = \frac{DN}{Dt} =$$

$$\lim_{\Delta t \to 0} \frac{\left(\iiint_{III} \eta\rho dV + \iiint_{II} \eta\rho dV\right)_{t+\Delta t} - \left(\iiint_{I} \eta\rho dV + \iiint_{II} \eta\rho dV\right)_{t}}{\Delta t}$$

The above equation can be arranged as following:

$$\frac{DN}{Dt} = \lim_{\Delta t \to 0} \left(\frac{\left(\iiint_{II} \eta\rho dV\right)_{t+\Delta t} - \left(\iiint_{II} \eta\rho dV\right)_{t}}{\Delta t} \right) + \tag{2.1}$$

$$\lim_{\Delta t \to 0} \frac{\left(\iiint_{III} \eta\rho dV\right)_{t+\Delta t}}{\Delta t} - \lim_{\Delta t \to 0} \frac{\left(\iiint_{I} \eta\rho dV\right)_{t}}{\Delta t}$$

In the first term on the right hand side of equation. 2.1, we can say that, as Δt goes to zero the region II becomes that of control volume ,cv,. Then:

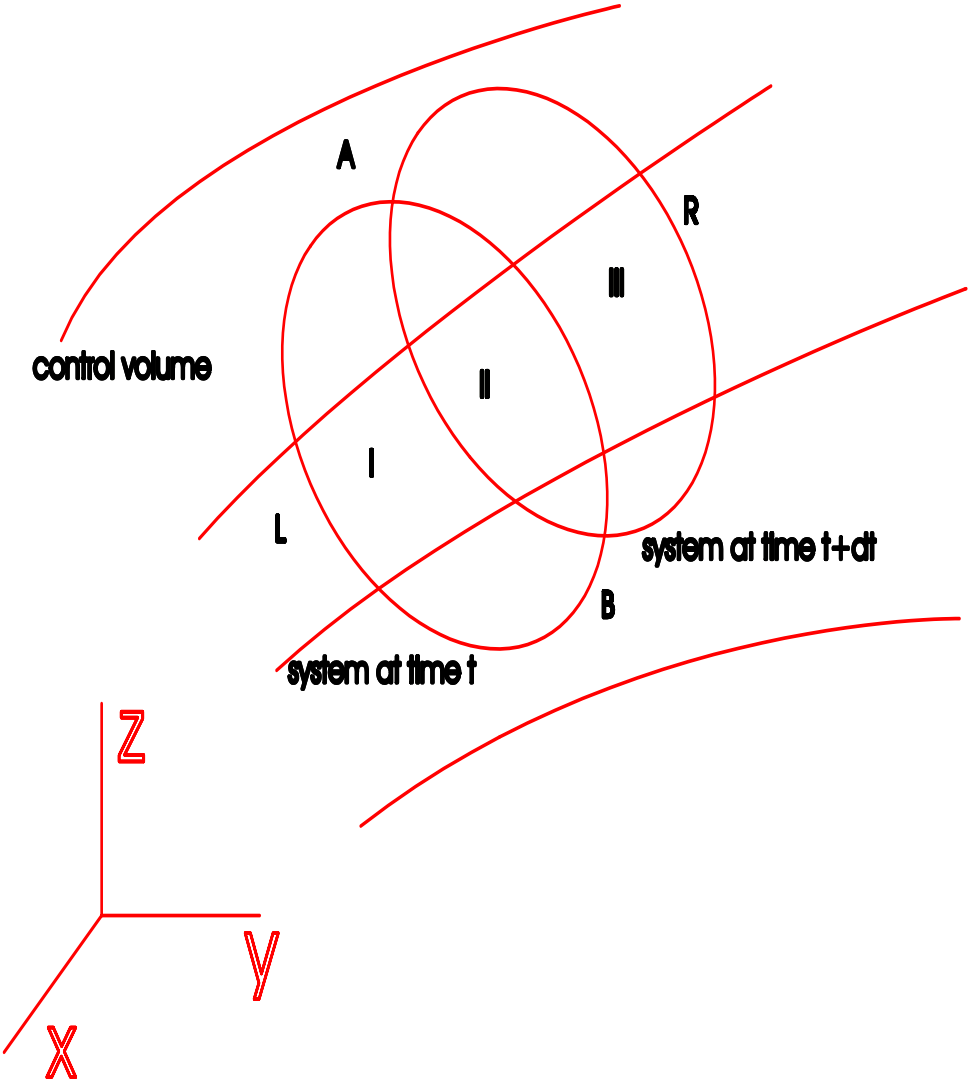

Figure 2.3: Moving system

$$\lim_{\Delta t\to 0}\left(\frac{\left(\iiint_{II}\eta\rho dV\right)_{t+\Delta t}-\left(\iiint_{II}\eta\rho dV\right)_{t}}{\Delta t}\right)=\frac{\partial}{\partial t}\iiint_{cv}\eta\rho dV \qquad (2.2)$$

The second term in equation 2.1 shows the amount of the property N that has crossed part of the control surface, cs, shown as ARB. Therefore, the second term is the average of efflux of N across ARB during time interval of Δt. As Δt goes to zero this becomes exact rate of efflux of N through the cs. Similarly, the third term approximates the amount of N that has passed into the cv during Δt through remaining of the cs (influx). Thus, the lase two integrals give the net rate of efflux of N from cv at time t as:

$$\lim_{\Delta t\to 0}\frac{\left(\iiint_{III}\eta\rho dV\right)_{t+\Delta t}}{\Delta t}-\lim_{\Delta t\to 0}\frac{\left(\iiint_{I}\eta\rho dV\right)_{t}}{\Delta t}=Net\ efflux\ rate\ of\ N\ from\ cs \qquad (2.3)$$

In conclusion, the rate of change of N for system at time t are sum of first, rate of change of N inside cv having the shape of the system at time t (equation 2.2)and second, the net rate of efflux of N through the cs at time t (equation 2.3).

In equation 2.3, the term dV can be written as:

$$dV=\mathbf{v}.d\mathbf{A}dt \qquad (2.4)$$

which is the volume of fluid that has crossed the cs in time dt. $d\mathbf{A}$ is the normal outward vector on control surface. Multiplying (equation 2.4) by ρ and dividing by dt then gives the instantaneous rate of mass flow of fluid $\rho\mathbf{v}.d\mathbf{A}$ leaving the control volume through the indicated area dA. For the fluid entering the control volume the expression $dV=\mathbf{v}.d\mathbf{A}dt$ is negative while for the fluid going out of the control volume the expression is positive. Therefore equation 2.3 can be written as follows:

$$\begin{aligned}
Efflux\ rate\ through\ cs &\approx \iint_{ARB}\eta\rho\mathbf{v}.d\mathbf{A}\\
Influx\ rate\ through\ cs &\approx -\iint_{ALB}\eta\rho\mathbf{v}.d\mathbf{A}\\
Net\ efflux\ rate\ through\ cs &\approx \iint_{ARB}\eta\rho\mathbf{v}.d\mathbf{A}+\iint_{ALB}\eta\rho\mathbf{v}.d\mathbf{A}
\end{aligned}$$

In the limit as $\Delta t \to 0$, the approximation becomes exact, so we can express the right side of the above equation as $\iint_{cs} \eta(\rho \mathbf{v}.d\mathbf{A})$, where the integral is the closed integral over the entire control surface.

Now the equation 2.1 can be written as:

$$\frac{DN}{Dt} = \iint_{cs} \eta(\rho \mathbf{v}.d\mathbf{A}) + \frac{\partial}{\partial t} \iiint_{cv} \eta \rho dV \tag{2.5}$$

This is called the Reynold Transport equation and it is a change from system approach to control volume approach. In the Reynole transport equation $\mathbf{v}$ is measured relative to some reference xyz and the control volume was fixed in this reference. Thus, $\mathbf{v}$ in the above equation is measured relative to control volume. As a consequences, the time rate of change of N is in effect observed from the control volume and velocities and time rates of changes are those seen from control volume. Since we could use a reference xyz having an arbitrary motion, it means that the control volume can have any motion. Thus the Reynold transport equation will then instantaneously be correct if we measure the time derivatives and velocities relative to the control volume, no matter what the motion of the control volume may be.

2.2.4 Continuity Equation

A system always entails the same quantity of matter. Therefore, the mass M would be constant. To go from system approach to control approach, we use Reynold transport equation in which N is for our case M, the mass of a fluid system and it is $M = \iiint \rho dV$. Therefore, $\eta = 1$. Thus for a constant mass in a system at any time t, we can write the Reynold transport equation as following:

$$\frac{DM}{Dt} = 0 = \iint_{cs} (\rho \mathbf{v}.d\mathbf{A}) + \frac{\partial}{\partial t} \iiint_{cv} \rho dV$$

The velocity $\mathbf{v}$ and the time derivative are measured relative to the control volume. Above equation can be written in the following form:

$$\iint_{cs} (\rho \mathbf{v}.d\mathbf{A}) = -\frac{\partial}{\partial t} \iiint_{cv} \rho dV \tag{2.6}$$

Equation 2.6 which is the final form of the continuity equation expresses that the net efflux rate of mass through the control surface equals the rate of

decrease of mass inside the control volume. Two special cases of continuity can be considered. The case of steady flow in which all fluid properties at any fixed position in the reference must remain invariant, the continuity equation can be written as:

$$\iint_{cs} (\rho \mathbf{v}.d\mathbf{A}) = \mathbf{0}$$

The other case is the case of incompressible fluid having constant ρ.The continuity equation can be written as:

$$\iint_{cs} \mathbf{v}.d\mathbf{A} = \mathbf{0}$$

A more detailed definition of compressibility is brought in the proceeding sections.

2.2.5 Linear Momentum Equation

If we take linear momentum as parameters N which is used as a general term (vector and scalar) in the Reynold transport equation, we have $N = \mathbf{P} = m\mathbf{v}$. The term η in this case would become momentum per unit mass, or simply $\mathbf{v}$, then, $\mathbf{P} = \iiint \mathbf{v}(\rho dV)$. Then the Reynold transport equation can be written as followings:

$$\frac{D\mathbf{P}}{Dt} = \iint_{cs} \mathbf{v}(\rho \mathbf{v}.d\mathbf{A}) + \frac{\partial}{\partial t} \iiint_{cv} \mathbf{v}\rho dV \tag{2.7}$$

The equation of linear momentum is a vector equation and can be divided into its three components.

Newton's second law states that:

$$\sum \mathbf{F} = \frac{d}{dt}_{system} \left[\iiint \mathbf{v} dm \right] = \frac{d\mathbf{P}}{dt}_{system}$$

In above equation, $\sum \mathbf{F}$ if the resultant of the all external forces acting on the system and $\mathbf{v}$ the time derivative are taken from the inertial references. Since, the second law of Newton is based on the Eulerian viewpoint, we are following a system. Thus, it can be written as:

$$\sum \mathbf{F} = \frac{D}{Dt}\left[\iiint \mathbf{v} dm\right] = \frac{D\mathbf{P}}{Dt}$$

There are two types of the external forces. Surface forces, $\mathbf{T}(x, y, z, t)$ given as forces per unit area on the boundary surface, bs. Force acting on the material inside the boundary, ib are called body force, $\mathbf{B}(x, y, z, t)$ given as force per unit mass. Thus, The above equation can be written as followings:

$$\iint_{bs} \mathbf{T} dA + \iiint_{ib} \mathbf{B}\rho dV = \frac{D\mathbf{P}}{Dt} \tag{2.8}$$

Equation 2.8 is the Newton's second law for a finite system. Knowing that the control volume and system are coincident at time t, if we fix the control volume in inertial space, then the derivatives in the right hand side is taken from a inertial references and we may use the Newton's second law (equation 2.8) to replace it in the Reynold equation and then we get:

$$\iint_{cs} \mathbf{T} dA + \iiint_{cv} \mathbf{B}\rho dV = \iint_{cs} \mathbf{v}(\rho \mathbf{v}.d\mathbf{A}) + \frac{\partial}{\partial t}\iiint_{cv} \mathbf{v}\rho dV \tag{2.9}$$

Equation 2.9 means that: Sum of surface forces acting on the control surface and body forces acting on the control volume are equal with the sum of the rate of the efflux of the linear momentum across the control surface and the rate of increase of linear momentum inside the control volume.

Equation 9 is a vector equation and can be written for each components. For example in x direction we can write it as follows:

$$\iint_{cs} T_x dA + \iiint_{cv} B_x \rho dV = \iint_{cs} v_x(\rho \mathbf{v}.d\mathbf{A}) + \frac{\partial}{\partial t}\iiint_{cv} v_x \rho dV \tag{2.10}$$

In this book for simplicity, the positive direction of the reference axis xyz are the same as the positive direction of the velocity components as well as the surface and body force components. Sign of $\mathbf{v}.d\mathbf{A}$ is independent of the sign consideration.

2.2.6 The Equation of the Motion

The continuity equation and the linear momentum equation was developed for finite systems and their were related to control volume. The equations give an average values of quantities or only components of resultant forces. They don't give any detail information of the flow everywhere inside the control volume. Here, we are trying to find out differential equations valid at any point of fluid.

Writing continuity equation in the form of differential equation, we consider an infinitesimal control volume in the shape of a rectangular parallelepiped fixed in xyz for a general flow $\mathbf{v}(x, y, z)$ measured relative to xyz.

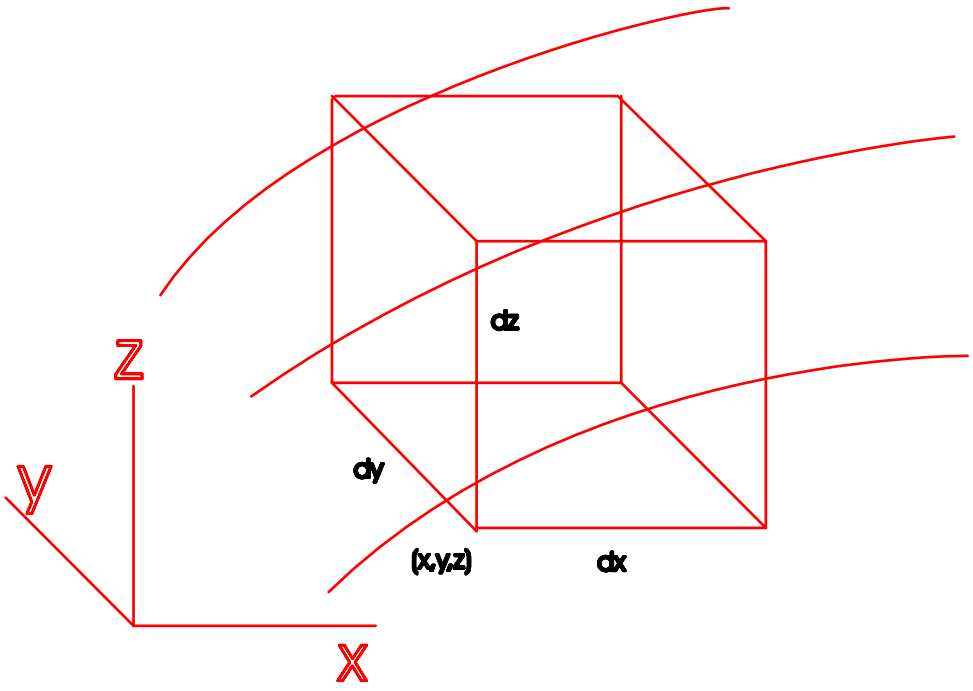

Figure 2.4: Volume element

The net efflux rate along the plane of control volume that are perpendicular to the x axis (x planes of the element) is, $\rho v_x \mid_{x+\Delta x} \Delta y \Delta z - \rho v_x \mid_x \Delta y \Delta z$ (figure 2.4) If we write the similar equation for the axis in y and z direction and add them up we get the net efflux rate as following:

$$\begin{aligned}\text{Net efflux rate} &= [\rho v_x \mid_{x+\Delta x} \Delta y\Delta z - \rho v_x \mid_x \Delta y\Delta z] \\ &+ [\rho v_y \mid_{y+\Delta y} \Delta x\Delta z - \rho v_y \mid_y \Delta x\Delta z] \\ &+ [\rho v_z \mid_{z+\Delta z} \Delta x\Delta y - \rho v_z \mid_z \Delta x\Delta y]\end{aligned}$$

The rate of mass accumulation inside the control volume would be $\frac{\partial \rho}{\partial t}\Delta x\Delta y\Delta z$. Equating the net efflux rate and the rate of decrease of mass inside the control volume and dividing all resulting equation by $\Delta x\Delta y\Delta z$ and taking the limit as Δx, Δy and Δz approach zero, we get:

$$\frac{\partial(\rho v_x)}{\partial x} + \frac{\partial(\rho v_y)}{\partial y} + \frac{\partial(\rho v_z)}{\partial z} = -\frac{\partial \rho}{\partial t} \tag{2.11}$$

This is called differentia continuity equation and one special cases of it would be case of steady flow which results in:

$$\frac{\partial(\rho v_x)}{\partial x} + \frac{\partial(\rho v_y)}{\partial y} + \frac{\partial(\rho v_z)}{\partial z} = 0$$

The other case of incompressible flow would be as following:

$$\frac{\partial v_x}{\partial x} + \frac{\partial v_y}{\partial y} + \frac{\partial v_z}{\partial z} = 0$$

Introducing the divergence operator which for a vector field $\mathbf{v}$ can be defined as:

$$\boldsymbol{\nabla}.\mathbf{v} = \frac{\partial v_x}{\partial x} + \frac{\partial v_y}{\partial y} + \frac{\partial v_z}{\partial z}$$

Then we can write the general form of the continuity equation 2.11 in the following form:

$$\boldsymbol{\nabla}.(\rho\mathbf{v}) = -\frac{\partial \rho}{\partial t}$$

Writing the linear momentum equation in the form of differential equation, we consider an infinitesimal system in the shape of a rectangular parallelepiped fixed in xyz (figure 2.5). The linear momentum equation is a form of Newton's second law which has an Eulerian viewpoint. Consider a volume element $\Delta x\Delta y\Delta z$ as shown in figure2.5. The surface stress on each side of

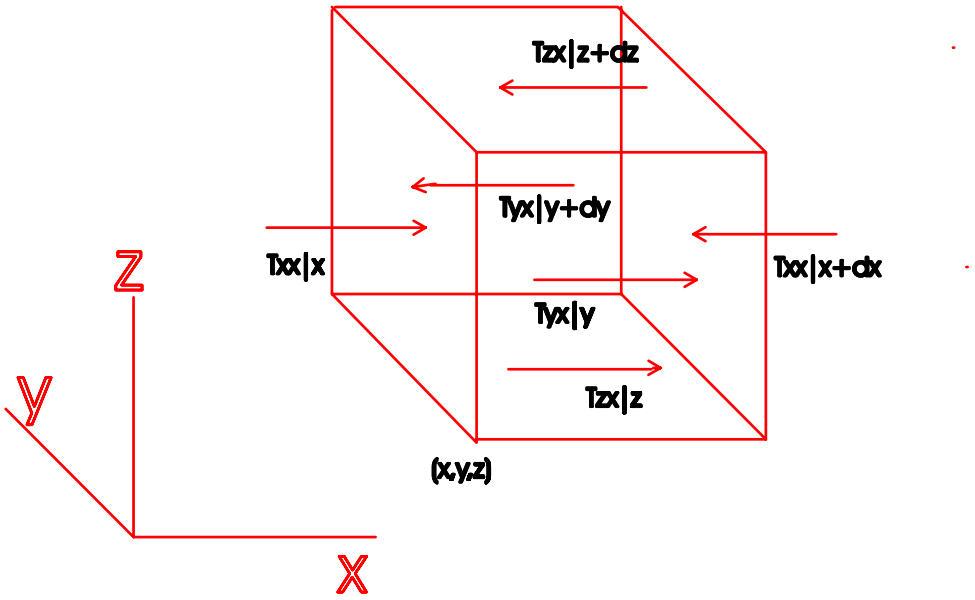

Figure 2.5: Rectangular Parallelpiped element

a cubic element cab be written as T_{ij}, $i, j = x, y, z$ where i is an indication of the side, plane, in which the stress is located on and j is the direction of the stress. For example $T_{xy}$is the components of the stress on a plane normal to x axis and directed toward y axis. It can be shown that for equilibrium we must have $T_{ij} = T_{ji}$. As it was already mentioned equation of linear momentum is a vector equation (equation 2.9). Thus we can write for each components of it. Here, we start by considering the x direction(equation 2.10). The first term on the left hand side of the equation 2.10 is all of the surface forces acting on the element at the x direction. The resultant forces acting on the x planes along the x directions is $T_{xx} \mid_{x+\Delta x} \Delta y \Delta z - T_{xx} \mid_x \Delta y \Delta z$. The resultant of forces acting on the y plane along the x direction is $T_{yx} \mid_{y+\Delta y} \Delta x \Delta z - T_{yx} \mid_y \Delta x \Delta z$. Similarly, for the forces on the z plane along the x direction is $T_{zx} \mid_{z+\Delta z} \Delta x \Delta z - T_{zx} \mid_z \Delta x \Delta y$. If we add all of the surface forces we will get:

$$[T_{xx} \mid_{x+\Delta x} \Delta y \Delta z - T_{xx} \mid_x \Delta y \Delta z] +$$
$$[T_{yx} \mid_{y+\Delta y} \Delta x \Delta z - T_{yx} \mid_y \Delta x \Delta z] +$$

$$[T_{zx} \mid_{z+\Delta z} \Delta x \Delta z - T_{zx} \mid_z \Delta x \Delta y]$$

The second term on the left hand side of the equation 2.10 is the body force and is:

$$\rho g_x \Delta x \Delta y \Delta z$$

where g_x is the component of the gravitational force along the x axis.

The first term on the right hand side of equation 2.10 is the net rate of efflux. the rate at which x component of momentum enters at x is $v_x \rho v_x \mid_x \Delta y \Delta z$ and the rate at which it leaves at $x + \Delta x$ is $v_x \rho v_x \mid_{x+\Delta x} \Delta y \Delta z$. The same can be written for the y and z planes. Thus if we add them up we get:

$$\begin{aligned}
&[v_x \rho v_x \mid_{x+\Delta x} - v_x \rho v_x \mid_x] \Delta y \Delta z + \\
&[v_x \rho v_y \mid_{y+\Delta y} - v_x \rho v_y \mid_y] \Delta x \Delta z + \\
&[v_x \rho v_z \mid_{z+\Delta z} - v_x \rho v_z \mid_z] \Delta x \Delta y
\end{aligned}$$

The second term on the right hand side of the equation 2.10 is the accumulation of the momentum inside the element and is:

$$\frac{\partial(\rho v_x)}{\partial t} \Delta x \Delta y \Delta z$$

If we substitute all the terms into the equation 2.10 from the above equations and dividing the entire resulting equation by $\Delta x \Delta y \Delta z$ and taking limit as Δx, Δy and Δz approaches zero, we obtain the x-component of the equation of the motion as:

$$\frac{\partial T_{xx}}{\partial x} + \frac{\partial T_{xy}}{\partial y} + \frac{\partial T_{xz}}{\partial z} + \rho g_x = \frac{\partial(v_x \rho v_x)}{\partial x} + \frac{\partial(v_x \rho v_y)}{\partial y} + \frac{\partial(v_x \rho v_z)}{\partial z} + \frac{\partial(\rho v_x)}{\partial t} \quad (2.12)$$

Similarly, for the components in the xx and y direction it can be written as:

$$\frac{\partial T_{xy}}{\partial x} + \frac{\partial T_{yy}}{\partial y} + \frac{\partial T_{zy}}{\partial z} + \rho g_y = \frac{\partial(v_y \rho v_x)}{\partial x} + \frac{\partial(v_y \rho v_y)}{\partial y} + \frac{\partial(v_y \rho v_z)}{\partial z} + \frac{\partial(\rho v_y)}{\partial t} \quad (2.13)$$

$$\frac{\partial T_{xz}}{\partial x} + \frac{\partial T_{yz}}{\partial y} + \frac{\partial T_{zz}}{\partial z} + \rho g_z = \frac{\partial(v_z \rho v_x)}{\partial x} + \frac{\partial(v_z \rho v_y)}{\partial y} + \frac{\partial(v_z \rho v_z)}{\partial z} + \frac{\partial(\rho v_z)}{\partial t} \quad (2.14)$$

The quantity ρv_x, ρv_y and ρv_z are the components of the $\rho\mathbf{v}$,mass velocity vector. The terms $\rho v_x v_x$, $\rho v_x v_y$, $\rho v_x v_z$, $\rho v_y v_z$, etc. are the nine components(six components because of symmetry) of the momentum flux $\rho\mathbf{vv}$, which is the dyadic product of $\rho\mathbf{v}$ and $\mathbf{v}$. Similarly, T_{xx}, T_{xy}, T_{xz}, T_{yx}, etc. are the nine components(six components because of symmetry) of the $\mathbf{T}$, known as the stress tensor. We can combine, the above three equations and write them in a vector format as followings:

$$\boldsymbol{\nabla}.\mathbf{T} + \rho\mathbf{g} = \boldsymbol{\nabla}.\rho\mathbf{vv} + \frac{\partial\rho\mathbf{v}}{\partial t} \tag{2.15}$$

There should be noticed that $\boldsymbol{\nabla}.\rho\mathbf{vv}$ and $\boldsymbol{\nabla}.\mathbf{T}$ are not simple divergence because of tensorial nature of the $\boldsymbol{\nabla}.\rho\mathbf{vv}$ and $\boldsymbol{\nabla}.\mathbf{T}$. The above equation is the general form of the linear momentum equation.

If we use the equation of continuity to substitute it in the equation 2.12, we will get:

$$\frac{\partial T_{xx}}{\partial x} + \frac{\partial T_{yx}}{\partial y} + \frac{\partial T_{zx}}{\partial z} + \rho g_x = \rho\frac{Dv_x}{Dt}$$

The same can be written for y and z components. When three components added together vectorially, we get:

$$\underbrace{\rho\frac{D\mathbf{v}}{Dt}}_{\substack{mass\ per\ unit\ volume \\ time\ acceleration}} = \underbrace{\boldsymbol{\nabla}.\mathbf{T}}_{\substack{surface\ forces\ on\ element \\ per\ unit\ volume}} + \underbrace{\rho\mathbf{g}}_{\substack{body\ forces\ on\ element \\ per\ unit\ volume}} \tag{2.16}$$

This is an statement of the Newton's second law which was developed for a volume of fluid element moving with acceleration because of the forces acting upon it. It can be seen that momentum balance is equivalent to Newton's second law of motion. The above equation is valid for any continuous medium. In equation 2.16 we can insert expressions for various stresses in forms of velocity gradient and pressure. Therefore, we need to find a relation between various stress and velocity gradient..

2.3 VISCOSITY

A fluid with zero viscosity is called a nonviscous, or inviscid fluid. Laminar flow can be described as a well-ordered pattern whereby fluid layers are assumed to slide over one another. In this case while fluid has irregular molecular motion, is macroscopically, well ordered flow. For a laminar flow, whereby fluid particles move in straight, parallel lines, called Newtonian fluids, the shear stress on an interface tangent to direction of flow is proportional to the distance rate of change of velocity, wherein differential is taken in a direction normal to the interface, $T_{xy} \propto \frac{\partial v_x}{\partial y}$ or $T_{xy} = \mu \frac{\partial v_x}{\partial y}$, Where μ is called the coefficient of viscosity with the dimension of $(F/L^2)t$ (figure 2.6).

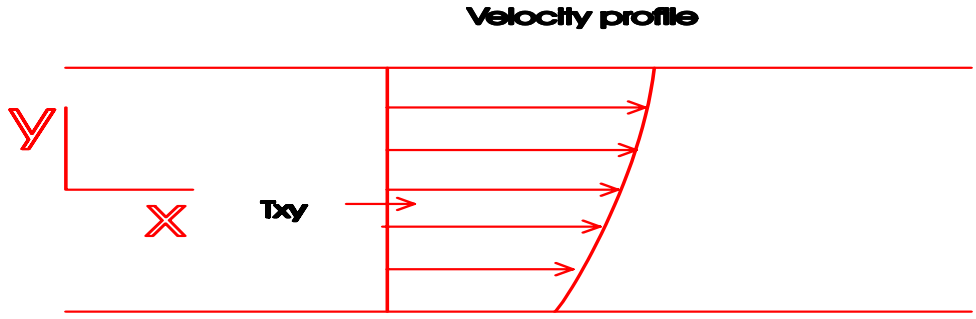

Figure 2.6: Well-ordered parallel flow

This unit in a system of centimeter (cm)-gram (g)-second(sec)is $g - cm^{-1} - \sec^{-1}$and is called the poise. At room temperature, μ is about 1 centi-poise for water and about 0.002 centi-pois for air. This is well-known Newton's viscosity law. All gases and simple liquids are described by the later formula. For gases at low density viscosity decrease as temperature increases. Whereas for liquids the viscosity usually decreases with increasing temperature. The reason may be that, in gases, molecules travel long distance between collisions and the momentum is transported by the molecules in free flight, which as in liquids the molecules travel only very short distances between collisions, the principal mechanism for momentum transfer is the actual colliding of the molecules.

In Newtonian law of viscosity for a given temperature and pressure μ is constant. Experiments show that in some fluids, $T_{xy}$is not proportional to the change of rate of velocity in normal direction of it. These few industrial

important materials, that are not described by the Newtonian law of viscosity are referred to non-newtonian fluids. In this case μ may be described as a function of $\frac{\partial v_x}{\partial y}$or T_{xy}.

In more general flows, there are more general relations between the stress field and the velocity field(namely constitutive law). Here, we consider Stoke's viscosity law. This is based on assumption that each stress is linearly related through a set of constants to each of the six strains rates ($\dot{\epsilon}_{ij}, i, j = x, y, z \mid \dot{\epsilon}_{ij}=\dot{\epsilon}_{ji}$). In addition each normal stress is directly related to pressure p. The constants are called viscosity coefficients and fluids behaving accordingly to this relation are called Newtonian fluid. The Stoke's viscosity law degenerates to Newton's viscosity law for the special case of parallel flow. Knowing that most Newtonian fluids have flow properties which are independent of direction of coordinates and also considering that for most fluid $p = -\bar{\sigma} = -\frac{1}{3}(T_{xx} + T_{yy} + T_{zz})$, we reach the following relationships:

$$\begin{aligned}
T_{xx} &= \mu(2\frac{\partial v_x}{\partial x} - \frac{2}{3}\boldsymbol{\nabla}.\mathbf{v}) - p \\
T_{yy} &= \mu(2\frac{\partial v_y}{\partial y} - \frac{2}{3}\boldsymbol{\nabla}.\mathbf{v}) - p \\
T_{zz} &= \mu(2\frac{\partial v_z}{\partial z} - \frac{2}{3}\boldsymbol{\nabla}.\mathbf{v}) - p \\
T_{xy} &= \mu(\frac{\partial v_x}{\partial y} + \frac{\partial v_y}{\partial x}) \\
T_{xz} &= \mu(\frac{\partial v_x}{\partial z} + \frac{\partial v_z}{\partial x}) \\
T_{yz} &= \mu(\frac{\partial v_y}{\partial z} + \frac{\partial v_z}{\partial y})
\end{aligned}$$

This is a common form of Stoke's viscosity law.

2.4 NAVIER-STOKES AND EULER EQUATIONS

Substituting the Stoke's viscosity law into the equations of the linear momentum (equations 2.12, 2.13, 2.14) for a newtonian fluid with varying density and viscosity, we get:

$$\rho\frac{Dv_x}{Dt} = \tag{2.17}$$

$$-\frac{\partial p}{\partial x}+\frac{\partial}{\partial x}\left[2\mu\frac{\partial v_x}{\partial x}-\frac{2}{3}\mu(\boldsymbol{\nabla}.\mathbf{v})\right]+\frac{\partial}{\partial y}\left[\mu(\frac{\partial v_x}{\partial y}+\frac{\partial v_y}{\partial x})\right]+\frac{\partial}{\partial z}\left[\mu(\frac{\partial v_z}{\partial x}+\frac{\partial v_x}{\partial z})\right]+B_x$$

$$\rho\frac{Dv_y}{Dt} = \tag{2.18}$$

$$-\frac{\partial p}{\partial y}+\frac{\partial}{\partial x}\left[\mu(\frac{\partial v_y}{\partial x}+\frac{\partial v_x}{\partial y})\right]+\frac{\partial}{\partial y}\left[2\mu\frac{\partial v_y}{\partial y}-\frac{2}{3}\mu(\boldsymbol{\nabla}.\mathbf{v})\right]+\frac{\partial}{\partial z}\left[\mu(\frac{\partial v_z}{\partial y}+\frac{\partial v_y}{\partial z})\right]+B_y$$

$$\rho\frac{Dv_z}{Dt} = \tag{2.19}$$

$$-\frac{\partial p}{\partial z}+\frac{\partial}{\partial x}\left[\mu(\frac{\partial v_z}{\partial x}+\frac{\partial v_x}{\partial z})\right]+\frac{\partial}{\partial y}\left[\mu(\frac{\partial v_z}{\partial y}+\frac{\partial v_x}{\partial z})\right]+\frac{\partial}{\partial z}\left[2\mu\frac{\partial v_z}{\partial z}-\frac{2}{3}\mu(\boldsymbol{\nabla}.\mathbf{v})\right]+B_z$$

These equations, along with the equation of continuity, the equation of $p = p(\rho)$, $\mu = \mu(\rho)$, and the boundary and initial conditions determine completely the pressure, density and velocity component in a flowing isothermal fluid.

For constant ρ and constant μ the equation may be simplified by using the equation of continuity ($\boldsymbol{\nabla}.\mathbf{v} = 0$) to results in:

$$\rho\frac{D\mathbf{v}}{Dt} = -\boldsymbol{\nabla}p + \mu\nabla^2\mathbf{v} + \mathbf{B}$$

The operator $\nabla^2 = \frac{\partial^2}{\partial x^2} + \frac{\partial^2}{\partial y^2} + \frac{\partial^2}{\partial z^2}$ is called the Laplacian operator. The above equation is called "Navier-Stokes equation which first developed by Navier in France.

For inviscid fluids, the equations 2.17, 2.18 and 2.19 will result in:

$$\rho\frac{D\mathbf{v}}{Dt} = -\boldsymbol{\nabla}p + \mathbf{B}$$

This is Euler equation which is widely used for describing flow systems in which viscous effects are relatively unimportant.

2.5 COMPRESSIBLE FLUID

Despite the existence of large pressure, fluids undergo very little change in density. Water needs a pressure change of $20,000kPa$ to have 1 percent change in its density. Fluids of constant density are termed incompressible fluids and assumed during computation the density is constant. A flowing fluid is said to be compressible when appreciable density changes are brought about the motion. The variation of density is usually accompanied by temperature changes as well as heat transfer. The variation of density means that a group of fluid elements can spread out into a larger region of space without requiring a simultaneous shift to be made of all fluid elements in the fluid. In compressible media a small shift of fluid element will induce similar small movements in adjacent elements and by this a disturbance called an acoustic wave propagates at a relatively high speed through the medium. In the incompressible flows, these propagation have infinite speed which adjustment (disturbance) took place simultaneously through the entire flow and there are now wave to be considered. Thus, compressibility means admission of elastic waves having finite velocity.

Up to now, we needed four scalar equations (the equation of continuity and three components of the equation of linear momentum) to describe fully a flow field. For compressible flow, the density and pressure changes are also accompanied by temperature changes. Thus we need equation of energy and equation of state($\rho = \rho(p, T)$). The general theory of compressible flow is very complicated, not only because of large number of the equations involved, but also because of the wave propagation phenomena that are predominant at flow speed higher than the speed of sound.

The speed of sound is defined as the rate of propagation of an infinitesimal pressure disturbance(wave) through a continuous medium. Sound is the propagation of compressible an expansion wave of finite but small amplitude such that the ear can detect them. Frequencies range from 20 to $20,000$ Hertz while the magnitude is typically less than 10 Pa.

Consider a long tube filled with motionless fluid and having a piston at one end, as shown in figure 2.7. By tapping the piston we may cause a pressure increase dp on the right of $A-A$. Now two things will happen. Due to molecular action, the pressure will increase to the left of $A-A$ and this increase in pressure will move in the tube at high speed C. We thus have a pressure wave of speed V moving to the left due to microscopic action. The second effect is on the macroscopic level. According to Newton's second law,

the fluid just to the left of wavefront described above must accelerate as a result of the pressure difference dp to a velocity dv. Once the pressure rise dp has been established in the fluid, there is no further change in velocity, so it remains at dv. Behind the wavefront, the fluid is thus moving to the left at speed dv. During an interval of dt the wave has progressed a distance Cdt and is shown at position B in figure 2.7. Meanwhile, fluid particle at A move a distance $dvdt$ to position A_1. At an intermediate position, such as halfway between A and B , shown in diagram as D, the fluid velocity dv has persisted for a time interval $\frac{dt}{2}$. Consequently, fluid initially at D has moved a distance $\frac{dvdt}{2}$ to position D_1.

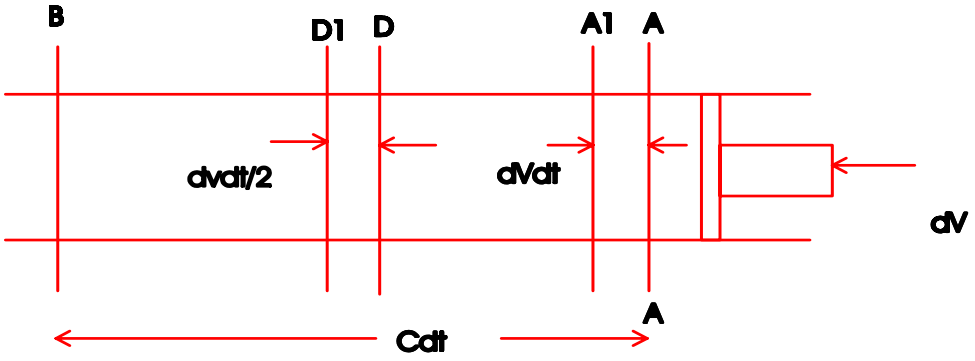

Figure 2.7: Wave front movement and fluid movement

By tapping, as infinitesimal pressure disturbance which will move down the tube at a constant speed, the fluid behind the wave is slightly compressed, while the fluid ahead of the wave remains undisturbed. This is an unsteady state problem. However, if we assume an infinitesimal control volume around the wave, travelling with the wave velocity C, we can apply a steady state analysis. The wave is thus stationary while the fluid flows with an approach velocity C, as shown in figure 2.8. Neglecting friction effects, the velocity profile can be assumed flat. The continuity equation may be written as:

$$\rho AC = (\rho + d\rho)(C - dv)A$$

Neglecting infinitesimal quantities of higher order ($d\rho dv$) gives:

$$Cd\rho - \rho dv = 0 \tag{2.20}$$

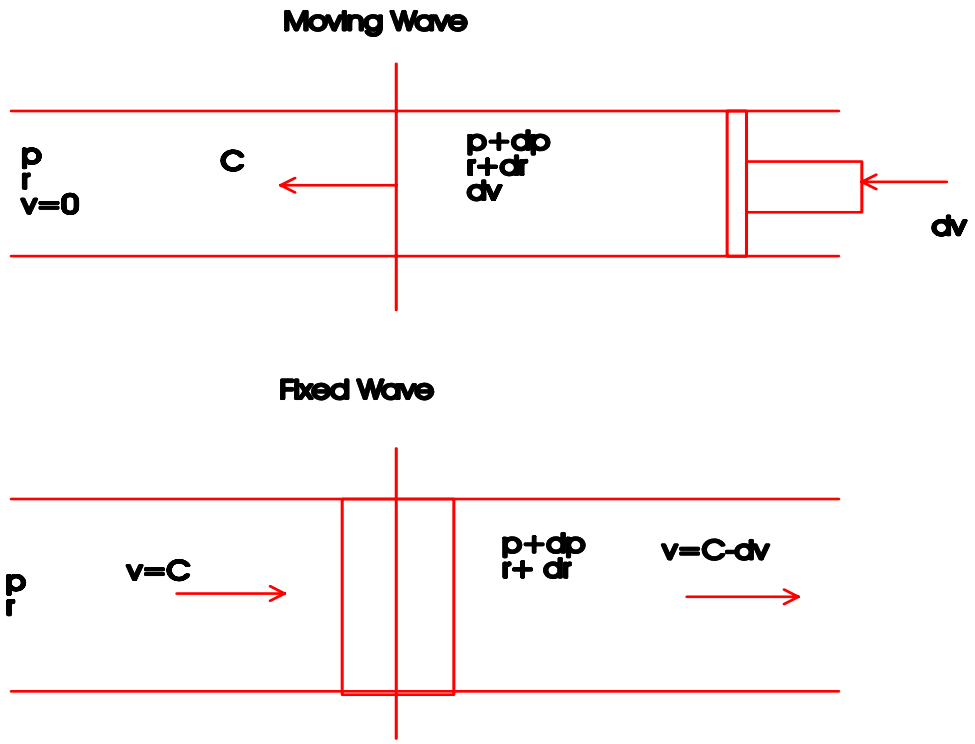

Figure 2.8: Moving pressure disturbance in a motionless fluid and fixed wave in a moving fluid

Applying linear momentum balance to the control volume, we get:

$$0 = C(\rho AC) - (C - dv)\rho AC + pA - (p + dp)A$$

Which further reduces to:

$$dp = \rho C dv \tag{2.21}$$

By combining equations 2.20 and 2.21 we get:

$$C^2 = \frac{dp}{d\rho} \tag{2.22}$$

This expression gives the velocity of propagation of a compressible wave. Since the propagation of infinitesimal expansion and compression waves is called sound, C is then the speed of sound. the above equation is valid for any continuum, be it a solid, a liquid, or a gas. Because of the high speed of travel of the wave there is very little time for any significant heat transfer to take place, so the process is very nearly adiabatic. It should be noted that C is measured relative to the fluid in which the front is propagating. We also assumed a constant value of C, that is we used an inertial control volume with steady flow relative to this control volume. The wave involve infinitesimal pressure variation. Wave with comparatively large pressure variation over a very narrow front are called shock waves. these waves move relative to fluid at speed in excess of the acoustic speed. Then we may consider acoustic wave as limiting cases of shock waves where the change in pressure across wave become infinitesimal. Therefore what we have developed is valid for any weak spherical and cylindrical waves which moves caused by any small disturbance of pressure.

If a continuum were incompressible, equation 2.22 would give an infinite speed of sound. However, no actual liquid or solid can be perfectly incompressible. All materials have a finite speed of sound. For example the speed of sound in water, air, ice and steel at 15^{oc} and a pressure of 101.325 kPa are 1490,340, 3200 and 5059 m/s, respectively.

For liquids and solids it is customary to define the bulk modulus as a parameter relating the volume (or density) change to the applied pressure change:

$$K = -\frac{\Delta p}{\frac{\Delta V}{V}} = \frac{\Delta p}{\frac{\Delta \rho}{\rho}} = \rho \frac{dp}{d\rho} \tag{2.23}$$

Water(at 20^{oc} and atmospheric pressure) has a bulk modulus of about $2.2 \times 10^6\ Pa$ while steel about $200 \times 10^6\ Pa$. The bulk modulus related to young's modulus of elasticity E by the expression:

$$\frac{K}{E} = 3(1 - 2\nu)$$

Where ν is the Poisson's ratio. For many common metals such as steel and aluminum $\nu \approx \frac{1}{3}$ and $E = K$.

By combining equations 2.22 and 2.23 we get:

$$C = \sqrt{\frac{K}{\rho}}$$

2.6 BOUNDARY-LAYER THEORY

For fluids with small viscosity such as air and water with a high degree of accuracy, we can consider frictionless flow over entire fluid except for their regions around the contact areas. Here, because of high velocity gradients, we could not properly neglect frictions (Newton's viscosity law) so we consider these regions apart from the main flow, terming the boundary layers.

In 1904 Ludwing Prandti introduced the concept of boundary layer and showed how Navier-Stokes equations could be simplified. This concept literally revolutionized the science of fluid mechanics. According to Prandti's boundary layer concept viscous effects at high Reynolds number ($\mathrm{Re} = \frac{\rho v L}{\mu} = \frac{Inertia\ Forces}{Viscous\ Forces} = \frac{v^2 L}{\mu v/\rho L^2}$) are confined in thin layers adjacent to solid boundaries. Outside these solid boundary layers the flow may be considered inviscid ($\mu = 0$) and can, thus be described by Euler equation. Within the boundary layer the velocity component in the main flow direction (x) changes from $v_x = 0$ (at the solid boundary) to $v_x = v_\infty$(the free stream velocity at the edge of the boundary layer).

We consider qualitatively the boundary layer flow over a flat plate. As it is shown in figure 2.9, a laminar region begins at the leading edge and grows in thickness. A transition region is reached where the flow changes from laminar to turbulent, with a consequent thickening of the boundary layer. The transition depends partly on the Reynold number($\frac{\rho v_\infty x}{\mu}$) where x is the distance downstream from the leading edge. Transition occurs in the range $\mathrm{Re}_x = 3 \times 10^5$ to $\mathrm{Re}_x = 10^6$. In the turbulent region we find, that as we get

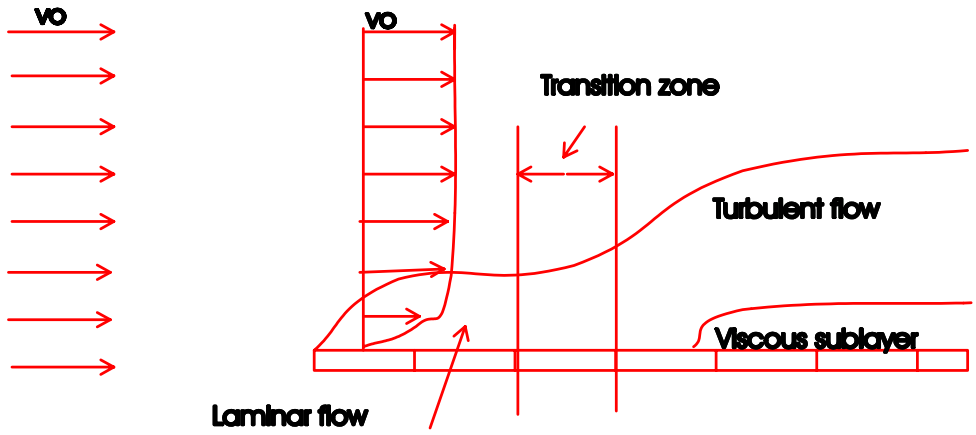

Figure 2.9: Details of boundary layers

near the boundary the turbulence becomes suppressed to such a degree that viscous effects predominate, leading us to formulate the concept of a viscous sublayer shown darkened in the diagram.

There is actually a smooth variation from boundary layer region to the region of constant velocity. The velocity profile merges smoothly into the main-stream profile. There are several definitions of boundary-layer thickness that are quite useful. One can consider that the thickness is the distance δ from the wall out to where the fluid velocity is 99 percent of the mainstream velocity. The experimental determination of the boundary layer thickness as defined above is very difficult because the velocity approaches asymptotically the free stream value v_∞. The edge of the boundary layer is poorly defined. For this reason alternative thicknesses which can be measured more accurately are often used. The displacement thickness δ^* defined as distance by which the boundary would have to be displaced if the entire flow were imagined to be frictionless and the same mass flow maintains at any section (figure 2.10). Thus, considering a unit width along the z across an infinite flat plate at zero angle of attack for incompressible fluid:

$$\int_0^\infty v_x dy = q = \int_{\delta^*}^\infty v_m dy$$

Hence, changing the lower limit on the second integral and solving for δ^* we get:

$$\delta^* = \int_0^\infty (1 - \frac{v_x}{v_m})dy$$

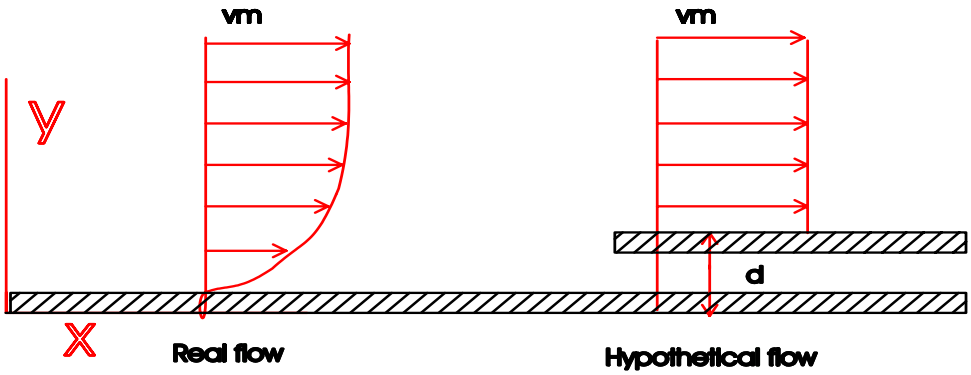

Figure 2.10: Displacement thickness in boundary layer

The motivation for using displacement thickness is to permit the use of a displaced body in place of the actual body, such that the frictionless mass flow around the displaced body is the same as the actual mass flow around the real body. Use is made of the displacement thickness in the design of wind tunnels, air intakes for airplane jet engine.

As the boundary layer thickness growth, the fluid is pushed away from the plate, which means that the velocity has also a component in the y direction , v_y. we would expect that $v_y \ll v_x$ because the boundary layer thickness is small compared to any significant body dimension. The boundary layer thickness, that is the value of y for which $v_x = 0.99v_\infty$, can be obtained as following:

$$\delta \approx 5.0\sqrt{\frac{\mu x}{\rho v_m}} = \frac{5x}{\sqrt{\mathrm{Re}_x}}$$

A rough comparison between the various thicknesses gives:

$$\delta^* = \frac{\delta}{3}$$

The effects of viscosity is influential as δ^* increases. In the case of concrete dams since δ^*/h ratio is very small, the viscous effect can be neglected, specially for the sudden ground acceleration on the base of the reservoir.

2.7 IRROTATIONAL FLOW

A fluid element can be subjected to three types of flow, namely: translation, rotation and deformation. These types of elemental motions are depicted in figure 2.11. The concept of translational motion is self-evident.. The deformational motion will occur when relative orientation of the axis changes as shown in figure 2.11. Deformational flow also exists if one or more axis are stretched or compressed. Here we focus our attention on rotational flow, which is depicted by the fluid element of figure 2.11 turning around.

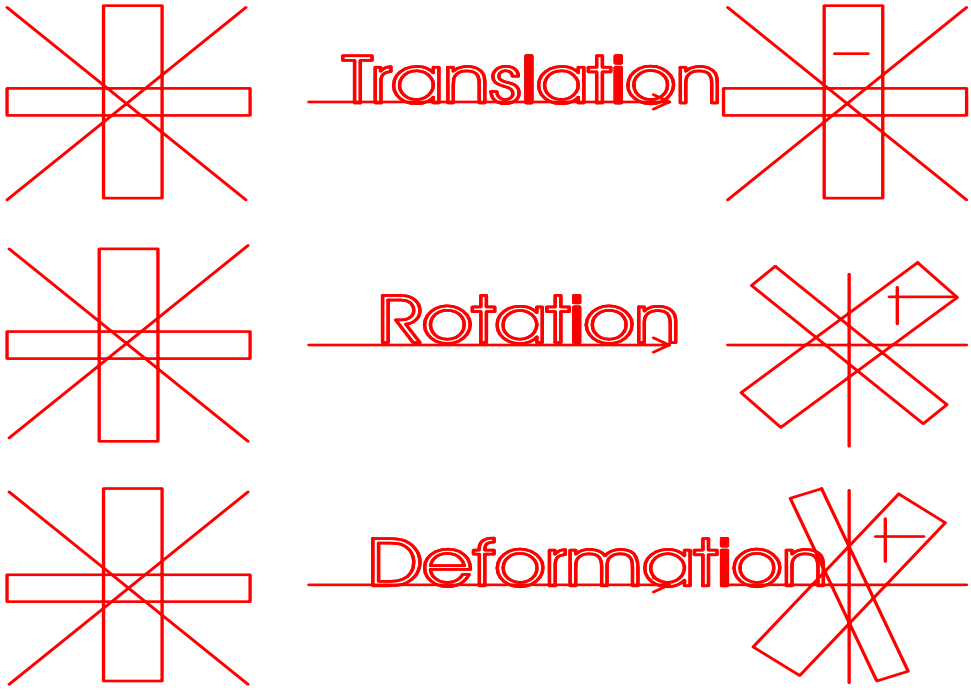

Figure 2.11: Three types of fluid motion

Let us examine the flow in a fluid with circular streamlines as shown in figure 2.12. The fluid rotates like a rigid body. each element turns around at a certain angular velocity. The arrows shown rotate at the same rate. This is unquestionably a case of rotational flow.

Now let us consider the flow between the two horizontal flat plates, where the bottom plate is stationary while the top one moves at velocity v_0 as shown in figure 2.13. we note that the horizontal arrow is simply translated, while

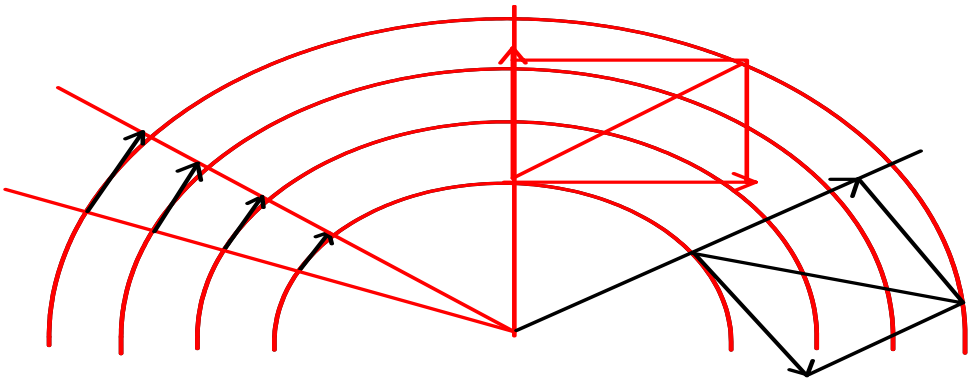

Figure 2.12: Fluid rotating like a rigid body

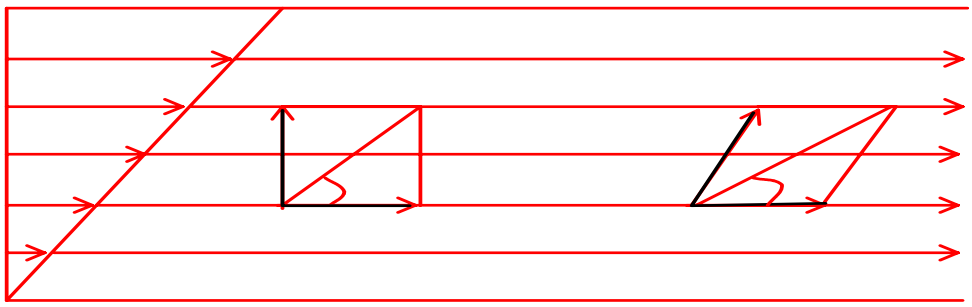

Figure 2.13: Shearing flow between two flat plates

the vertical one turns. It is not clear wether this is a case of rotational flow or not. To determine that we propose to use the average rate at rotation of the two arrows as a measure. If the average rate of rotation is zero the flow is said to be irrotational, if not the flow is rotational. For generality we refer to figure 2.14.

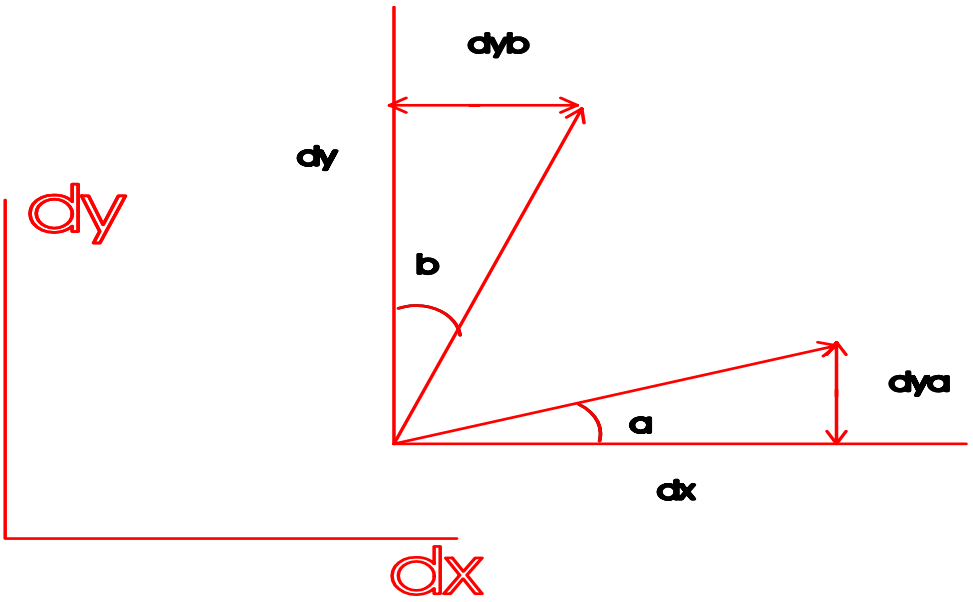

Figure 2.14: Change of relative positions in an arbitrary flow field

We define the angular velocity ω_z about the axis z as the average rate of counterclockwise rotation of the two lines:

$$\omega_z = \frac{1}{2}(\frac{d\alpha}{dt} - \frac{d\beta}{dt})$$

In the limit of small angles we would have:

$$\frac{d\alpha}{dt} = \frac{d(\frac{\Delta y_\alpha}{\Delta x})}{dt} = \frac{d(\frac{\Delta y_\alpha}{\Delta t})}{dx} = \frac{\partial v_y}{\partial x}$$

$$\frac{d\beta}{dt} = \frac{d(\frac{\Delta x_\beta}{\Delta y})}{dt} = \frac{d(\frac{\Delta x_\beta}{\Delta t})}{dy} = \frac{\partial v_x}{\partial y}$$

Thus,

$$\omega_z = \frac{1}{2}(\frac{\partial v_y}{\partial x} - \frac{\partial v_x}{\partial y})$$

Similarly:

$$\omega_x = \frac{1}{2}(\frac{\partial v_z}{\partial y} - \frac{\partial v_y}{\partial z})$$

$$\omega_y = \frac{1}{2}(\frac{\partial v_x}{\partial z} - \frac{\partial v_z}{\partial x})$$

The vector $\boldsymbol{\omega}$ is thus one-half of the vorticity vector:The vector $\boldsymbol{\omega}$ is thus one-half of the vorticity vector:

$$\boldsymbol{\omega} = \frac{1}{2}\boldsymbol{\nabla} \times \mathbf{v} = \frac{1}{2}\begin{bmatrix} \mathbf{i} & \mathbf{j} & \mathbf{k} \\ \frac{\partial}{\partial x} & \frac{\partial}{\partial y} & \frac{\partial}{\partial z} \\ v_x & v_y & v_z \end{bmatrix}$$

To avoid the factor $\frac{1}{2}$ we define the vorticity $\boldsymbol{\zeta}$ as equal to twice the rotational vector $\boldsymbol{\omega}$, then:

$$\boldsymbol{\zeta} = 2\boldsymbol{\omega} = \boldsymbol{\nabla} \times \mathbf{v}$$

Referring back to simple flow configuration of figure 2.13 we note that $v_y = v_z = 0$ and $v_x = v_0 y$, then we have:

$$\omega_z = \frac{1}{2}(0 - v_0) = -\frac{1}{2}v_0$$

Thus, the flow is rotational. At this time we define irrotational flows as those where $\boldsymbol{\omega} = \mathbf{0}$ at each point in the flow. Rotational flows are those where $\boldsymbol{\omega} \neq \mathbf{0}$ at points in the flow.

The normal strain rates give the rate of stretching or shrinking of the two lines shown in figure 2.14, while the shear strain rates give rate of change of angularity of the two lines. What's left of the relative motion must be rigid body motion. Thus the expression $\frac{1}{2}(\frac{\partial v_y}{\partial x} - \frac{\partial v_x}{\partial y})$ is actually more than just average rotation of the line segments about the z axis. It represent the rigid body angular velocity ω_z of the line segments about the z axis.

A development of rotation in a fluid particle in an initially irrotational flow would require shear stress to be present on the particle surface. Thus the shear stress(Newton'sss viscosity law) in such flows and in more general flows will depend on the viscosity of the fluid and the rate of variation of the velocity in region. For fluids with small viscosity such as water and air, assumption of irrotational flow is valid for great part of the flow except region with large velocity gradient. Thus the boundary layer regions are the places that element of fluid rotates. Irrotational analysis may be carried out if the boundary layer thickness is small in comparison with the scale of the fluid.

2.8 RESERVOIR'S EQUATION OF MOTION

Based on the information presented in the previous sections, the Euler equation is valid for the case of dam's reservoir. In the Euler equation, if we divide the pressure into static and dynamic pressure we can write for static pressure $-\boldsymbol{\nabla} p_s + \mathbf{B} = 0$, therefore for only hydrodynamic pressure we can write the following:

$$\rho \frac{D\mathbf{v}}{Dt} = -\boldsymbol{\nabla} p$$

The p is the dynamic pressure in excess of static pressure. The above equation can be written as:

$$\rho(\boldsymbol{\nabla}.\mathbf{v})\ \mathbf{v} + \rho \frac{\partial \mathbf{v}}{\partial t} = -\boldsymbol{\nabla} p$$

For small amplitude motion the effect of convective term of the left hand side of the above equation is negligible, thus we can write:

$$\rho \frac{\partial \mathbf{v}}{\partial t} = -\boldsymbol{\nabla} p \tag{2.24}$$

For a linearly compressible fluid, we define the following:

$$p = -K(\epsilon_{xx} + \epsilon_{yy} + \epsilon_{zz}) \tag{2.25}$$

Derivating of whole equation with respect to time:

$$\dot{p} = -K(\dot{\epsilon}_{xx} + \dot{\epsilon}_{yy} + \dot{\epsilon}_{zz})$$

The $\dot{\epsilon}_{xx}$can be written as following:

$$\dot{\epsilon}_{xx}= \frac{\partial}{\partial t}\left(\epsilon_{xx}\right) = \frac{\partial}{\partial t}\left(\frac{\partial u_x}{\partial x}\right) = \frac{\partial}{\partial x}\left(\frac{\partial u_x}{\partial t}\right) = \frac{\partial v_x}{\partial x}$$

In which u_x is the displacement in the x-direction. Thus we can write:

$$\dot{p}= -K(\boldsymbol{\nabla}.\mathbf{v}) \tag{2.26}$$

If we use equation 2.24 to take the divergence of the whole equation we get:

$$\boldsymbol{\nabla}.(\rho\frac{\partial \mathbf{v}}{\partial t}) = \boldsymbol{\nabla}.(-\boldsymbol{\nabla}p)$$

Or we can write the following:

$$\rho\frac{\partial}{\partial t}(\boldsymbol{\nabla}.\mathbf{v}) = -\boldsymbol{\nabla}^2 p \tag{2.27}$$

Using equation 2.26 and substitute it in equation 2.27 we get:

$$\frac{\rho}{K}\frac{\partial^2 p}{\partial t^2} = \boldsymbol{\nabla}^2 p \tag{2.28}$$

We define $c = \sqrt{\frac{\rho}{K}}$, in which is the velocity of pressure wave in fluid. For incompressible fluid ($K = \infty$), therefore, $C = \infty$and then we have:

$$\boldsymbol{\nabla}^2 p = 0$$

The above equation is the Laplace equation of motion for incompressible fluid.

The equation of motion for reservoir (equation 2.28) obtained based on the following assumption:

a) inviscid fluid, $\mu = 0$

b)small amplitude motion, convective terms are neglected

c)linear compressible fluid, equation 2.25

2.9 RESERVOIR BOUNDARY CONDITIONS

The formulation of the boundary conditions associated with the reservoir boundaries is simply the expression in mathematical terms of the physical situations. There are an infinite number of solutions to the differential

equation. The task is to find the solution that is relevant to the boundary condition. It should be noted that in addition to the spatial (or geometric) boundary conditions, there are temporal boundary conditions which specify the state of the variable of the interest at some points at time. This temporal condition is called an "initial condition".

In case of dam-reservoir we have four spatial (geometric) boundary conditions namely, dam-reservoir, reservoir-foundation, free surface, and reservoir far-end boundary conditions (figure 2.15).

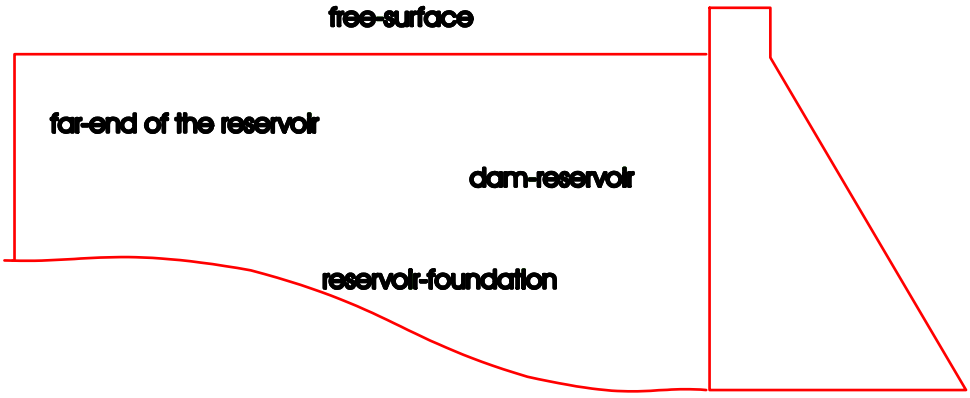

Figure 2.15: Boundaries of the dam-reservoir system

2.9.1 Dam-Reservoir Boundary Condition

At the surface of fluid-structure, it is clear that there must be no flow across the interface. This is based on the fact that face of the concrete dams are impermeable. This results into the condition that at the normal to the boundary there is no relative velocity or another word we can write it mathematically:

$$v_n^s = v_n$$

in which n is the unit normal vector to the boundary at the dam-reservoir interface and v_n^s and v_n are the velocity of the structure (dam) and fluid along the n respectively (figure 2.16). The above equation can be rewritten as following:

$$v_n^s = \mathbf{v}.\mathbf{n}$$

Differentiating the above equation with respect to time will give:

$$\frac{\partial v_n^s}{\partial t} = \frac{\partial \mathbf{v}}{\partial t}.\mathbf{n}$$

It must be noted that n is normal to the surface and it direction is constant as well as its value at a point. From the Euler equation and knowing that $\frac{\partial v_n^s}{\partial t}$ is normal acceleration of the dam at the interface we can write:

$$a_n^s = -\frac{1}{\rho}\boldsymbol{\nabla} p.\mathbf{n}$$

or:

$$\frac{\partial p}{\partial n} = -\rho a_n^s$$

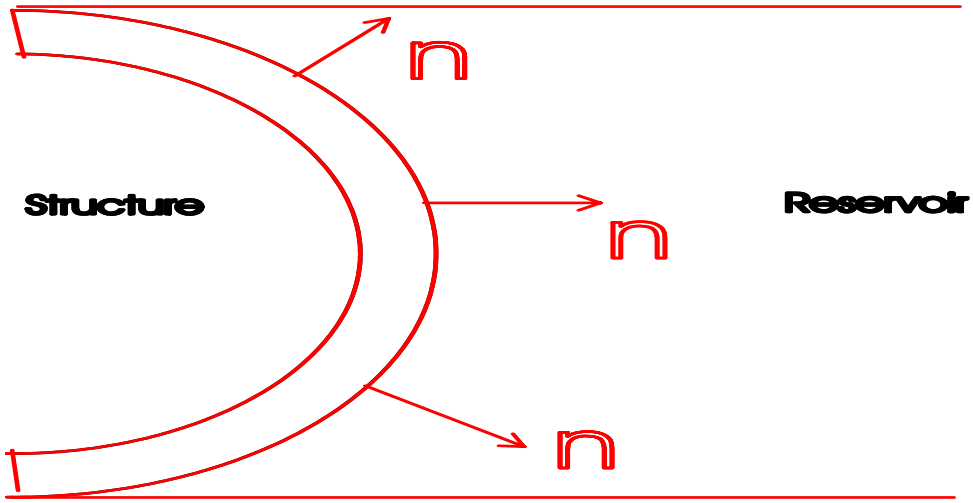

Figure 2.16: Dam-reservoir interface

2.9.2 Reservoir-Foundation Boundary Condition

If there is no absorption or penetration of water into the reservoir bottom, the same dam-reservoir boundary condition that was obtained previously, can be

used for reservoir-foundation boundary. In case of reservoir with sediment at the bottom, we can account it in a very simplified manner.

The boundary condition at the reservoir bottom relates the hydrodynamic pressure to the sum of the normal acceleration and acceleration due to interaction between impounded water and the reservoir bottom material. Here, we consider only interaction in the normal direction due to the assumption that the hydrodynamic pressure waves incident on the reservoir bottom only excite vertically propagating dilatational waves in the reservoir bottom materials. The hydrodynamic pressure $p(n,t)$ in the water is governed by the one-dimensional wave equation:

$$\frac{\partial^2 p}{\partial n^2} = \frac{1}{C^2}\frac{\partial^2 p}{\partial t^2} \qquad n \geq 0 \tag{2.29}$$

Similarly, the interaction displacement $\varkappa(n,t)$ in the layer of reservoir bottom materials is governed by:

$$\frac{\partial^2 \varkappa}{\partial n^2} = \frac{1}{C_r^2}\frac{\partial^2 \varkappa}{\partial t^2} \qquad n \leq 0 \tag{2.30}$$

Where $C_r = \sqrt{\frac{E_r}{\rho_r}}$, E_r is the Young's modulus of elasticity and $\rho_r$is the density of the reservoir bottom materials. At the reservoir bottom, the accelerative boundary condition states that the normal pressure gradient is proportional to the total acceleration:

$$\frac{\partial p(0,t)}{\partial n} = -\rho\left[a_n(t) + \ddot{\varkappa}\,(0,t)\right] \tag{2.31}$$

Where $\ddot{\varkappa}\,(0,t)$ is the acceleration of the reservoir bottom due to interaction between the impounded water and the reservoir bottom materials. Equilibrium at the surface of the reservoir bottom materials requires that:

$$p(0,t) = -E_r\frac{\partial \varkappa}{\partial y}(0,t) \tag{2.32}$$

the D'alembert solution to equation 2.30 is $\varkappa = g_r(n + C_r t)$ where g_r is the wavefront of the refracted wave propagating vertically downward in the reservoir bottom materials. An upward propagating wave does not exist because of the radiation condition for the assumed infinitely thick layer of reservoir bottom materials. Note that $\frac{\partial \varkappa}{\partial t}(0,t) = C_r\ g_r^{'}(C_r t)$ and $\ddot{\varkappa}\,(0,t) =$

$C_r^2 g_r''(C_r t)$, where the prime indicates the derivative of g_r with respect to argument $(n + C_r t)$. Differentiating equation 2.32 with respect to t gives:

$$\frac{\partial p(0,t)}{\partial t} = E_r C_r g_r''(C_r t)$$

or:

$$\frac{\partial p(0,t)}{\partial t} = -\frac{E_r}{C_r}\, \ddot{\varkappa}\,(0,t) \tag{2.33}$$

The solution for $\ddot{\varkappa}\,(0,t)$ from equation 2.33, when substituted into equation 2.31 with the identity $\frac{C_r}{E_r} = \frac{1}{\rho_r C_r}$, gives:

$$\frac{\partial p(0,t)}{\partial n} - q\frac{\partial p(0,t)}{\partial t} = -\rho a_n(t) \tag{2.34}$$

Where $q = \frac{\rho}{\rho_r C_r}$. For rigid reservoir bottom materials, $C_r = \infty$ and $q = 0$, so the second term on the right hand side of the above equation is zero giving the boundary condition for a rigid reservoir bottom. The fundamental parameter that characterizes the effects of absorption of hydrodynamic pressure waves at the reservoir bottom is the admittance or damping coefficient q. The wave reflection coefficient κ, which is the ratio of the amplitude of the reflected hydrodynamic pressure wave to the amplitude of a vertically propagating pressure wave incident on the reservoir bottom can be related to the damping coefficient.

The wave reflection coefficient κ can be obtained by considering the reflection of a harmonic pressure wave in the impounded water impinging vertically on the reservoir bottom. The downward vertically propagating incident wave of unit amplitude is $p_i = \exp\left[i\frac{\omega}{C}(n + Ct)\right]$, while the resulting upward propagating wave is $p_r = \kappa \exp\left[i\frac{\omega}{C}(-n + Ct)\right]$. Both p_i and p_r satisfy the wave equation (equation 2.29) The substitution of the sum $p_i + p_r$ of the two hydrodynamic pressure waves into the boundary condition at the reservoir bottom, equation 2.34, with no normal acceleration results in an equation which can be solved to results in:

$$\kappa = \frac{1 - qC}{1 + qC}$$

The wave reflection coefficient is independent of excitation frequency ω. In general, it depends on the angle of incident of the pressure wave at the reservoir bottom. The wave reflection coefficient may range within the limiting

values of 1 and -1. For rigid reservoir bottom $C_r = \infty$ and $q = 0$, resulting in $\kappa = 1$. For very soft material, C_r approaches zero and $q = \infty$, resulting in $\kappa = -1$. The material properties of the reservoir bottom medium are highly variable and depend upon many factors. It is believed the κ values from 1 to 0 would cover the wide range of materials encountered at the bottom of actual reservoirs.

2.9.3 Free Surface Boundary Condition

The geometry of free surface boundary is not known a priori. This shape is part of the solution, which means we have a very difficult boundary condition to cope with. In the case of surface wave of negligible surface tension, we call them gravity wave. The free surface of a wave can be described as:

$$F(x, y, z, t) = z - \varphi(x, y, z, t) = 0 \tag{2.35}$$

where φ is the displacement of the free surface above the horizontal plane,

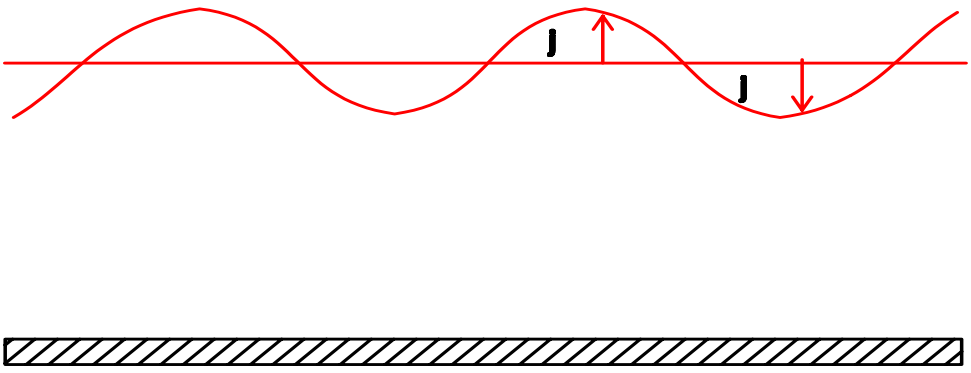

Figure 2.17: Free surface wave

say $z = 0$,. If the surface varies with time, as would the water surface, then the total derivative of the surface with respect to time would be zero on the surface. In other word, if we move with the surface, it does not changes.

$$\frac{DF(x, y, z, t)}{Dt} = 0 = \frac{\partial \varphi}{\partial t} + v_x \frac{\partial F}{\partial x} + v_y \frac{\partial F}{\partial y} + v_z \frac{\partial F}{\partial z} \qquad on\ F(x, y, z, t) = 0$$

Or:

$$-\frac{\partial F}{\partial t} = \mathbf{v}.\boldsymbol{\nabla} F = \mathbf{v}.\mathbf{n}\,|\boldsymbol{\nabla} F|$$

Where the unit vector normal to the surface has been introduced as $\mathbf{n} = \frac{\boldsymbol{\nabla} F}{|\boldsymbol{\nabla} F|}$. Rearranging the above equation, we get:

$$\mathbf{v}.\mathbf{n} = \frac{-\frac{\partial F}{\partial t}}{|\boldsymbol{\nabla} F|} \qquad on\ F(x,y,z,t) = 0$$

The boundary condition at the free surface using equation 2.35 is:

$$\mathbf{v}.\mathbf{n} = \frac{\frac{\partial F}{\partial t}}{\sqrt{\left(\frac{\partial \varphi}{\partial x}\right)^2 + \left(\frac{\partial \varphi}{\partial z}\right)^2 + 1}} \qquad on\ z = \varphi(x,t)$$

Where:

$$\mathbf{n} = \frac{-\frac{\partial \varphi}{\partial x}\mathbf{i} - \frac{\partial \varphi}{\partial y}\mathbf{j} + \mathbf{k}}{\sqrt{\left(\frac{\partial \varphi}{\partial x}\right)^2 + \left(\frac{\partial \varphi}{\partial z}\right)^2 + 1}}$$

Carrying out the dot product:

$$v_z = \frac{\partial \varphi}{\partial t} + v_x \frac{\partial \varphi}{\partial x} + v_z \frac{\partial \varphi}{\partial z} \qquad on\ z = \varphi(x,t)$$

Neglecting the convection terms and approximating pressure we get:

$$p = \rho g \varphi \qquad at\ z = 0 \tag{2.36}$$

$$v_z = \frac{\partial \varphi}{\partial t} \qquad at\ z = 0 \tag{2.37}$$

We also know:

$$\frac{\partial v_z}{\partial t} = -\frac{1}{\rho}\frac{\partial p}{\partial z} + g \tag{2.38}$$

Differentiating equation 2.36 with respect to t and cancelling φ with equation 2.37 gives:

$$\frac{1}{\rho g}\frac{\partial p}{\partial t} = v_z$$

A second differentiation with respect to t and elimination of v_z with equation 2.38 then substitution of $p_{total} = p + \rho g\varphi$, in which p represent the excess pressure due to motion and $\rho g\varphi$stands for hydrostatic pressure, we get:

$$\frac{1}{g}\frac{\partial^2 p}{\partial t^2} + \frac{\partial p}{\partial z} = 0 \qquad\qquad at\ z = 0$$

This is an approximate to the surface boundary condition.

The above boundary condition is usually replaced with the boundary condition that:

$$p = 0 \qquad\qquad at\ z = 0$$

This assumption of no surface wave is common assumption in concrete dams and is valid. It was shown that the surface waves are negligible.

The more complicated free surface boundary condition can be established in which we can assume pressure distribution due to interaction of wind and surface. These cases are above the scope of the book and can be found in appropriate references of water wave mechanics.

2.10 SOLUTION OF THE RESERVOIR EQUATION

Westergard's classic work (1933) on the hydrodynamic water pressure on dams during the earthquake started a new area for the researcher in this field. Westergaard's solution to wave equation for rigid dams during earthquakes was obtained based on the assumptions of dam with rectangular reservoir subjected to horizontal earthquake. In the solution, the reservoir extended to infinity in the upstream direction and the effect of surface wave was neglected. The system was subjected to the horizontal ground acceleration which was perpendicular to the dam axis. The motion was assumed to be small amplitude motion and water was taken inviscid fluid.

The pressure equation for the system shown in figure 2.18 is found under the following boundary conditions:

$p = 0$ at $y = h$
$u_y = 0$ at $y = 0$
$\ddot{u}_x = ag\cos(\frac{2\pi t}{T})$ at $x = 0$
$p = 0$when $x \to \infty$

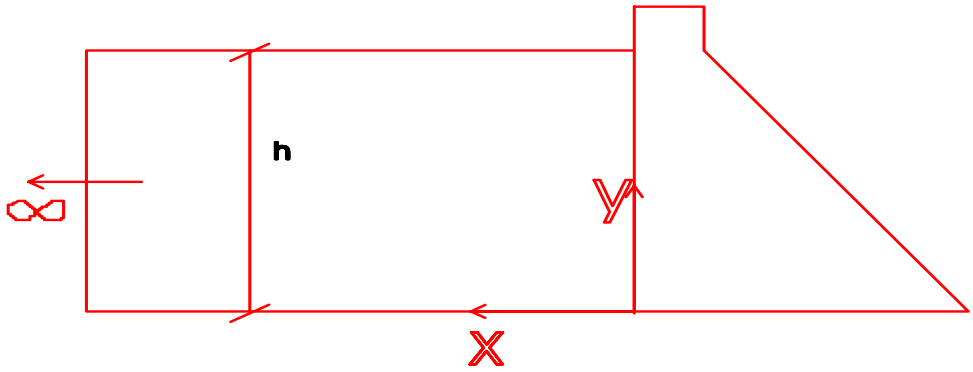

Figure 2.18: Rigid dam-infinite reservoir system

The hydrodynamic pressure for the above mentioned boundary conditions is as follows:

$$p(x,y,t) = \frac{8a\rho gh}{\pi^2}\cos(\frac{2\pi t}{T})\sum_{n=1,3,5,\ldots}^{\infty}\left(\frac{1}{n^2c_n}e^{-q_n}\sin(\frac{n\pi(h-y)}{2h})\right) \qquad (2.39)$$

in equation 2.39 q_n and $c_n$are defined as followings:

$$q_n = \frac{n\pi c_n x}{2h}$$

$$c_n = \sqrt{1-\frac{16\rho h^2}{n^2KT^2}} = \sqrt{1-\frac{16h^2}{n^2C^2T^2}}$$

The maximum pressure at $x = 0$ occurs when $t = 0, T, 2T, \ldots$ and can be written as:

$$p_{\max}(x,y,t) = \frac{8a\rho gh}{\pi^2}\sum_{n=1,3,5,\ldots}^{\infty}\left(\frac{1}{n^2c_n}\sin(\frac{n\pi(h-y)}{2h})\right) \qquad (2.40)$$

The maximum pressure at a given time on the upstream face ($x = 0$) happens at the bottom of the reservoir. The shape of the pressure diagram is such that the curve has a horizontal tangent at the top and a vertical tangent at the bottom.

In an approximation, the maximum pressure (equation 2.40) can be replaced by a parabolic curve. The maximum hydrodynamic pressure to be added to the hydrostatic pressure is as follows:

$$p_{\max}(0,y,t) = \frac{0.0255\ ton - ft^3\ a\sqrt{h(h-y)}}{\sqrt{1-0.72(\frac{h\ \sec}{1000T\ ft})}}$$

To further simplify the hydrodynamic pressure on the dam, one may consider the hydrodynamic pressure as a certain body of water moves with dam. This is called as added mass approach. This is possible because of the fact that the hydrodynamic pressure obtained (equation 2.39) has same phase compared to ground acceleration. Thus, we need to find the mass of water that attached to the dam and moves with it. For water with unit weight of $0.03125 ton - ft^3$ the width of water along the x-direction is as follows(figure 2.19):

$$b = \frac{7}{8}\sqrt{h(h-y)}$$

The mass of water that moves with the dam body can be transferred in to extra mass of concrete attached to the dam body. For a dam concrete with the unit mass of $144 lb.percu.ft$ the width of concrete would be:

$$b' = 0.38\sqrt{h(h-y)}$$

As it was already mentioned the Westergaard approach gives a pressure distribution which is in phase with ground acceleration. Also we imposed the boundary condition at far-end of the reservoir that as $x \to \infty$ then $p \to 0$. This boundary condition is an indication of energy dissipation at the far-end. The Westergaard solution is valid if the value of $c_n$is real. Another word, we can write:

$$1 - \frac{16h^2}{n^2C^2T^2} \geq 0$$

This will result in:

$$T > \frac{4h}{nc} \qquad\qquad n = 2m-1,\ m = 1,2,3,...$$

The term, $\frac{4h}{(2m-1)c}$ is the m^{th}period of the reservoir, T_m,. Therefore, the westergaard's solution is valid if the period of loading, T, is greater than the

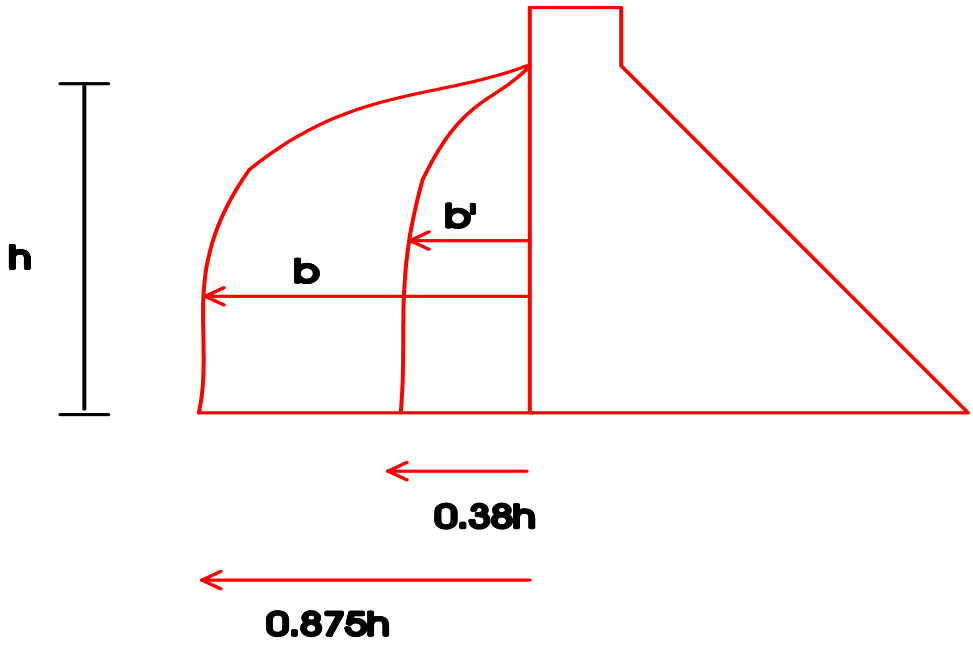

Figure 2.19: Added mass approach

first period of the reservoir, $T_1 = \frac{4h}{c}$,. If $T = T_m$, then $p = \infty$ and we have resonance.

The Westergaard pressure equation at the upstream face of the dam can be written as followings:

$$p(0, y, t) = \frac{4a\rho g}{\pi} \left[\cos \omega t \sum_{m=1}^{\infty} \frac{(-1)^{m-1}}{(2m-1)\sqrt{\lambda_m^2 - \frac{\omega^2}{C^2}}} \cos \lambda_m y \right]$$

in which ω_m and T_n are the circular frequency and period of the m^{th} mode of the reservoir and ω is the circular frequency of the earthquake.. They can be written as follows:

$$\lambda_m = \frac{\omega_m}{C} \qquad\qquad \omega = \frac{2\pi}{T}$$

$$\omega_m = \frac{2\pi}{T_m} = \frac{(2m-1)\pi C}{2h} \qquad\qquad m = 1, 2, 3, ...$$

Another solution to the wave equation presented by Chopra. Chopra (1967) presented a closed form solution for hydrodynamic pressure in the case of rigid dam with the vertical up-stream face under the horizontal and vertical ground motion. For the excitation frequency less than the fundamental frequency of the reservoir, both Westergaard and Chopra's solution are the same. The greater excitation frequency causes an out-of-phase pressure compared to Westergard's solution. In this case the hydrodynamic pressures cannot be represented by inertia effect on an added mass moving with the dam. Also it was found that the response to vertical ground motion is a real valued function and there is no decay with time so that the system is truly undamped in this case.

In his solution for the horizontal earthquake, the wave equation for a rigid dam with rectangular reservoir (figure 2.18)presented subjected to the following boundary conditions:

$p = 0$ at $y = h$
$\frac{\partial p}{\partial y} = 0$ at $y = 0$
$\frac{\partial p}{\partial x} = -\rho \ \ddot{u_g}$ at $x = 0$

The hydrodynamic pressure for a harmonic ground excitation of $\ddot{u}_g = e^{iwt}$ would be:

$$p(x,y,t) = \frac{4\rho}{\pi}\sum_{m=1}^{\infty}\frac{(-1)^{m-1}}{(2m-1)\sqrt{\lambda_m^2-\frac{\omega^2}{C^2}}}\exp\left(-x\sqrt{\lambda_m^2-\frac{\omega^2}{C^2}}\right)\cos\lambda_m y \;\; e^{iwt} \tag{2.41}$$

It can be seen that as $x \to \infty$ the pressure does not approach zero if $\lambda_m < \frac{\omega}{C}$ which was the fourth boundary condition imposed in Westergaard solution. To compare the above solution with Westergaard's solution, we can consider the real part of the ground motion as well as coefficient ag ($\ddot{u}_g = ag\cos(\frac{2\pi t}{T})$).The Solution in this case consist of the real part of the pressure solution (equation 2.41) and would be as:

$$p(0,y,t) =$$

$$\frac{4a\rho g}{\pi}\sin\omega t\sum_{m=1}^{m_1-1}\frac{(-1)^{m-1}}{(2m-1)\sqrt{\frac{\omega^2}{C^2}-\lambda_m^2}}\cos\lambda_m y +$$

$$\frac{4a\rho g}{\pi}\cos\omega t\sum_{m=m_1}^{\infty}\frac{(-1)^{m-1}}{(2m-1)\sqrt{\lambda_m^2-\frac{\omega^2}{C^2}}}\cos\lambda_m y$$

in which m_1 is the minimum value of m such that $\lambda_m > \frac{\omega}{C}$. If $m_1 = 1$ which is an indication of $\lambda_1 > \frac{\omega}{C}$ or $\omega < \omega_1$, then the term involving $\sin\omega t$ vanishes and the solution of the wave equation is same as Westergaard's solution. Here, again it can be noticed that the Westergaard's solution is valid if the frequency of the excitation is less than the fundamental frequency of the reservoir system. For $\omega > \omega_1$ the term involving $\sin\omega t$ does not vanish and represent existence of pressure at infinite distance up the reservoir. The pressure response has two terms one is in phase with ground motion and the other is in opposite phase of ground motion. Therefore, the hydrodynamic pressure cannot be represented by added mass approach.

For $m_1 > 1$ we have pressure at infinite distance. This means that for the case of $\omega_m < \omega < \omega_{m+1}$the pressure would be zero at $x = \infty$ for $\omega_{m+1}$and higher modes. While for ω_m and lower modes we expect to have pressure at very far-end of the reservoir.

The solution of wave equation subjected to the vertical ground motion for a rigid dam with rectangular reservoir is investigated. The reservoir have the following boundary conditions:

$\frac{\partial p}{\partial y} = -\rho\, \ddot{u_y}$ at $y = 0$

$\frac{1}{g}\frac{\partial^2 p}{\partial t^2} + \frac{\partial p}{\partial y} = 0$ at $y = h$

$\frac{\partial p}{\partial x} = 0$ at $x = 0$

The pressure solution when the reservoir is subjected to the vertical ground motion of $\ddot{u_y}$= $ag\cos(\omega t)$ would be as follows:

$$p(x,y,t) = \frac{ag\rho C}{\omega}\frac{\sin\frac{\omega}{C}(h-y) - \frac{g}{\omega C}\cos\frac{\omega}{C}(h-y)}{\cos\frac{\omega}{C}h + \frac{g}{\omega C}\sin\frac{\omega}{C}h}\cos(\omega t)$$

The solution is independent of the $x-$coordinate.

If we ignore the free surface wave and change the second boundary condition by:

$p = 0$ at $y = h$

then the solution would be:

$$p(x,y,t) = \frac{ag\rho C}{\omega}\frac{\sin\frac{\omega}{C}(h-y)}{\cos\frac{\omega}{C}h}\cos(\omega t) \tag{2.42}$$

The difference between the two solutions depends on the magnitude of the quantity $\frac{g}{\omega C}$. Analysis of strong ground motions of the past earthquakes seems to indicate that frequencies of most of the significant harmonic components lie in the range $1 < \omega < 120\ rad/sec$. Thus, the largest value of $\frac{g}{\omega C}$ may be taken as $6.82 \times 10^{-3}(\omega = 1,\ C = 4720 fps)$. However, such low frequency harmonics contribute little to the response in the case of typical reservoir depths encountered, because natural frequencies for the reservoir are rather high: e.g. for a 300 ft deep reservoir $\omega_1 = 24.72$ radians per sec. The magnitude of $\frac{g}{\omega C}$ for harmonics of significance is therefore considerably less than 6.82×10^{-3}, and errors introduced by dropping terms involving $\frac{g}{\omega C}$ will be small, except possibly near the free surface. Therefore, equation2.42 is sufficiently accurate.

Most investigator have ignored the waves that may be generated at the free surface of water. For compressible fluid, and harmonic excitation it was found that the error ,e , introduced by ignoring surface wave, varies as follows:

$$e < 0.05 \qquad if \qquad \frac{h}{T} > 4.2\sqrt{h}$$

$$0.05 < e < 0.20 \qquad if \qquad 2.6\sqrt{h} < \frac{h}{T} < 4.2\sqrt{h}$$

$$e < 0.20 \qquad if \qquad \frac{h}{T} < 2.6\sqrt{h}$$

Most of significant harmonic in typical strong ground motion have a period below 3 sec. Thus for $T = 3$ sec, the error $e < 0.05$ if $h > 158.5m$. For a reservoir depth 100 ft, $e < 0.05$ if $T < 1.32\,\text{sec}$. Because the natural periods of the system are very small (first natural period for 100 ft depth of water is 0.085 sec), the contributions to the total response from harmonic components of ground motion with the periods longer than 1.32 sec will be small. This is particularly so because we are dealing with an fluid. Hence, it may be concluded that errors introduced by neglecting surface wave is on the order of 0.05. Similar conclusions can be derived for other depth between 100 ft and 520 ft. On this basis, it seems that the effect of surface waves can be ignored with little loss of accuracy.

2.11 RESERVOIR FAR-END TRUNCATED BOUNDARY CONDITION

The truncated boundary for the finite element and boundary element modeling of the infinite reservoir was worked by so many researchers. Sommerfeld boundary condition is the most common one that is based on the assumption that at long distance from the dam face, water wave can be considered as plane wave. A plane wave can be represented by an equation of the form:

$$p = F(x - Ct)$$

This equation leads to the following condition:

$$\frac{\partial p}{\partial x} = \frac{\partial p}{\partial n} = -\frac{1}{C}\frac{\partial p}{\partial t} \tag{2.43}$$

in which n is the normal at the truncation boundary. This represents well-known Sommerfeld radiation condition. It introduces a damping in the system and models the loss of energy in the outgoing waves. Under this condition

for the far end reservoir, the classical solution for the hydrodynamic pressure was obtained in which there are in-phase and out-of-phase pressures. As a rule for the truncated boundary there is no reflection for the outgoing wave and all of our effort is in modeling the energy loss in outgoing wave such that all energy can be absorbed on the truncated boundaries. The solution to the wave equation can be investigated for a rigid dam with rectangular reservoir subjected to horizontal ground motion and the following boundary conditions:

$p = 0$ at $y = h$
$\frac{\partial p}{\partial y} = 0$ at $y = 0$
$\frac{\partial p}{\partial x} = -\rho\ \ddot{u}$ at $x = 0$
$\frac{\partial p}{\partial x} = \frac{\partial p}{\partial n} = -\frac{1}{C}\frac{\partial p}{\partial t}$ at $x = L$

The hydrodynamic pressure for a harmonic ground excitation of $\ddot{u}_g = e^{iwt}$ would be:

$$p(x,y,t) = \frac{4\rho}{\pi}\sum_{m=1}^{\infty}\frac{(-1)^{m-1}}{(2m-1)q_m}\frac{e^{q_m(L-x)} + Z_m e^{-q_m(L-x)}}{e^{q_m L} - Z_m e^{-q_m L}}\cos\lambda_m y \quad e^{iwt} \tag{2.44}$$

Where:

$$q_m = \sqrt{\lambda_m^2 - \frac{\omega^2}{C^2}}\ , Z_m = \frac{q_m - i\frac{\omega}{C}}{q_m + i\frac{\omega}{C}}\ , i = \sqrt{-1} \tag{2.45}$$

It was found that the Sommerfeld radiation damping condition does not yield good approximation for the infinite reservoir for excitation frequencies between the first and second natural frequencies of the reservoir. Within this range of frequencies an increase in the length of reservoir does not lead to any increase in the accuracy(Humar and Roufaiel, 1983).

Humar and Roufaiel (1983) used a radiation condition which adequately models the loss over a wide range of excitation frequencies, also it was shown that the conditions give much better results as compared to the plane wave Sommerfeld condition. Their radiation condition derived only for the horizontal ground motion in the case of dam with vertical up-stream face. The Solution of the equation 2.41 when $\ddot{u}_g = e^{i\omega t}$ can be represented as following:

$$p(x,y,t) = \left[\sum_{m=m_1}^{m_1-1}\frac{A_m}{q_n}e^{-q_n x}\cos\lambda_m y + \sum_{m=m_1}^{\infty}\frac{A_m}{\sqrt{\lambda_m^2 - \frac{\omega^2}{C^2}}}\cos\lambda_m y\right] e^{i\omega t}$$

It was already shown that at large distance from the dam, the second term in the equation vanishes, and the pressure is given as:

$$p(x,y,t) = \sum_{m=1}^{m_1-1} A_m e^{-\left(\sqrt{\lambda_m^2 - \frac{\omega^2}{C^2}}\right)x} \cos\lambda_m y \; e^{i\omega t} = \sum_{m=1}^{m_1-1} p_m \tag{2.46}$$

From the above equation we can write:

$$p\frac{\partial p}{\partial x} = -\frac{1}{\omega}\sum_{m=1}^{m_1-1}\left(\sqrt{\frac{\omega^2}{C^2} - \lambda_m^2}\right) p_m \frac{\partial p}{\partial t} \tag{2.47}$$

For the case of $m = 2$ (when ω lies between $\omega_1$and ω_2) equation 2.46 gives $p = p_1$ and equation 2.47 becomes:

$$\frac{\partial p}{\partial x} = -\frac{1}{C}\left(\sqrt{1 - \left(\frac{\omega_1}{\omega}\right)^2}\right)\frac{\partial p}{\partial t}$$

Therefore, it can be said that the following condition should be applied at the truncated boundary:

$$\frac{\partial p}{\partial n} = 0 \qquad\qquad \omega < \omega_1 \tag{2.48}$$

$$\frac{\partial p}{\partial n} = -\frac{1}{C}\left(\sqrt{1 - \left(\frac{\omega_1}{\omega}\right)^2}\right)\frac{\partial p}{\partial t} \qquad\qquad \omega > \omega_1 \tag{2.49}$$

Apparently, the preceding condition is not exact when ω is greater than ω_2. For large value of ω equation 2.49 reduces to equation 2.43.

The hydrodynamic pressure obtained by applying the modified boundary condition at $x = L$ represented by equations 2.48 and 2.49 will be given by an expression similar to equation 2.44, except that $Z_m$will now be as follows:

$$Z_m = 1 \qquad\qquad \omega < \omega_1$$

$$Z_m = \frac{q_m - i\frac{\omega}{C}\sqrt{1 - \left(\frac{\omega_1}{\omega}\right)^2}}{q_m + i\frac{\omega}{C}\sqrt{1 - \left(\frac{\omega_1}{\omega}\right)^2}} \qquad\qquad \omega > \omega_1$$

The modified boundary condition at the far end was obtained with ignoring the second term in the pressure equation at the large distance from the dam. It was found that the modified radiation boundary condition gives much better results as compared to the Sommerfeld one for excitation frequencies between 0.0 and 2.

Sharan (1984) showed that the condition of $\frac{\partial p}{\partial n} = 0$ for incompressible fluid at the far end is the form of that for a rigid stationary boundary and the behavior of the fluid motion at the truncated boundary is not truly presented. A large extent of the fluid domain is required to be included in the analysis. The above condition is same as Sommerfeld condition for the incompressible fluid ($C = \infty$). Under the assumption of incompressible fluid in the rectangular reservoir and rigid dam, the governing equation of the pressure would be the Laplace equation. Knowing the pressure equation, he found that at large distance from upstream face condition would be:

$$\frac{\partial p}{\partial n} = -\frac{\pi}{2h}p$$

It can be observed that at very large distance away from the dam face $p = 0.0$ therefore $\frac{\partial p}{\partial n} = 0$ which is same condition at the infinity for the infinite reservoir. He found that under the assumption of the rigid dam and rigid rectangular reservoir bottom, for the horizontal vibration. the truncated boundary can be located very close to the structure. It was found that although the proposed boundary condition was derived for the dam with the vertical upstream face, the results for an inclined face are relatively more accurate than those for a vertical face.

Sharan (1985) used the radiation condition for the submerged structure surrounded by unbounded extent of compressible fluid as following:

$$\frac{\partial p}{\partial n} = -\Psi p$$

Deferent geometry of the solid-fluid interface was used to find the accuracy of the proposed radiation boundary condition.

Sharan (1987) proposed a damper radiation boundary condition for the time domain analysis of the compressible fluid with small amplitude. The structure submerged in unbounded fluid in the upstream direction. The proposed radiation condition was:

$$\frac{\partial p}{\partial n} = -\frac{\pi}{2h}p - \frac{1}{C}\frac{\partial p}{\partial t}$$

The above boundary condition was found to be very effective and efficient for a wide range of the excitation frequency. For the finite value of c and h, the effectiveness of the proposed damper depends on the period of excitation T, $(\frac{2\pi}{\omega})$. If the value of T be near the natural period of vibration of the fluid domain $(\frac{TC}{h} \rightarrow 4)$, the magnitude of $p$and $\frac{\partial p}{\partial t}$ become infinitely large. In this case approximated boundary condition for the truncated surface may be written as $\frac{\partial p}{\partial n} = 0$. Therefore for such a case, neither Sommerfeld damper nor the proposed one would be effective. In the case of $\frac{TC}{h} \ll 4$, the magnitude of , $\frac{pC}{h}$, becomes small compared to that of $\frac{\partial p}{\partial t}$. For the limiting case $p \rightarrow 0$ when $T \rightarrow 0$. On the other hand, for $\frac{TC}{h} \gg 4$, $\frac{\partial p}{\partial t}$ is much less than that of $\frac{pC}{h}$. For the limiting case $\frac{\partial p}{\partial t} \rightarrow 0$ when $T \rightarrow \infty$. Thus in both case, one of the terms on the right hand side of proposed equation of damping would be small compare to the other. As a general, it was found that proposed boundary condition at the truncated surface is more efficient and needs less computational time. In the case of $\frac{TC}{h} = 1$ (high excitation frequency) both methods shows discrepancy with the case of $L = \infty$. It is not an important problem because in high frequency excitation the hydrodynamic forces are not comparable so that its error in hydrodynamic pressure is not significant.

Sharan (1985) expressed the condition at the truncated face as:

$$\frac{\partial p}{\partial x} = -\frac{\alpha}{C}\frac{\partial p}{\partial t} + \frac{\beta\omega}{C}p$$

For $(\Omega = \frac{\omega h}{C})$ less than $\frac{3\pi}{2}$ which is for excitation frequency less than the second natural frequency of the reservoir if $\frac{x}{h}$ is sufficiently large, then $\alpha = 0$ and $\beta = -\sqrt{(\frac{\pi}{2\Omega})^2 - 1}$ and for $\frac{\pi}{2} < \Omega < \frac{3\pi}{2}$, $\beta = 0$ and $\alpha = \sqrt{1 - (\frac{\pi}{2\Omega})^2}$. For $\Omega < \frac{\pi}{2}$, $\frac{\partial p}{\partial n}$ is function of p instead of $\frac{\partial p}{\partial t}$, therefore Sommerfeld radiation boundary condition is not justified for $\Omega < \frac{\pi}{2}$. For these range of frequencies values of p,$\frac{\partial p}{\partial t}$,and $\frac{\partial p}{\partial x}$ approach zeroes as the ratio $\frac{x}{h}$ is increases. This explains why satisfactory results may be obtained even with use of improper boundary condition such as $\frac{\partial p}{\partial n} = 0$ and $\frac{\partial p}{\partial n} = -\frac{1}{C}\frac{\partial p}{\partial t}$ by considering a very large extent of the reservoir. For $\Omega > \frac{3\pi}{2}$ even for large value of $\frac{x}{h}$, the parameters α and β are sensitive to x and y coordinate point on the truncated surface.

Chapter 3

FINITE ELEMENT MODELLING OF THE DAM-RESERVOIR SYSTEM

The first step in dynamic analysis of a system is to properly model the actual system. In mathematical modelling, we need to formulate the equation of the motion. Having formulated the equation of the motion, we then procced to solve the equation of the motion. In previous Chapter, reservoir's equation of the motion was formulated. Here we will find the structure's equation of the motion and its finite element equation in addition to reservoir finite element equation.

3.1 FINITE ELEMENT MODELLING OF THE STRUCTURE

3.1.1 Single-Degree-Of-Freedom Systems

A single-degree-of-freedom system (SDF) is defined as a system whose motion can defined by a single parameter. Systems shown in figure 3.1 are systems of SDF. As shown in the figure only one parameter (u, x or θ) is required to define the position of the particle at each second.

For a system shown in $3.1-a$, if we try to apply a dynamic force $f(t)$, the equation of the motion can be written as:

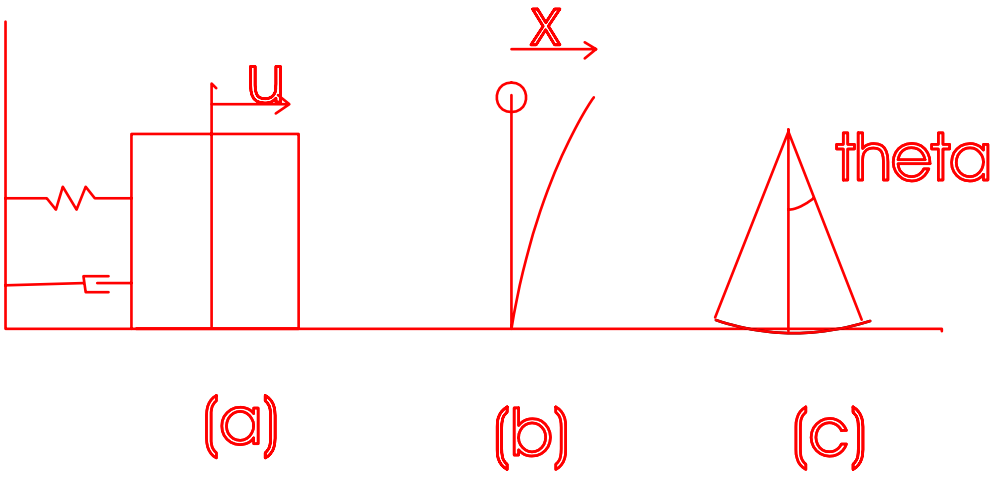

Figure 3.1: Systems of single degree of freedom

$$f(t) = F_I + F_D + F_S$$

in which F_I, F_D and F_S are inertial, damping and spring (stiffness) forces, respectively. The inertial force is equivalent to the total acceleration of the mass M and can be written as $M\ \ddot{u}$ when there is no base motion. If there is a base motion, the inertial force can be written as $M(\ddot{u} + \ddot{u}_g)$. As is shown in figure3.2 $\ddot{u}$ is the acceleration of the mass M relative to the base and $\ddot{u}_g$is the ground acceleration.The spring force can be written as Ku, which is a linear spring or linear stiffness. Other form of spring may be proposed which result in nonlinear equation. The damping force is viscous damping force and is given by $F_D = C\ \dot{u}$ which C is the damping coefficient. This is a valid assumption when velocity is small. For high velocity, damping force is proportional to the square of the velocity. Thus the equation of the motion for a SDF system can be written as:

$$M(\ddot{u} + \ddot{u}_g) + C\ \dot{u} + Ku = f(t)$$

This is a differential equation of second order. The equation can be rewritten into the following form:

$$M\ \ddot{u} + C\ \dot{u} + Ku = f(t) - M\ \ddot{u}_g$$

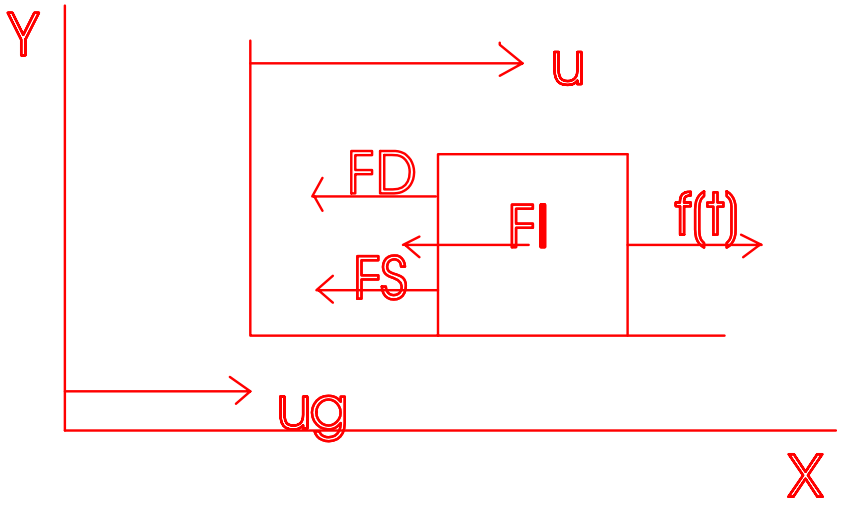

Figure 3.2: Forces on a single degree of freedom

It can be seen that the base acceleration is equivallent of a force acting on the mass in the opposite direction of its motion. In the other word, the base motion can be interpreted as a force acting on the mass in opposite direction of its motion.

3.1.2 Multi-Degree-Of-Freedom System

In a multi-degree-of-freedom (MDF) sytem, it is required to know the values of the displacement in more than one point in order to define its motion at any instant of time. Consider a system with n degrees of freedom which accelerate in the y direction as shown in figure 3.3.

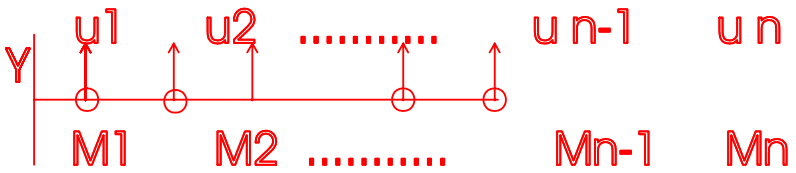

Figure 3.3: An example of multi-degree-of-freedom (MDF) sytem with degrees of freedom in y direction

The inertial forces can be written as:

$$F_I = \left\{ \begin{array}{c} F_{I1} \\ F_{I2} \\ . \\ . \\ F_{I(n-1)} \\ F_{In} \end{array} \right\} = \left[\begin{array}{l} M_1 \ldots\ldots\ldots\ldots\ldots\ldots \\ \ldots . M_2 \ldots\ldots\ldots\ldots\ldots \\ \ldots\ldots\ldots\ldots\ldots\ldots\ldots \\ \ldots\ldots\ldots\ldots\ldots\ldots\ldots \\ \ldots\ldots\ldots\ldots\ldots M_{I(n-1)..} \\ \ldots\ldots\ldots\ldots\ldots\ldots M_{In} \end{array} \right] \left\{ \begin{array}{c} \ddot{u}_1 \\ \ddot{u}_2 \\ . \\ . \\ \ddot{u}_{n-1} \\ \ddot{u}_n \end{array} \right\}_g$$

or it can be write as:

$$F_I = [M]\{\ddot{U}\}^t$$

The mass matrix $[M]$ is a diagonal matrix and in general it can be a non-diagonal symmetric matrix.

The forces due to elasticity can be written as:

$$F_S = \left\{ \begin{array}{c} F_{S1} \\ F_{S2} \\ . \\ . \\ . \\ F_{Sn} \end{array} \right\} = \left[\begin{array}{l} K_{11} K_{12} \ldots\ldots\ldots\ldots\ldots K_{1n} \\ K_{21} K_{21} \ldots\ldots\ldots\ldots\ldots K_{2n} \\ \ldots\ldots\ldots\ldots\ldots\ldots\ldots\ldots \\ \ldots\ldots\ldots\ldots\ldots\ldots\ldots\ldots \\ \ldots\ldots\ldots\ldots\ldots\ldots\ldots\ldots \\ K_{n1} K_{n2} \ldots\ldots\ldots\ldots\ldots K_{nn} \end{array} \right] \left\{ \begin{array}{c} u_1 \\ u_2 \\ . \\ . \\ . \\ u_n \end{array} \right\}$$

or it can be written as:

$$F_S = [K]\{U\}$$

where $[K]$ is the stiffness matrix. A detailed description of the stiffness matrix can be found in finite element books.

The damping matrix can be written as :

$$F_D = \left\{ \begin{array}{c} F_{D1} \\ F_{D2} \\ . \\ . \\ . \\ F_{Dn} \end{array} \right\} = \left[\begin{array}{l} C_{11} C_{12} \ldots\ldots\ldots\ldots\ldots C_{1n} \\ C_{21} C_{21} \ldots\ldots\ldots\ldots\ldots C_{2n} \\ \ldots\ldots\ldots\ldots\ldots\ldots\ldots\ldots \\ \ldots\ldots\ldots\ldots\ldots\ldots\ldots\ldots \\ \ldots\ldots\ldots\ldots\ldots\ldots\ldots\ldots \\ C_{n1} C_{n2} \ldots\ldots\ldots\ldots\ldots C_{nn} \end{array} \right] \left\{ \begin{array}{c} \dot{u}_1 \\ \dot{u}_2 \\ . \\ . \\ . \\ \dot{u}_n \end{array} \right\}$$

or it can be written as:

$$F_D = [C]\{\dot{U}\}$$

where $[C]$ is the damping matrix.

Equating of the external forces and internal forces will results in:

$$[M]\{\ddot{U}_t\} + [C]\{\dot{U}\} + [K]\{U\} = \{f(t)\}$$

which $\{f(t)\}$ is the external forces act on the structures and can be written as:

$$\{f(t)\} = \begin{Bmatrix} f_1(t) \\ f_2(t) \\ . \\ . \\ . \\ f_n(t) \end{Bmatrix}$$

If there is a base displacement like ground acceleration along y direction as shown in figure 3.3, the equation of motion for a multi-degree-of-freedom system can be written as:

$$[M]\{\ddot{U}_t\} + [C]\{\dot{U}\} + [K]\{U\} = \{f(t)\}$$

in which $\{\ddot{U}_t\} = \{\ddot{U_{gy}}\} + \{\ddot{U}\}$. The vector of ground acceleration can be written as:

$$\{\ddot{U_g}\} = \begin{Bmatrix} \ddot{u}_{gy} \\ \ddot{u}_{gy} \\ . \\ . \\ \ddot{u}_{gy} \\ \ddot{u}_{gy} \end{Bmatrix} = \ddot{u}_{gy} \begin{Bmatrix} 1 \\ 1 \\ . \\ . \\ 1 \\ 1 \end{Bmatrix} = \ddot{u}_{gy}\ \{I\}$$

Where $\ddot{u}_{gy}$is the ground acceleration at the base along y direction. Thus, the equation of motion can be written as:

$$[M]\{\ddot{U}\} + [C]\{\dot{U}\} + [K]\{U\} = \{f(t)\} - [M]\{\ddot{U}_{gy}\}$$

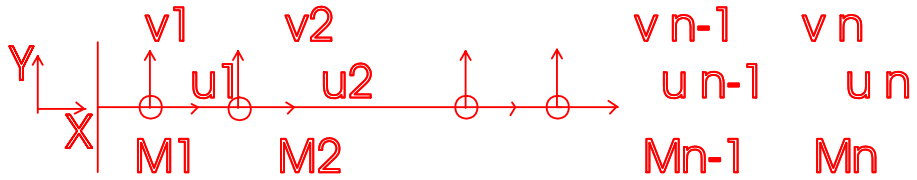

Figure 3.4: An example of MDF system with two degrees of freedom at each mass

For a system of MDF system when subjected to ground acceleration in two directions and there are two degree of freedoms for each mass,as shown in figure 3.4,we can write the equation of motion based on the both degrees of freedom at each mass.For this system, we can write the displacement vector as:

$$\{U\} = \begin{Bmatrix} u_1 \\ v_1 \\ u_2 \\ v_2 \\ . \\ . \\ . \\ u_n \\ v_n \end{Bmatrix}$$

The same can be written for $\{\dot{U}\}$ and $\{\ddot{U}\}$. The equation of motion can be written as following:

$$[M]\{\ddot{U}\} + [C]\{\dot{U}\} + [K]\{U\} = \{f(t)\} - [M]\{\ddot{U}_g\}$$

In which $\{\ddot{U}_g\}$ can be written as:

$$\{\ddot{U}_g\} = \ddot{u}_{gx} \begin{Bmatrix} 1 \\ 0 \\ 1 \\ 0 \\ . \\ . \\ 1 \\ 0 \\ 1 \\ 0 \end{Bmatrix} + \ddot{u}_{gy} \begin{Bmatrix} 0 \\ 1 \\ 0 \\ 1 \\ . \\ . \\ 0 \\ 1 \\ 0 \\ 1 \end{Bmatrix}$$

When $\ddot{u}_{gx}$and $\ddot{u}_{gy}$are the ground acceleration along the x and y direction, respectively. In the above equation of motion $\{f(t)\}$ can be written as:

$$\{f(t)\} = \begin{Bmatrix} f_{1x}(t) \\ f_{1y}(t) \\ f_{2x}(t) \\ f_{2y}(t) \\ . \\ . \\ . \\ f_{nx}(t) \\ f_{ny}(t) \end{Bmatrix}$$

Which $f_{ix}(t)$ and $f_{iy}(t)$ are the forces acting on the ith mass along x and y direction, respectively. In the case of concrete dams, $\{f(t)\}$ can be seperated into hydrodynamic pressure $\{f\}$ and resultant of all the other forces, $\{f_1\}$, that act on the structure. Thus, the final form of the equation of the motion can be written as:

$$[M]\{\ddot{U}\} + [C]\{\dot{U}\} + [K]\{U\} = \{f\} + \{f_1\} - [M]\{\ddot{U}_g\}$$

In a MDF sytem, a system is discretized into its degrees of freedom. The number of degrees of freedom depend on the number of elements and the degree of freedom for each element. Usually in the case of concrete gravity dams isoparametric plane stress or plane strain are used. These types of elements are used for two dimensional problems. In some cases triangular

elements may be used. In both plane stress or plane strain the displacement field is given by the u and v in directions of cartisian x and y axis. In the case of concrete gravity dam, assumption of 2-D analysis is a valid assumption.

In 3-D analysis the simplest case is the case of tetrahedron element. Based on the nature of the problem each node may have 3 different components u, v and w in the direction of X, Y and Z. For more complex type of element we may add rotational degrees of freedom in to each node. Three dimensional analysis of concrete gravity dams requires a large number of DOF.

3.2 COUPLING MATRIX OF THE DAM-RESERVOIR

The coupling matrix relates the pressure of the reservoir and the forces on the dam-reservoir interface as following:

$$[Q]\{p\} = \{f\}$$

where $\{f\}$ is the force vector acting on the structure due to the hydrodynamic pressure.

Figure **??** shows a line element on the interaction boundary of the dam-reservoir. The work done by the hydrodynamic pressure on the interaction surface of the structure must be equal to the work of the equivalent nodal forces on the interface boundary of an element. Thus, for unit thickness elements as shown in figure **??**, the following expression can be written:

$$\int_{s_e} pU_n ds = \{f\}^{e^T}\{\delta\} = \left\{ \begin{array}{cccc} fx_1 & fy_1 & fx_2 & fy_2 \end{array} \right\} \left\{ \begin{array}{c} u_1 \\ v_1 \\ u_2 \\ v_2 \end{array} \right\} \tag{3.1}$$

where p and U_n are the values of the hydrodynamic pressure and normal displacement along the element interface, respectively. $\{\delta\}$ and $\{f\}^e$ are the displacement and force vector of an interface element. u_i and v_i (fx_i and fy_i) are the displacements (forces) at node i of the interface element along the global X and Y coordinates, respectively. The integration is performed along each element on the dam-reservoir interface. The superscript and subscript 'e' refer to the element on the dam-reservoir interface. Writing u and v,

displacements along the global X and Y coordinates of the interface element, in terms of structure shape functions, then:

$$u = u_1 N_1 + u_2 N_2 \qquad v = v_1 N_1 + v_2 N_2$$

where $N_i$is the structure shape function at node$i$ of the interface element. For the normal displacement along the element surface, U_n, we have:

$$U_n = u_n + v_n = \eta u_1 N_1 + \eta u_2 N_2 + \beta v_1 N_1 + \beta v_2 N_2 \tag{3.2}$$

In equation 3.2, $\eta$and $\beta$are the absolute values of the normal vector on the boundary in the global directions of X and Y, respectively. Equation 3.2 can be written in the following form:

$$U_n = \left\{ \begin{array}{cccc} \eta N_1 & \beta N_1 & \eta N_2 & \beta N_2 \end{array} \right\} \{\delta\} = \{N_n^s\}^T \{\delta\} \tag{3.3}$$

The hydrodynamic pressure can be expressed as shape function of the fluid in the form:

$$p = \{N^f\}^T \{p\}^e = \left\{ \begin{array}{cc} N_1^f & N_2^f \end{array} \right\} \{p\}^e \tag{3.4}$$

where N_i^f is the fluid shape function at node $i$of the interface element. Combining equations 3.1, 3.3 and 3.4, there is obtained:

$$\{f\}^e = \int_{s_e} \{N_n^s\}\{N^f\}^T ds \ \{p\}^e = [Q]^e \{p\}^e \tag{3.5}$$

where $[Q]^e$ and $\{p\}^e$ are the coupling matrix and hydrodynamic pressure vector of an element on the dam-reservoir interface. The total coupling matrix$[Q]$ is obtained by assembling all element coupling matrices. From equation 3.5, $[Q]^e$ is written as:

$$[Q]^e = \int_{s_e} \{N_n^s\}\{N^f\}^T ds$$

For an interface element as shown in figure 3.5, then:

$$[Q]^e = \int_{s_e} \left[\begin{array}{cc} \eta N_1 N_1^f & \eta N_1 N_2^f \\ \beta N_1 N_1^f & \beta N_1 N_2^f \\ \eta N_2 N_1^f & \eta N_2 N_2^f \\ \beta N_2 N_1^f & \beta N_2 N_2^f \end{array} \right]$$

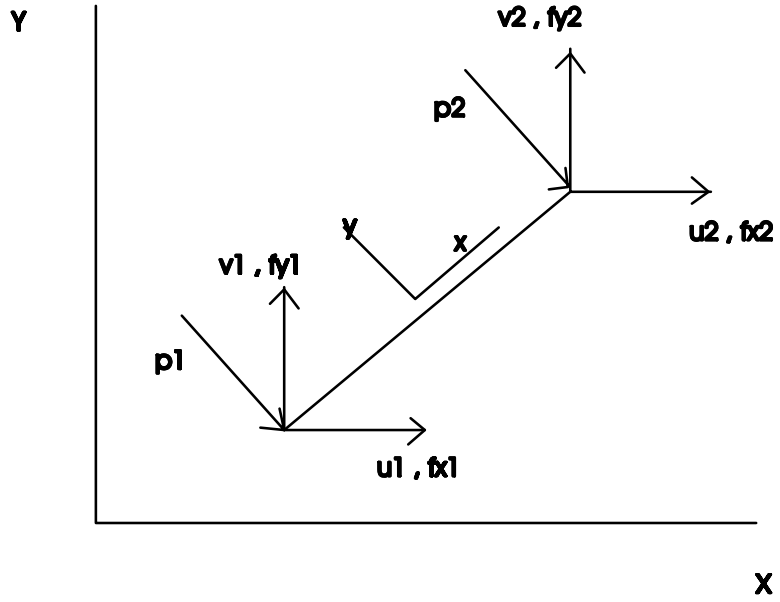

Figure 3.5: Interface element on the dam-reservoir interaction boundary

3.3 FINITE ELEMENT MODELLING OF THE RESERVOIR

As it was discussed in previous Chapter, the hydrodynamic pressure distribution in the reservoir is governed by the pressure wave equation. Assuming that water is linearly compressible and neglecting its viscosity, the small amplitude irrotational motion of water is governed by the two-dimensional wave equation:

$$\nabla^2 p(x,y,t) = \frac{1}{C^2}\,\ddot{p}\,(x,y,t) \tag{3.6}$$

where $p(x,y,t)$ is the hydrodynamic pressure in excess of hydrostatic pressure, C is the velocity of pressure wave in water and$x$and y are the coordinate axes.

The hydrodynamic pressure in the impounded water governed by equation 3.6, is due to the horizontal and the vertical accelerations of the upstream face of the dam, the reservoir bottom as well as the far end of the reservoir in the case of finite reservoir length. The motion of these boundaries is related

to the hydrodynamic pressure by the boundary conditions.

For earthquake excitation, the condition at the boundaries of the dam-reservoir, reservoir-foundation and the reservoir-far-end are governed by the equation:

$$\frac{\partial p(x,y,t)}{\partial n} = -\rho a_n(x,y,t)$$

whereρ is density of water and $a_n(x,y,t)$ is the component of acceleration on the boundary along the direction of the inward normal n. No wave absorption is considered at the boundaries of the reservoir.

Neglecting the free surface wave, the boundary condition at the free surface is written as:

$$p(x,y,t) = 0$$

where$h$ is the height of the reservoir.

Using finite element discretization of the fluid domain and the discretized formulation of equation 3.6, the wave equation can be written in the following matrix form:

$$[G]\{\ddot{p}\} + [H]\{p\} = \{F\} \tag{3.7}$$

where $G_{ij} = \sum G^e_{ij}$, $H_{ij} = \sum H^e_{ij}$ and $F = \sum F^e_i$. The coefficient G^e_{ij}, H^e_{ij} and F^e_i for an individual element are determined using the following expressions:

$$G^e_{ij} = \frac{1}{C^2} \int_{A_e} N_i N_j dA$$

$$H^e_{ij} = \int_{A_e} (\frac{\partial N_i}{\partial x}\frac{\partial N_j}{\partial x} + \frac{\partial N_i}{\partial y}\frac{\partial N_j}{\partial y})dA$$

$$F^e_i = \int_{s_e} N_i \frac{\partial p}{\partial n} ds$$

where N_i is the element shape function, A_e is the element area and s_e is the prescribed length along the boundary of the elements. In the above formulation, matrices $[H]$ and $[G]$ are constant during the analysis while the force vector $\{F\}$ and the pressure vector $\{p\}$ and its derivatives are the variable quantities in equation 3.7.

3.3.1 Truncated Boundary of the Reservoir's Far-End

The Sharan boundary condition, which was already described, at the far-end truncated boundary can be written as:

$$\frac{\partial p}{\partial n} = -\frac{\pi}{2h}p - \frac{1}{C}\,\dot{p}$$

Implementation of the truncated boundary condition in the finite element model, can be done by separating the force vector $\{F\}$ in equation 3.7 into two components:

$$\{F\} = \{FF_1\} + \{FF_2\} \tag{3.8}$$

where $\{FF_1\}$ is the component of the force due to acceleration at the boundaries of the dam-reservoir and reservoir-foundation while $\{FF_2\}$ is due to truncation at the far boundary and can be written as:

$$\{FF_2\} = -\frac{\pi}{2h}[D]\{p\} - \frac{1}{C}[D]\{\dot{p}\} \tag{3.9}$$

where $D_{ij} = D^e_{ij}$ and D^e_{ij} is defined as:

$$D^e_{ij} = \int_{\ell^e_T} N_i N_j d\ell_T \tag{3.10}$$

In equation 3.10, ℓ^e_T is the side of the element on the truncated boundary. Substituting equations 3.8 and 3.9 into equation 3.7 results in:

$$[G]\{\ddot{p}\} + \frac{1}{C}[D]\{\dot{p}\} + ([H] + \frac{\pi}{2h}[D])\{p\} = \{FF_1\} \tag{3.11}$$

In general form, we can write the finite element form of the equation of the reservoir as:

$$[G]\{\ddot{p}\} + [C']\{\dot{p}\} + [K']\{p\} = \{F\} - \rho[Q]^T(\{\ddot{U}\} + \{\ddot{U}_g\}) = \{F_2\} - \rho[Q]^T\{\ddot{U}\}$$

Putting equation 3.11 in the format of the above equation, the following relationships are obtained:

$$[C'] = \frac{1}{C}[D]$$

$$[K'] = [H] + \frac{\pi}{2h}[D]$$

$$\{F_2\} - \rho[Q]^T\{\ddot{U}\} = \{FF_1\}$$

Where $\{F_2\}$ is forces due to ground acceleration on the dam-reservoir boundaries and total acceleration on the rest of the boundaries.

3.4 EQUATION OF THE COUPLED DAM-RESERVOIR SYSTEM

As we discussed, it can be seen that the dam-reservoir interaction is a classic coupled problem which contains two differential equations of the second order. The equations of the dam structure and the reservoir can be written in the following form:

$$[M]\{\ddot{U}\} + [C]\{\dot{U}\} + [K]\{U\} = \{f_1\} - [M]\{\ddot{U}_g\} + [Q]\{p\} = \{F_1\} + [Q]\{p\}$$

$$[G]\{\ddot{p}\} + [C']\{\dot{p}\} + [K']\{p\} = \{F\} - \rho[Q]^T(\{\ddot{U}\} + \{\ddot{U}_g\}) = \{F_2\} - \rho[Q]^T\{\ddot{U}\}$$

where$[M]$, $[C]$ and $[K]$ are mass, damping and stiffness matrices of the structure and $[G]$, $[C']$ and $[K']$are matrices representing mass, damping and stiffness of the reservoir, respectively. Detailed definitions of the$[G]$,$[C']$ and $[K']$ matrices and vector $\{F\}$, are presented in the previous sections.$[Q]$ is the coupling matrix; $\{f_1\}$ is the vector of body force and hydrostatic force; and $\{p\}$ and $\{U\}$ are the vectors of hydrodynamic pressures and displacements. $\{\ddot{U}_g\}$ is the ground acceleration and ρ is the density of the fluid. The dot represents the time derivative.

Chapter 4

DYNAMIC ANALYSIS OF DAM-RESERVOIR SYSTEM

4.1 INTRODUCTION

The dam-reservoir system can be categorized as a coupled field system in which two physical domains of fluid and structure interact only at their interface. In such a problem, the presence of interaction implies that the time response of both subsystems must be evaluated simultaneously. Different approaches to the solution of the coupled field problem exist. Field elimination, simultaneous solution and partitioned solution are the three classes of solutions for the coupled field system. The advantages and disadvantages of each method were addressed by Felippa and Park (1980). The field elimination approach is not feasible in the case of nonlinear problems. The reduced system of equations has high order derivatives which cause some difficulties in applying the initial conditions. The simultaneous solution is time consuming and involves many operations, especially when a large number of elements is used. This method contains matrices with a large bandwidth and consequently requires a large amount of memory especially for the cases when the existing matrices are not symmetric. In addition, the main disadvantage of the first two classes of solution arises from the difficulties encountered in using available software while the partitioned solution has the capability of using existing software for each subsystem. Staggered solution was described by Felippa and Park (1980) as a partitioned solution procedure that can be organized in terms of sequential execution of single-field analyser.

Most of the physical systems are made of subsystems which interact with each other. These physical systems which are referred to as coupled systems, have been investigated by several researchers. Methods of solution vary depending on the governing differential equations of the subystems and may lead to different degrees of accuracy and stability of the solution (Park 1980). Coupled problems and their numerical solutions were addressed by Felippa and Park (1980); Park and Felippa (1984). Zienkiewicz and Chan (1989) proposed an unconditionally stable method for staggered solution of soil-pore fluid interaction problem. Huang (1995) proposed two unconditionally stable methods for the analysis of soil-pore fluid problem. The methods were named pressure correction method and displacement correction method. Zienkiewicz and Chan (1989) presented an unconditionally stable method for staggered solution procedure for the fluid-structure interaction problem. Their method was proved to be unconditionally stable when no damping term was included in the equations of the fluid and the structure. However, when the damping term is included in the equation of the subsystems, the proposed method may not be unconditionally stable. The problem of solutions instability when the damping term is included in the differential equation, was recognized by researchers. Most of the staggered solution applications in the field of fluid-structure interaction were conducted using a method which is not unconditionally stable.

There are two method of solution for dynamic analysis of a system. Time domain and frequency domain solutions are two methods of solutions and have different application depending on the nature of the system. For a linear system both method can be used while for a nonlinear system only time domain solution can be used to evaluate the dynamic response of the system.

The behaviour of a nonlinear system is different than the linear system. Lack of superposition property, multiplicity of equilibria and domains of attraction, local and global stability, frequency dependence of amplitude of free oscilation, the jump response, subharmonic and superharmonic generation are some of characteristics of a nonlinear system. In particular, when a linear system is subjected to harmonic excitation, the steady state response will be another harmonic with the same frequency and will be independent of the initial conditions. A nonlinear system may behave in a different manner. This character of nonlinear systems make them unable to be solved using frequency domain method.

In this Chapter, two methods of staggered solution procedure are applied

to the dam-reservoir interaction problem. Both methods are shown to be unconditionally stable when the two differential equations of the fluid and structure include damping terms. The accuracy of the solution using both of the proposed methods, is investigated. Two different configurations of concrete gravity dams are analysed to illustrate the application of the proposed procedure and to compare the solution with available finite element solutions.

4.2 THE COUPLED DAM-RESERVOIR PROBLEM

As it was discussed in previous Chapter, The dam-reservoir interaction is a classic coupled problem which contains two differential equations of the second order. The equations of the dam structure and the reservoir can be written in the following form:

$$[M]\{\ddot{U}\}+[C]\{\dot{U}\}+[K]\{U\} = \{f_1\}-[M]\{\ddot{U}_g\}+[Q]\{p\} = \{F_1\}+[Q]\{p\} \quad (4.1)$$

$$[G]\{\ddot{p}\} + [C']\{\dot{p}\} + [K']\{p\} = \{F\} - \rho[Q]^T(\{\ddot{U}\} + \{\ddot{U}_g\}) = \{F_2\} - \rho[Q]^T\{\ddot{U}\} \quad (4.2)$$

where$[M]$, $[C]$ and $[K]$ are mass, damping and stiffness matrices of the structure and $[G]$, $[C']$ and $[K']$are matrices representing mass, damping and stiffness of the reservoir, respectively. Detailed definitions of the$[G]$,$[C']$ and $[K']$ matrices and vector $\{F\}$, are presented in the following sections.$[Q]$ is the coupling matrix; $\{f_1\}$ is the vector of body force and hydrostatic force; and $\{p\}$ and $\{U\}$ are the vectors of hydrodynamic pressures and displacements. $\{\ddot{U}_g\}$ is the ground acceleration and ρ is the density of the fluid. The dot represents the time derivative.

4.3 DIRECT INTEGRATION OF THE EQUATION OF MOTION

In direct integration the equation of motion are integrated using a numerical step-by-step procedure. The term direct means that no transformation of the

equation of motion into the different form is carried out.The direct integration of the equations of motion provides the response of the system at discrete intervals of time which are usually spaced. In this procedure three basic parameters of displacement, velocitiy aand acceleration are computed. The integration algorithms are based on appropriately selected expressions that relate the response parameters at a given interval of time to their values at one or more previous time points. In general two independent expressions of this nature must be specified. The equation of motion written for the time interval under consideration provides the third expression necessary to determine the three unknown parameters. If the equation of motion is written at a time step which the three parameters are unknown$(t + \Delta t)$, the time integration scheme is called implicite integration method. In explicit integration method, the equilibrium equation is written at the time step which all the three basis parameters are known (t).

In time integration scheme, the basic parameters are known at the begining of the integration or any points preceding the integration time. These specified or computed values permit the marching scheme to be begun so that response can be computed at as many subsequent points as desired. The accuracy and stability of the scheme depend on the magnitude of the time interval and marching algorithm.

There are several method of direct integration. Newmark method, Wilson, Houbolt are implicit integration methods while Central Difference Method is the explicit integration method.

The stability of each method depends on the time steps taken and some of the methods are unconditionally stable. In an unconditionaly stable method, solution does not blow up choosing a big time step. However, the accuracy of the solution might be affected. To achieve an accurate solution a small time step must be chosen based on the natural period of the system as well as the characteristics of the exciting force.

All the above integration schemes are for the solution of a single equation of motion. While, in the couples dam-reservoir equation we are dealing with a couple of equilibrium equation. The stability of an integration scheme for a single equation does not guarantee the stability of a coupled equation. Therefore, It is needed to develope an approach for solution of coupled equation using the above methods.

4.4 USING NEWMARK-β METHOD FOR THE COUPLED EQUATIONS

Direct integration scheme is used to find the displacement and hydrodynamic pressure at the end of the time increment $i+1$ given the displacement and hydrodynamic pressure at time i. The Newmark-β method is used for discretization of both equations (implicit-implicit method). In this method $\{\dot{U}\}_{i+1}$, $\{U\}_{i+1}$, $\{\dot{P}\}_{i+1}$ and $\{P\}_{i+1}$ can be written as follows:

$$\begin{aligned} \{\dot{U}\}_{i+1} &= \{\dot{U}\}^p_{i+1} + \gamma\Delta t\{\ddot{U}\}_{i+1} \\ \{\dot{U}\}^p_{i+1} &= \{\dot{U}\}_i + (1-\gamma)\Delta t\{\ddot{U}\}_i \end{aligned} \tag{4.3}$$

$$\begin{aligned} \{U\}_{i+1} &= \{U\}^p_{i+1} + \beta\Delta t^2\{\ddot{U}\}_{i+1} \\ \{U\}^p_{i+1} &= \{U\}_i + \Delta t\{\dot{U}\}_i + (0.5-\beta)\Delta t^2\{\ddot{U}\}_i \end{aligned} \tag{4.4}$$

$$\begin{aligned} \{\dot{p}\}_{i+1} &= \{\dot{p}\}^p_{i+1} + \gamma\Delta t\{\ddot{p}\}_{i+1} \\ \{\dot{p}\}^p_{i+1} &= \{\dot{p}\}_i + (1-\gamma)\Delta t\{\ddot{p}\}_i \end{aligned} \tag{4.5}$$

$$\begin{aligned} \{p\}_{i+1} &= \{p\}^p_{i+1} + \beta\Delta t^2\{\ddot{p}\}_{i+1} \\ \{p\}^p_{i+1} &= \{p\}_i + \Delta t\{\dot{p}\}_i + (0.5-\beta)\Delta t^2\{\ddot{p}\}_i \end{aligned} \tag{4.6}$$

where $\gamma$and β are the integration parameters.The governing field equations at time $i+1$ can be written as follows:

$$[M]\{\ddot{U}\}_{i+1} + [C]\{\dot{U}\}_{i+1} + [K]\{U\}_{i+1} = \{F_1\}_{i+1} + [Q]\{p\}_{i+1} \tag{4.7}$$

$$[G]\{\ddot{p}\}_{i+1} + [C']\{\dot{p}\}_{i+1} + [K']\{p\}_{i+1} = \{F_2\}_{i+1} - \rho[Q]^T\{\ddot{U}\}_{i+1} \tag{4.8}$$

The coupled field equations 4.7 and 4.8 can be solved using the staggered solution scheme. The procedure can be started by guessing $\{P\}_{i+1}$

in equation 4.7 to solve for $\{U\}_{i+1}$ and its derivatives. Then equation 4.8 can be solved to find $\{P\}_{i+1}$. This method can not guarantee the unconditional stability of the solution. Similarly, guessing$\{\ddot{U}\}_{i+1}$ at first to calculate $\{P\}_{i+1}$ from equation 4.8 and then calculating $\{U\}_{i+1}$from equation 4.7 can not provide unconditionally stable procedure.

In the following sections, two methods of staggered solution are proposed which are shown to be unconditionally stable.

4.5 STAGGERED DISPLACEMENT METHOD

In this method, equation 4.7 can be approximated as following:

$$[M]\{\ddot{U}\}^*_{i+1} = \{F_1\}_{i+1} + [Q]\{p\}^p_{i+1} - [C]\{\dot{U}\}^p_{i+1} - [K]\{U\}^p_{i+1} \tag{4.9}$$

Combining equations 4.9 and 4.7 gives:

$$[M]\{\ddot{U}\}_{i+1} = [M]\{\ddot{U}\}^*_{i+1} + \beta\Delta t^2[Q]\{\ddot{p}\}_{i+1} - \gamma\Delta t[C]\{\ddot{U}\}_{i+1} - \beta\Delta t^2[K]\{\ddot{U}\}_{i+1} \tag{4.10}$$

Taking advantage of the lumped mass which results in a diagonal mass matrix, equation 4.10 can be modified as:

$$[M]\{\ddot{U}\}_{i+1} = [M]\{\ddot{U}\}^*_{i+1} + \beta\Delta t^2[Q]\{\ddot{p}\}_{i+1} \tag{4.11}$$

Substituting equation 4.11 into equation 4.8, then:

$$([G]+\rho\beta\Delta t^2[Q]^T[M]^{-1}[Q])\{\ddot{p}\}_{i+1}+[C']\{\dot{p}\}_{i+1}+[K']\{p\}_{i+1} = \{F_2\}_{i+1}-\rho[Q]^T\{\ddot{U}\}^*_{i+1} \tag{4.12}$$

In equation 4.12, the right hand side terms are known, thus, $\{P\}_{i+1}$ can be obtained. In order to correct the approximation made in equation 4.11, $\{P\}_{i+1}$ can be substituted in equation 4.7 to calculate $\{U\}_{i+1}$ and its derivatives.

Therefore, the procedure of the staggered displacement method can be summarized by the following steps:

1. Solving equation 4.9 to calculate $\{\ddot{U}\}^*_{i+1}$.
2. Substituting $\{\ddot{U}\}^*_{i+1}$in equation 4.12 to calculate $\{P\}_{i+1}$.
3. Substituting $\{P\}_{i+1}$ in equation 4.7 to calculate $\{U\}_{i+1}$ and its derivatives.

4.5.1 Stability of the Staggered Displacement Method

In an unconditionally stable solution method, instability can be attributed to that of structure. While in a conditionally stable method, the instability may be due to numerical or structural instability. To show that the described method of staggered displacement is unconditionally stable, consider a modally decomposed system with scalar values. In such a system, displacement and the pressure must not grow. Thus for$|\mu| < 1$ we have:

$$\{U\}_{i+1} = \mu\{U\}_i \qquad \{\dot{U}\}_{i+1} = \mu\{\dot{U}\}_i \qquad \{\ddot{U}\}_{i+1} = \mu\{\ddot{U}\}_i \tag{4.13}$$

$$\{p\}_{i+1} = \mu\{p\}_i \qquad \{\dot{p}\}_{i+1} = \mu\{\dot{p}\}_i \qquad \{\ddot{p}\}_{i+1} = \mu\{\ddot{p}\}_i \tag{4.14}$$

Using z-transformation of $\mu = \frac{1+z}{1-z}$, the condition for stability requires that the real part of z is negative ($Re(z) \leq 0$) and that the Routh-Hurwitz criterion is satisfied. For $\beta = 0.25$ and $\gamma = 0.5$, equations 4.3, 4.4, 4.5 and 4.6 become:

$$\begin{aligned} \{\ddot{U}\}_{i+1} &= \frac{4z^2}{\Delta t^2}\{U\}_{i+1} \qquad \{\dot{U}\}_{i+1} = \frac{2z}{\Delta t}\{U\}_{i+1} \\ \{\dot{U}\}^p_{i+1} &= \frac{2z - z^2}{\Delta t}\{U\}_{i+1} \qquad \{U\}^p_{i+1} = (1 - z^2)\{U\}_{i+1} \end{aligned} \tag{4.15}$$

$$\begin{aligned} \{\ddot{p}\}_{i+1} &= \frac{4z^2}{\Delta t^2}\{p\}_{i+1} \qquad \{\dot{p}\}_{i+1} = \frac{2z}{\Delta t}\{p\}_{i+1} \\ \{\dot{p}\}^p_{i+1} &= \frac{2z - z^2}{\Delta t}\{p\}_{i+1} \qquad \{p\}^p_{i+1} = (1 - z^2)\{p\}_{i+1} \end{aligned} \tag{4.16}$$

Rewriting equation 4.7 without the force term, then:

$$[M]\{\ddot{U}\}_{i+1} + [C]\{\dot{U}\}_{i+1} + [K]\{U\}_{i+1} - [Q]\{p\}_{i+1} = 0 \tag{4.17}$$

Combining equations 4.10 and 4.12 and substituting them into equation 4.8 without the force term, gives:

$$[G]\{\ddot{p}\}_{i+1}+[C']\{\dot{p}\}_{i+1}+[K']\{p\}_{i+1}+\rho[Q]^T[M]^{-1}([M]+\gamma\Delta t[C]+\beta\Delta t^2[K])\{\ddot{U}\}_{i+1} = 0 \tag{4.18}$$

The modally decomposed system is represented by a single degree of freedom equation. The single degree of freedom equivalent of equations 4.17 and 4.18 will be obtained by substituting the mass, damping and stiffness values m, c and k instead of $[M]$, $[C]$ and $[K]$ in equation 4.17 and g, $c^{'}$ and$k^{'}$ instead of $[G]$, $[C^{'}]$ and $[K^{'}]$ in equation 4.18. The coupling matrix $[Q]$ would be represented by scalar quantity q. The characteristic equation of the coupled field can be written by substituting equations 4.15 and 4.16 into equations 4.17 and 4.18 as follows:

$$\begin{vmatrix} m\frac{4z^2}{\Delta t^2} + c\frac{2z}{\Delta t} + k & -q \\ \frac{\rho q}{m}(m + \frac{\Delta t}{2}c + \frac{\Delta t^2}{4}k)\frac{4z2}{\Delta t^2} & g\frac{4z^2}{\Delta t^2} + c'\frac{2z}{\Delta t} + k' \end{vmatrix} = 0 \tag{4.19}$$

or

$$a_0 z^4 + a_1 z^3 + a_2 z^2 + a_1 z + a4 = 0 \tag{4.20}$$

where:

$$\begin{aligned} a_0 &= \frac{16mg}{\Delta t^2} \qquad a_1 = \frac{8mc'}{\Delta t^3} + \frac{8gc}{\Delta t^3} \\ a_2 &= \frac{4mk'}{\Delta t^2} + \frac{4cc'}{\Delta t^2} + \frac{4gk}{\Delta t^2} + \frac{4\rho q^2}{\Delta t^2} + \frac{2\rho q^2 c}{m\Delta t} + \frac{\rho q^2 k}{m} \\ a_3 &= \frac{2c'k}{\Delta t} + \frac{2ck'}{\Delta t} \qquad a_4 = kk' \end{aligned}$$

The Routh-Hurwitz conditions for stability are:

$$a_0 > 0 \qquad a_1, a_2, a_3, a_4 \geq 0 \qquad \begin{vmatrix} a_1 & a_3 \\ a_0 & a_2 \end{vmatrix} > 0 \qquad \begin{vmatrix} a_1 & a_3 & 0 \\ a_0 & a_2 & a_4 \\ 0 & a_1 & a_3 \end{vmatrix} > 0 \tag{4.21}$$

For the structural system of dam and reservoir;m,c, k, g, c' andk' are positive quantities. Therefore, a_0, a_1, a_2,$a_3$and a_4 are always positive. The values of the two determinants in equation 4.21 are given as:

$$\begin{aligned} a_1 a_2 - a_3 a_0 &= \\ & \frac{32}{\Delta t^5} m^2 c' k' + \frac{32}{\Delta t^5} m c'^2 c + \frac{32\rho}{\Delta t^5} m c' q^2 + \frac{16\rho}{\Delta t^4} c' q^2 c \\ & + \frac{8\rho}{\Delta t^3} c' q^2 k + \frac{32}{\Delta t^5} g c^2 c' + \frac{32}{\Delta t^5} g^2 c k \end{aligned} \tag{4.22}$$

$$+\frac{32\rho}{\Delta t^5}gcq^2+\frac{16\rho}{\Delta t^4}gc^2q^2+\frac{8\rho}{\Delta t^3}gcq^2k$$

$$\begin{aligned}a_1a_2a_3-a_1^2a_4-a_3^2a_0 \;=\; & \\ & \frac{64}{\Delta t^6}(mk'\sqrt{cc'}-gk\sqrt{cc'})^2+\frac{64}{\Delta t^6}mc'^3ck+\frac{64}{\Delta t^6}mc'^2c^2k' \\ & +\frac{64\rho}{\Delta t^6}mc'^2q^2k+\frac{64\rho}{\Delta t^6}mc'q^2ck'+\frac{32\rho}{\Delta t^5}c'^2q^2ck \\ & +\frac{32\rho}{\Delta t^5}c'q^2c^2k'+\frac{16\rho}{\Delta t^4}c'^2q^2k^2+\frac{16\rho}{\Delta t^4}c'q^2kck' \\ & +\frac{64}{\Delta t^6}gc^2c'^2k+\frac{64}{\Delta t^6}gc^3c'k'+\frac{64\rho}{\Delta t^6}gcq^2c'k \\ & +\frac{64\rho}{\Delta t^6}gc^2q^2k'+\frac{32\rho}{\Delta t^5}gc^2q^2c'k+\frac{32\rho}{\Delta t^5}gc^3q^2k' \\ & +\frac{16\rho}{\Delta t^4}gcq^2k^2c'+\frac{16\rho}{\Delta t^4}gc^2q^2kk'\end{aligned} \tag{4.23}$$

All the terms in equation 4.22 and 4.23 are positive. Recalling the condition of stability (equation 4.21), then the method of staggered displacement is unconditionally stable.

4.6 STAGGERED PRESSURE METHOD

In this method, the pressure can be approximated using equation 4.8 as following:

$$[G]\{\ddot{p}\}^*_{i+1}=\{F_2\}_{i+1}-[C']\{\dot{p}\}^p_{i+1}-[K']\{p\}^p_{i+1} \tag{4.24}$$

Substituting equation 4.24 into equation 4.8, there is obtained:

$$[G]\{\ddot{p}\}_{i+1}=[G]\{\ddot{p}\}^*_{i+1}-\rho[Q]^T\{\ddot{U}\}_{i+1}-\gamma\Delta t[C']\{\ddot{p}\}_{i+1}-\beta\Delta t^2[K']\{\ddot{p}\}_{i+1} \tag{4.25}$$

or:

$$([G]+\beta\Delta t^2[K']+\gamma\Delta t[C'])\{\ddot{p}\}_{i+1}=[G]\{\ddot{p}\}^*_{i+1}-\rho[Q]^T\{\ddot{U}\}_{i+1} \tag{4.26}$$

Substituting equation 4.26 into equation 4.7 with $[H]=[G]+\beta\Delta t^2[K']+\gamma\Delta t[C']$, gives:

$$([M]+\rho\beta\Delta t^2[Q][H]^{-1}[Q]^T)\{\ddot{U}\}_{i+1}+[C]\{\dot{U}\}_{i+1}+[K]\{U\}_{i+1}= \quad (4.27)$$

$$\{F_1\}_{i+1}+[Q](\{p\}^p_{i+1}+\beta\Delta t^2[H]^{-1}[G]\{\ddot{p}\}^*_{i+1})$$

Using equation 4.27, the variable $\{\ddot{U}\}_{i+1}$can be calculated. Substituting $\{\ddot{U}\}_{i+1}$ into equation 4.7 gives $\{p\}_{i+1}$ and its derivatives.

Therefore, the procedure of the staggered pressure method can be summarized by the following steps:

1. Solving equation 4.24 to calculate $\{\ddot{p}\}^*_{i+1}$.
2. Substituting $\{\ddot{p}\}^*_{i+1}$in equation 4.27 to calculate $\{\ddot{U}\}_{i+1}$.
3. Substituting $\{\ddot{U}\}_{i+1}$in equation 4.26 to calculate $\{p\}_{i+1}$ and its derivatives.

4.6.1 Stability of the Staggered Pressure Method

For stability check, similar procedure as that used in the displacement method can be applied. Rewriting equations 4.7 and 4.8 without the force terms, then:

$$[M]\{\ddot{U}\}_{i+1}+[C]\{\dot{U}\}_{i+1}+[K]\{U\}_{i+1}-[Q]\{p\}_{i+1}=0 \quad (4.28)$$

$$[G]\{\ddot{p}\}_{i+1}+[C']\{\dot{p}\}_{i+1}+[K']\{p\}_{i+1}+\rho[Q]^T\{\ddot{U}\}_{i+1}=0 \quad (4.29)$$

The characteristic equation of the coupled field for a modally decomposed system with scalar values, can be written by substituting equations 4.15 and 4.16 into equations 4.28 and 4.29:

$$\begin{vmatrix} m\frac{4z^2}{\Delta t^2}+c\frac{2z}{\Delta t}+k & -q \\ \rho q\frac{4z^2}{\Delta t^2} & g\frac{4z^2}{\Delta t^2}+c'\frac{2z}{\Delta t}+k' \end{vmatrix}=0$$

or

$$a_0z^4+a_1z^3+a_2z^2+a_1z+a4=0 \quad (4.30)$$

where:

$$\begin{aligned} a_0 &= \frac{16mg}{\Delta t^4} \qquad a_1=\frac{8mc'}{\Delta t^3}+\frac{8gc}{\Delta t^3} \\ a_2 &= \frac{4mk'}{\Delta t^2}+\frac{4cc'}{\Delta t^2}+\frac{4gk}{\Delta t^2}+\frac{4\rho q^2}{\Delta t^2} \\ a_3 &= \frac{2c'k}{\Delta t}+\frac{2ck'}{\Delta t} \qquad a_4=kk' \end{aligned}$$

The coefficients of the polynomial are all positive. The determinants in the Routh-Hurwitz conditions (equation 4.21), give:

$$a_1a_2 - a_3a_0 = \frac{32}{\Delta t^5}m^2c'k' + \frac{32}{\Delta t^5}mc'^2c + \frac{32\rho}{\Delta t^5}mc'q^2 + \frac{32}{\Delta t^5}gc^2c' + \frac{32}{\Delta t^5}g^2ck + \frac{32\rho}{\Delta t^5}gcq^2 \tag{4.31}$$

$$a_1a_2a_3 - a_1^2a_4 - a_3^2a_0 = \frac{64}{\Delta t^6}(mk'\sqrt{cc'} - gk\sqrt{cc'})^2 + \frac{64}{\Delta t^6}mc'^3ck + \frac{64}{\Delta t^6}mc'^2c^2k' + \frac{64\rho}{\Delta t^6}mc'^2q^2k + \frac{64\rho}{\Delta t^6}mc'q^2ck' + \frac{64}{\Delta t^6}gc^3c'k' + \tag{4.32}$$

$$+\frac{64\rho}{\Delta t^6}gc^2c'^2k + \frac{64\rho}{\Delta t^6}gc^2q^2k' + \frac{64\rho}{\Delta t^6}gcq^2c'k \tag{4.33}$$

These terms are all positive. Therefore, given the stability condition of equation 4.21, the method of staggered pressure is unconditionally stable.

4.7 MODIFIED STAGGERED PRESSURE METHOD

Most of the available nonlinear solutions assume a diagonal mass matrix for the purpose of analysis. The staggered displacement method is the most suitable coupled field problem solution procedure for the case of nonlinear analysis. In the case of the staggered pressure method some difficulties may arise due to added mass effect in equation 4.27 which changes the mass matrix from diagonal to a full matrix. For this reason the staggered pressure method was modified to apply to nonlinear analysis.

The staggered pressure method is modified by rewriting equation 4.27 in the following approximate form:

$$[M]\{\ddot{U}\}_{i+1}+[C]\{\dot{U}\}_{i+1}+[K]\{U\}_{i+1} = \{F_1\}_{i+1}+[Q]\,(\{p\}^p_{i+1}+\beta\Delta t^2[H]^{-1}(\,[G]\{\ddot{p}\}^*_{i+1}-\rho[Q]^T\{\ddot{U}\}_i)\,) \tag{4.34}$$

Therefore, the procedure of the modified staggered pressure method can be summarized by the following steps:

1. Solving equation 4.24 to calculate $\{\ddot{p}\}^*_{i+1}$.
2. Substituting $\{\ddot{p}\}^*_{i+1}$in equation 4.34 to calculate $\{\ddot{U}\}_{i+1}$.
3. Substituting $\{\ddot{U}\}_{i+1}$ in equation 4.26 to calculate $\{p\}_{i+1}$ and its derivatives.

The modified staggered pressure method does not guarantee unconditional stability of the solution. In the following analysis, the modified staggered pressure method is used instead of the staggered pressure method and the results are compared with those obtained using the staggered displacement analysis procedure.

4.8 USING α-METHOD FOR THE COUPLED EQUATIONS

In this method, $\{\dot{U}\}_{i+1}$, $\{U\}_{i+1}$, $\{\dot{p}\}_{i+1}$ and $\{p\}_{i+1}$ can be written same as Newmark-β method. The governing field equations at time $i+1$ can be written as follows:

$$[M]\{\ddot{U}\}_{i+1}+[C]\{\dot{U}\}_{i+1}+(1+\alpha)[K]\{U\}_{i+1} = \{F_1\}_{i+1}+[Q]\{p\}_{i+1}+\alpha[K]\{U\}_i \tag{4.35}$$

$$[G]\{\ddot{p}\}_{i+1}+[C']\{\dot{p}\}_{i+1}+(1+\alpha)[K']\{p\}_{i+1} = \{F_2\}_{i+1}-\rho[Q]^T\{\ddot{U}\}_{i+1}+\alpha[K']\{p\}_i \tag{4.36}$$

where α is the integration parameter which is introduced in the coupled field equation. The coupled field equations 4.35 and 4.36 can be solved using the staggered displacement solution scheme.

4.8.1 Staggered Displacement Method

In this method, equation 4.35 can be approximated as following:

$$[M]\{\ddot{U}\}^*_{i+1} = \{F_1\}_{i+1}+[Q]\{p\}^p_{i+1}-[C]\{\dot{U}\}^p_{i+1}-(1+\alpha)[K]\{U\}^p_{i+1}+\alpha[K]\{U\}_i \tag{4.37}$$

Combining equations 4.37 and 4.35 gives:

$$[M]\{\ddot{U}\}_{i+1} = [M]\{\ddot{U}\}^*_{i+1}+\beta\Delta t^2[Q]\{\ddot{p}\}_{i+1}-\gamma\Delta t[C]\{\ddot{U}\}_{i+1}-(1+\alpha)\beta\Delta t^2[K]\{\ddot{U}\}_{i+1} \tag{4.38}$$

Taking advantage of the lumped mass which results in a diagonal mass matrix, equation 4.38 can be modified as:

$$[M]\{\ddot{U}\}_{i+1} = [M]\{\ddot{U}\}^*_{i+1} + \beta\Delta t^2[Q]\{\ddot{p}\}_{i+1} \tag{4.39}$$

Substituting equation 4.39 into equation 4.36, then:

$$([G] + \rho\beta\Delta t^2[Q]^T[M]^{-1}[Q])\{\ddot{p}\}_{i+1} + [C']\{\dot{p}\}_{i+1} + (1+\alpha)[K']\{p\}_{i+1} =$$

$$\{F_2\}_{i+1} - \rho[Q]^T\ \ddot{U}\}^*_{i+1} + \alpha[K']\{p\}_i \tag{4.40}$$

In equation 4.40, the right hand side terms are known, thus, $\{p\}_{i+1}$ can be obtained. In order to correct the approximation made in equation 4.39, $\{p\}_{i+1}$ can be substituted in equation 4.35 to calculate $\{U\}_{i+1}$ and its derivatives.

Therefore, the procedure of the staggered displacement method can be summarized by the following steps:

1. Solving equation 4.37 to calculate $\{\ddot{U}\}^*_{i+1}$.
2. Substituting $\{\ddot{U}\}^*_{i+1}$in equation 4.40 to calculate $\{p\}_{i+1}$.
3. Substituting $\{p\}_{i+1}$ in equation 4.35 to calculate $\{U\}_{i+1}$ and its derivatives.

It can be shown that the method of staggered displacement is unconditionally stable for the linear coupled equations of the dam-reservoir system with structural damping when $\alpha = 0$. For the nonlinear equations, the numerical solution is based on piece-wise linear solution. The solution stability depends on the length of the time steps and the introduced numerical damping. The dam-reservoir interaction representation using the staggered solution technique using α-method is suitable for nonlinear fracture analysis of concrete dams.

The nonlinear seismic analysis of concrete gravity dams includes opening and closing of the cracks due to the cyclic nature of the earthquake. When the cracks are closed, cracked elements recover their strength and therefore the structure gains stiffness. As the cracks open, the stiffness of the structure reduces. The effect of opening and closing of cracks introduce high frequency shock waves into the structure. The numerical difficulties due to opening and closing of cracks can be overcome by using the α-method (Hilber et al., 1977; Hilber and Hughes, 1978).

The α-method of time integration algorithms introduces numerical damping to the system. It is an efficient method that is accurate in lower modes and dissipate energy in the higher modes when compared with other time integration techniques. Thus, using the α-method ensures that the response of higher modes is damped out. Direct integration is used to determine the displacement and hydrodynamic pressure at the time increment $i+1$. The α-method is used for discretization of both equations of the coupled field problem (implicit-implicit method). The dam-reservoir interaction representation using the staggered solution technique is introduced to the nonlinear fracture analysis of concrete dams.

4.9 SEISMIC ENERGY BALANCE

In the design of structure subjected to earthquake loading, the energy equation can be used to study the energy absorbtion of different components. In a satisfactory design, the energy supply must be larger than the energy demand. In this regard, two approaches can be considered for the energy equation. Uang and Bertero (1990) used absolute and relative energy formulations for a single degree of freedom system. They found that absolute energy formulation is simple and more straightforward. Filiatrault et al. (1994) used energy balance to study the nonlinear behaviour of different structures under variable earthquake ground motion. Different time stepping algorithms were used to investigate the effect of numerical damping. Without the numerical damping, exact energy balance can be achieved. The two approaches to energy formulation were found to give different energy responses.

The energy equation of the dam structure governed by equation (2.1), can be written as:

$$\frac{1}{2}\{\dot{U}_t\}^T[M]\{\dot{U}_t\} + \int\{\dot{U}\}^T[C]\{dU\} + \int\{r\}^T\{dU\} = \tag{4.41}$$

$$\int\{f_1\}^T\{dU\} + \int\{\ddot{U}_t\}^T[M]\{dU_g\} + \int([Q]\{p\})^T\{dU\}$$

or:

$$EK + ED + ER = EP + EQ + EH \tag{4.42}$$

In equations **??** and 4.42, $\{r\}$ is the vector of the nonlinear restoring force. The absolute kinetic energy is EK, the viscous damping energy is ED, the nonlinear restoring work is ER, the work of preseismic applied force is EP, the absolute seismic input energy is EQ and the work done by the hydrodynamic pressure is EH. The relative displacement is $\{U\}$ while $\{U_t\}$ is the total (absolute) displacement vector $\{U_t\} = \{U\} + \{U_g\}$. $\{U_g\}$ is the ground displacement vector. The restoring energy, ER contributes to the stored elastic energy in a system EE, and the energy dissipated due to fracture $EF(EF = ER - EE)$, Thus:

$$EK + EE + ED + EF = EI$$

EK and EE contribute to the stored energy while ED and EF represent the dissipated energy. The input energy EI, is the sum of the seismic input energy due to the inertial force EQ, hydrodynamic force EH and work of preseismic applied load EP.

The energy balance error is computed as:

$$Error = \frac{(EP + EQ + EH) - (EK + ED + ER)}{(EQ + EH)} \times 100$$

When the dam-reservoir interaction effects are represented by added masses, the hydrodynamic energy EH is excluded from the energy equation, $EH = 0$. However, energy is added to the seismic input energy EQ and kinetic energy EK through the mass added to the structural system. In the analysis, the results of the fracture response are presented for the time before the five percent energy balance error is reached. The error in the energy balance represents an excessive amount of damage when numerical damping is introduced.

4.10 ACCURACY OF THE SOLUTION SCHEME

The accuracy of the staggered solution scheme can be improved by increasing the number of iterations and/or by decreasing the time step. Increasing the number of iterations of the staggering scheme is a time consuming process. The accuracy of the proposed methods is based on the selection of the appropriate time step. In all of the following analyses no iterations have been made for the purpose of improving accuracy. The staggered displacement method and the modified staggered pressure method are compared with the

finite element solution of example problems for the purpose of evaluating the accuracy of the analysis.

Chapter 5

NONLINEAR FRACTURE MODELS OF CONCRETE GRAVITY DAMS

5.1 INTRODUCTION

The cracking behaviour of concrete dams has been the subject of extensive research during the past decade because few dams suffered severe cracking during earthquakes. Rescher (1990) indicated that most concrete gravity dams will experience cracking even under operational loading conditions and moderate earthquake ground motions. Therefore, the assumption of linear behavior may not be appropriate in the analysis of the seismic response of concrete gravity dams.

Concrete dams are distinguished from other structures because of their size and their interactions with the reservoir and foundation. The results obtained from the nonlinear analysis of concrete dams are strongly dependent on the approach to modelling of these interactions. It is a difficult task to develop a comprehensive analytical model to include both nonlinearity and interaction effects. The size effect can also influence the properties of the dam concrete. The fracture properties of normal concrete can be determined using laboratory tests. However, the dam concrete differs from the normal weight concrete because of aggregate size and its poor strength. Little information is available on the fracture properties of the dam concrete. The fracture surface of the dam concrete specimens is characterized by mainly aggregate failure.

Saouma et al. (1991) attempted to measure fracture toughness of a concrete specimen in the laboratory which was considered to be similar to dam concrete. They concluded that a definitive decision cannot be made concerning the results and their accuracy. Bruhwiler and Wittmann (1990) carried out a dynamic test to determine the material properties of the dam concrete under high rate of loading and an initially applied compression load. They found that the fracture energy of dam concrete is 2 to 3 times higher than that of ordinary concrete. The reason is related to the tensile strength characteristic of dam concrete. The tensile behavior of concrete can be divided into two stages. In the first stage, the behavior is linear until the tensile strength is reached. In the second stage, strain softening behavior is observed. Fracture energy is sensitive to the tensile stress. In addition, increasing the preloading decreases the fracture energy.

To understand the nonlinear behaviour of concrete dams, modelling of the cracking and damage process is needed. Bazant and Oh (1983) proposed a fracture mechanics approach as a blunt smeared crack band. The proposed approach represented a significant advance in comparison to the linear fracture theory. The strain softening of the material was considered based on the fracture parameters, fracture energy, uniaxial tensile strength and crack band width. Fracture energy can be determined from the complete stress-strain curve. Formulas were derived to give the fracture parameters.

Two classes of solutions can be found in the nonlinear study of concrete gravity dams. Discrete crack approach is the first class of solutions which is based on the variable mesh approach. Two methods of linear elastic fracture mechanics LEFM, and nonlinear fracture mechanics NLFM, can be used in this approach. The second class of solutions is the continuum model in which a fixed finite element mesh is used. Smeared crack model and damage mechanics are the two methods of solution in this class. These two families of fracture model have been investigated in parallel. They also called global approach and local approach. In the global approach, the cracks are simulated by discontinuity in the continuum and the stresses are obtained using linear elastic fracture mechanics(LEFM). This method is coupled to a numerical technique such as finite elements or boundary elements. On the other hand, the local approach of fracture is based on changes in the constitutive law governing the behaviour of concrete. The integrity of the structure is not required during the solution process.

Bhattacharjee and Léger (1994) applied NLFM to predict the response of concrete gravity dams. The experimental work done on a model of a concrete

gravity dam and a small beam specimen confirmed the applicability of the proposed NLFM approach. The coaxial rotation crack model gives a better response than the fixed crack model. Léger and Leclerc (1996) studied the nonlinear response of concrete gravity dams subjected to different earthquake ground motions. They found that the response is sensitive to time variation of the input motion. Most of the time, cracking response showed that the crack starts from the downstream side and moves toward the upstream side. This form of cracking does not promote dam instability. The cracks are either horizontal or they sloped downward. They found that the vertical ground motion acceleration component is not critical in seismic cracking response of dams.

The nonlinear response of a concrete gravity dam with an initial distribution of temperature gradient when subjected to the earthquake was studied by Léger and Bhattacharjee (1995). They used frequency-independent added mass matrix as a representative of dam-reservoir-foundation interaction. The reservoir and foundation were modelled as a series of dampers and springs such that the same response can be obtained for the linear response of the crest when compared with the case of actual interaction. Under earthquake excitation, when a rigid foundation is assumed with no reservoir bottom absorption, no crack was observed at the top part of the dam. A crack was formed at the foundation level.

Bhattacharjee and Léger (1993); Léger and Bhattacharjee (1994) studied the energy response of concrete gravity dams. They used a stiffness proportional damping with -method of integration. Newton-Raphson iteration technique was used to remove the unbalanced load. An energy balance error approach is used as a measure of damage. The seismic analysis of Koyna dam under both horizontal and vertical components of the earthquake was conducted. Without introducing the numerical damping, the analysis stopped after the first few seconds because of energy balance error due to spurious deformation of some elements. No discrepancies were found in the results of the analysis before the occurrence of instability, when compared with the case of = -0.2 in which the analysis was successfully completed. Dissipated fracture energy is negligible in comparison to other sources of energy dissipation. The reservoir effect was represented by added mass technique.

The effect of hydrodynamic pressure inside the crack in the seismic analysis of concrete gravity dams was investigated by Tinawi and Guizani (1994). The pressure inside the crack does not change the response of the dam significantly. It was found that under high frequency content earthquakes, the

hydrodynamic pressure inside the crack may increase when higher modes are significant. At the base of the dam, the hydrodynamic pressure may be 50% higher than the hydrostatic pressure.

The nonlinear response of the Pine Flat dam was studied using the discrete approach (Wepf et al. 1993). A fictitious crack approach was used to model the crack tip. Reservoir interaction was modelled using a boundary element. Linear response of the dam was compared with EAGD-84 code analysis and good agreement was found. The nonlinear response of the dam including reservoir interaction was strongly affected in comparison with the added mass approach. The slope of the reservoir bottom strongly influenced the nonlinear response. The aggregate interlock effect was found to be important in the final cracking configuration of the dam.

The cracking response of a concrete gravity dam when subjected to earthquake loading can be different if nonuniform damping or uniform damping including the damping due to cracking is considered (Barrett et al., 1991). In the analysis, the dam was represented by a small number of elements. When the bottom few elements were cracked, a noticeable change in the response was observed.

Using different computer codes, Singhal (1991) found that the Westergaard's added mass approach yields higher values for crest displacement and stress than that obtained using other approaches. The reservoir bottom absorbtion and water compressibility did not change the response significantly.

Pekau et al. (1991, 1995) and Pekau and Batta (1991) presented a method to study the cracking of concrete gravity dams using the principle of Linear Elastic Fracture Mechanics (LEFM) and boundary element mode superposition analysis. The model was checked by a shake table test of cantilever beam made of gypsum. The impact of cracking surface was modeled as a load pulse.

Ayari and Saouma (1990) proposed a model for simulation of discrete crack closure. The model was applied in the dynamic analysis of the Koyna dam (India) under both horizontal and vertical components of the earthquake. The results were obtained for 5 seconds only of the earthquake in which the numerical damping was less than 10%.

Nonlinear seismic response of concrete gravity dams was studied by Skrikerud and Bachmann (1986). Fracture mechanics analysis using discrete crack approach was applied. The model was capable of initiation, opening, closing and reopening of discrete cracks. Special treatment was used to model aggregate interlock effect. The model was applied to a dam of rigid foundation

with empty reservoir. The crack pattern was found to be very sensitive to the parameters chosen for the analysis. The first four seconds of an artificially generated time history was used for the purpose of analysis. The analysis stopped due to excessive damage. Nonlinear response of concrete gravity dams was also studied by Feltrin et al. (1990). A rigid foundation was assumed for Pine Flat dam and the reservoir interaction was included. The nonlinearity in concrete behaviour included the strain softening and aggregate interlock. Response of the linear model with and without the reservoir interaction was determined. Nonlinear response of the empty reservoir was studied by scaling the ground motion until cracking occurred. The cracks started at the top part from down stream face of the dam near the slope discontinuity and moved horizontally. A different response was observed under the effect of reservoir interaction. The first crack started at the foundation level and then it followed by a crack at the top part of the dam at the same location of the crack of empty reservoir case. The crest displacement was found to be higher than that of the empty reservoir. They concluded that the effect of dam-reservoir interaction must be included in the nonlinear analysis.

El-Aidi and Hall (1989 a,b) investigated the nonlinear response of concrete gravity dams. The water cavitation in addition to cracking of concrete was considered. Despite the difficulties involved, the nonlinear model was applied for the case of preformed base crack, top crack and homogeneous dam without any cracks. In the case of homogeneous dam, the top crack initiated at $t = 1.95$ sec. Soon after initiation of the top crack, it went through the dam body and almost separated the top part from the rest of the dam. During the rest of the analysis, no other cracks were observed and only rocking and opening and closing of the crack were observed.

Fenves and Vargas-Loli (1988) proposed a method for dam-reservoir interaction which resulted in a symmetric matrix representation of the total equation of the system. The nonlinearity of the reservoir was introduced into the proposed method to investigate the reservoir interaction effect. They found that the effect of cavitation is not significant in the response of the structure.

Mlakar (1987) studied the nonlinear dynamic behaviour of concrete gravity dams using the ADINA code. It was found that the crack first started at the base. Then cracking initiated at the top part near slope discontinuity. The cracks near the slope discontinuity propagated instantaneously and passed through the cross section.

In this chapter the nonlinear fracture response of concrete gravity dams

due to seismic loading is investigated. The dam-reservoir interaction is included in the time domain analysis using the method of staggered displacement. Smeard crack approach based on a nonlinear fracture mechanics crack propagation criterion is used to study the cracking and response of concrete gravity dams.

5.2 A BRIEF STUDY OF NONLINEAR PARAMETERS

Modelling the constitutive behaviour of concrete is the most important part of nonlinear seismic response study of the dams. Analytical models for two-dimensional fracture propagation studies are well developed now, but the constitutive behaviour of concrete is the most important part of nonlinear seismic response study of the dams. Analytical models for two-dimensional fracture propagation studies are well developed now, but the three-dimensional application of the fracture models is still in its infancy. Unlike the circumstance in arch dams, where the nonlinear joint behaviour in the arch direction could be a decisive factor in the stability of the structure , the structural response of gravity dams is mainly determined by gravity action. The concrete gravity dam monoliths, usually unkeyed or lightly grouted, are expected to vibrate independently under severe ground excitations. Hence, two-dimensional plane-stress idealizations seem to be appropriate for nonlinear seismic response study of concrete gravity dams.

A state-of-the-art review on the constitutive models for two-dimensional finite element crack propagation analysis of concrete gravity is presented in this part. Special emphasis is put on the applications of the models in seismic analyses of the dams and the limitations of past investigations are examined.

5.2.1 Finite element models of crack propagation

Two approaches have generally been followed for the spatial representation of tensile crack propagation in finite element analysis of concrete structures: the discrete crack model and the continuum crack model. Both models have been used over the decades because of the advantages and inconveniences that they bring to the constitutive models for finite element crack propagation analysis of concrete structures.

5.2.2 Discrete crack propagation model ,DCPM,(variable mesh)

In the DCPM, global approach, a crack is represented as a discrete gap along the inter-element boundary. The growth of the crack is determined by strength or fracture mechanics based constitutive models. The progressive physical discontinuity in the system is reflected instantaneously in the finite element model by modifying the mesh during the analysis. It is generally argued that the nonlinear response of concrete dams is dominated by a few discrete long cracks. From this consideration, the discrete crack model may be a sensible choice for dam fracture analysis.. The specific advantages of the DCPM are the abilities to consider explicitly the water penetration and uplift pressure on the crack-open surfaces, the aggregate interlock in the rough cracks, and the direct estimation of crack-opening displacement (COD) profile. The principal disadvantages in applying this model are the difficulty and high computational cost due to continuous change of the finite element topology during the analysis, and the unobjective effects of finite element mesh and crack length increment. A special case of discrete crack modelling is the application of special elements to represent the a priori weak joints in the system, such as the dam-foundation interface and construction joints.

5.2.3 Continuum crack propagation models (CCPM)

The continuum crack can be divided into Smeared crack propagation model (SCPM) and Damage mechanics crack propagation model. In these models the fracture is idealized to propagate as a blunt front smeared over an entire element or a certain band width of the element. After initiation of the fracture process, determined by a suitable constitutive model, the pre-crack material stress- strain relationship is replaced by an orthotropic relationship with material reference axis system aligned with the fracture direction. The tension stiffness across the crack plane is either eliminated suddenly or a gradual stress-release criterion is applied. Thus, only the constitutive relationship is updated with propagation of cracks and the finite element mesh is kept unchanged. The advantage of the models lies in its simplicity and cost effectiveness, although the physical nature of crack representation is questionable. The tendency of the model to cause diffused crack pattern and the directional bias caused by slanted finite element mesh are still significant computational difficulties. However, the model has been extensively used in

the seismic response study of concrete gravity dams.

5.3 Constitutive models for crack propagation

To conduct a comprehensive fracture propagation analysis, the selected constitutive model should describe the prefracture material stress-strain behavior, the fracture initiation and propagation criteria, and the post-crack behaviour. It is a usual practice in concrete structure analysis to presume linear elastic behaviour before the onset of tensile fracture process. The behaviour of concrete under high compressive loading is predominantly nonlinear. Several models based on the concepts of elastoplasticity and elasto-viscoplasticity have been proposed, to study the nonlinear behaviour of concrete under compression. However, the compressive stresses in concrete gravity dams are expected to be low even under severe ground excitations. A reasonable assumption of linear elastic behaviour under compressive loading has been applied in almost all previous investigations. It is almost universal in the constitutive models of fracture analysis to assume the initiation of new cracks in a homogenous structure when the principal tensile stress reaches the tensile strength of concrete. Diversity in various models lies in the definition of the fracture propagation criteria after the crack has been introduced in the structure. Major developments in the realms of crack propagation analysis and their relative merits are presented in the following sections.

5.3.1 Strength-based criteria

The early investigations on cracking of concrete have mostly applied simple criteria based on the concepts of strength of material (SOM). A crack is assumed to propagate when the predicted stress or strain at the crack-tip exceeds the critical value representative of the strength of the material. The crack propagation criterion, in this approach, is identical to the new crack initiation criterion. A sudden release of stress on the fracture plane is commonly assumed upon reaching the material tensile strength. The gradual release of stress with increasing strain has also been used, mainly for numerical stability reasons, in finite element analyses of cracking problems. The SOM criterion of crack propagation has been used in discrete and smeared crack propagation finite element models. Comparison of computed tensile

stress with the strength of the material is not rational for a cracked structure because spurious results may be obtained depending on the size of the finite element ahead of the propagating crack. The lack of finite element mesh objectivity of the SOM criterion was reported.

5.3.2 Fracture mechanics criteria

Fracture mechanics is the theory dealing with propagation of cracks, based on the concept of energy dissipation by the structure undergoing fracturing process. It has been recognized only recently that the failure mechanism in concrete structures is different from the usual strength based concept, due to the progressive growth of a fracture process. The fracture mechanics of concrete has drawn significant attention of the research community over the last decade; as a consequence, the literature on the subject is voluminous. Here, only the principal developments in fracture mechanics, relevant to the seismic analysis of concrete dams, are reviewed.

Figure 5.1: Modes of failure: (a) mode I - Tensile fracture; (b) mode II - planar shear fracture; (c) mode III - tearing fracture

Three elementary modes of failure are recognized in the fracture theory (Figure 5.1). For two- dimensional idealizations, modes I and II (the opening mode and the planar shear mode) are usually considered. The third one, the tearing mode (mode III), is considered for three- dimensional fracture propagation studies. Fracture mechanics crack propagation models can be

broadly classified into two categories the linear elastic fracture mechanics (LEFM) models and the nonlinear fracture mechanics (NLFM) models.

According to LEFM, the fracture process occurs right at the crack-tip and the entire volume of the material remains elastic (Figure5.2-a). The stress field around the tip of a sharp crack is characterized by the stress intensity factors, Ki, determined from linear elastic solutions:

$$\left\{ \begin{array}{c} K_I \\ K_{II} \\ K_{III} \end{array} \right\} = \lim_{r \to 0, \theta \to 0} \sqrt{2\pi t} \left\{ \begin{array}{c} \sigma_{22} \\ \sigma_{12} \\ \sigma_{23} \end{array} \right\}$$

where σ_{ij} are the near crack-tip stresses, r and θ are polar coordinates, and K_i are associated with three fundamental fracture modes. Once the stress intensity factors, K_i, have been numerically (or analytically) computed and the material fracture toughness (sometimes named critical stress intensity factor), K_{1c}, experimentally determined, a suitable functional relationship is applied for propagation of an existing crack:

$$f(K_I, K_{II}, K_{III}, K_{1c}) = 0 \tag{5.1}$$

Several functional forms of equation 5.1 have been proposed in the literature. In LEFM models, a sudden release of stress on the surface is assumed with the extension of the crack. Most investigators adopt the discrete crack propagation finite element model (DCPM) with the LEFM constitutive models. Techniques to apply the LEFM criteria in smeared crack propagation finite element model have also been reported in the literature. Pekau et al. (1991) have proposed a numerical procedure to apply the linear elastic fracture mechanics criterion in discrete crack propagation analysis with boundary element model for the dams.

The question of whether the fracture process in concrete can take place at a localized point has been a subject of intense debate for quite long time. In reality, the fracture process zone (FPZ) must have some finite size (Figure5.2-b). It is argued that the LEFM could be applied if the FPZ is much smaller than the dimension of the structure under consideration. Very large concrete structures like dams are usually cited as the possible candidates for application of LEFM models. However, no rational experimental evidence has ever been put forward appraising the extent of FPZ in dam concrete. The disregard of nonlinear behaviour in the FPZ is an assumption of unknown consequences in influencing the global response of the structure. It seems

Figure 5.2: Fracture process zone (FPZ); (a) LEFM; (b) NLFM

appropriate to consider the nonlinear behaviour in the FPZ if the localization of the crack profile is a primary objective of the finite element analysis. In a gravity dam, a relatively stiff structure, crack opening displacements may be very small, which means that a long fracture process zone may exist (Dungar et al. 1991). Hence the argument of small fracture process zone in comparison to the thickness of the structure, usually cited to apply LEFM models, may not be true even for concrete gravity dams. The choice between LEFM and NLFM models could also be influenced by the strain rate under consideration.

The primary characteristic of nonlinear fracture mechanics (NLFM) is the recognition of the strain softening behaviour of concrete in the FPZ. Two apparently different models have been proposed in the literature considering only the model I nonlinear fracture propagation in concrete. The most referenced work is due to Hillerborg et al. (1976). They characterized the existence of FPZ as a fictitious crack lying ahead of the real crack tip (figure5.3-a). The behaviour of concrete in the FPZ was represented by a diminishing stress, σ, versus crack opening displacement (COD), δ, relationship; the tensile resistance being ceased at a critical COD value, δ, (Figure 5.3-b). The area under the $\sigma - \delta$ curve represents the energy, G_f, dissipated during fracture Process on unit area:

$$G_f = \int_0^{\delta^f} \sigma(\delta) d\delta$$

G_f is a material property and often referred to as fracture energy or specific fracture energy. The special feature of the Hillerborg's fictitious crack model is the dissipation of energy over a discrete line crack. The basic nature of the model has made its extensive applications possible in discrete crack propagation analysis.

The LEFM models, in the context of discrete crack propagation, have also been modified to take account of the FPZ through an effective crack length calculated as the true crack length plus a portion of the fictitious crack. In some recent studies the key assumption of Hillerborg's model, that the tensile stress at the tip of fictitious crack is equal to the tensile strength of concrete has been modified using the concept of singular stress distribution at the fictitious crack tip.

Bazant and Oh (1983) came forward with the argument that the energy dissipation cannot take place in a diminishing volume, it must involve a finite

Figure 5.3: Nonlinear fracture mechanics models: (a,b) fictitious crack model,(c,d) crack band model

volume of the material. The fracture process is thus assumed to propagate as a blunt front (Figure5.3-c). The width of the blunt crack (or the band of micro-cracks), w_c, is assumed to be a material property in this model. The strain softening behaviour of concrete in the FPZ is represented by a stress-strain relationship (Figure5.3-d) and the fracture energy, G_f, is given by

$$G_f = w_c \int_0^{\varepsilon_f} \sigma(\varepsilon) d\varepsilon$$

The inherent characteristic of the proposed crack band model is the smeared nature of crack distribution over a band width, w_c, The crack band width, w_c, however, has not been determined by any direct experimental investigation. Bazant and Oh (1983), in the original presentation, attempted to establish the value of w_c by fitting their proposed model in a series of stress-strain and fracture energy data collected from the literature. The values of w_c in the range of single aggregate dimension to six times that size gave equally good results. The assumption of fracture energy dissipation over a certain band area of material characteristic dimension, thus, seems to be a numerical speculation.

An important aspect of the nonlinear fracture mechanics models is the shape of the softening branch. Various proposals have been made in the literature about the form of $\sigma - \delta$ and $\sigma - \varepsilon$ softening relationships. A bilinear relationship is usually applied to interpret the experimental observations (Briihwiler 1990; Nomura et al. 1991). The precise shape of the softening diagram has been reported to have considerable influence on the numerical results (ACI 1991). There has been an unrelenting debate as to which softening model, the fictitious crack model or the crack band model, should be used. The smeared nature of the crack band model is a tempting feature for application in finite element analysis when the direction and location of crack propagation are not known a priori. Application of the crack band model, in its original form, to smeared fracture propagation analysis requires the size of finite elements to be limited to w_c. The very small value of w_c, according to the definition presented by Bazant and Oh (1983), renders any practical finite element analysis of large concrete gravity dams too expensive.

Special finite element techniques have been proposed to ease this limit on element size, where the fracture process effects are smeared over a zone of the finite element and the average stress-strain relationship is adjusted to conserve the fracture energy. A linear strain softening relationship has been

Figure 5.4: (a) average stress-strain curve for smeared crack element; (b) characteristic dimension, $l_c = l_1, l_2$; (c) characteristic dimension. lc=$\sqrt{l'l''}$

assumed in most of these models. The area under the average stress-strain curve for a finite element undergoing fracture process is adjusted such that the dissipated fracture energy,G_f, for unit area of crack extension remains independent of the element characteristic dimension, l_c, (Figure5.4-a) . A favored approach in the nonlinear smeared fracture models (NSFM) is to adjust the slope of the softening branch, assuming that the softening process initiates when the tensile stress reaches the material tensile strength. The strain-softening modulus, E_t, in figure5.4-a can be derived as:

$$E_t = \frac{\sigma_t^2 E}{\sigma_t^2 - \frac{2EG_f}{l_c}} \tag{5.2}$$

if the tensile strength, σ_t, the elastic modulus, E, and the strain fracture energy, G_f, are known for the material, the strain softening modulus for the particular element size, l_c, can be determined from equation 5.2. For a special case of , $l_c = w_c$ (w_c is the width of crack band), the nonlinear smeared fracture model reduces to the crack band model of Bazant and Oh (1983). Unlike the crack band width, w_c, the characteristic dimension, l_c, is a geometric property of the element. For cracks parallel to a side of square finite elements, as in Figure5.4-b, the characteristic dimension, l_c, equals the element dimension across the crack plane ($l_c = l_1$, l_2,l_3, etc.) For oblique crack propagation, l_c can be taken as the square root of the element area under consideration (Figure5.4-c).

The softening modulus, E_t, given by equation 5.2, becomes stiffer for increasing value of l_c up to a certain limit, beyond which an unrealistic snap-back appears in the tensile stress strain relationship of concrete. In the limit case, the softening constitutive model degenerates to the traditional elastobrittle failure criterion, dissipating the stored elastic strain energy instantly upon reaching the tensile strength of material. The maximum finite element size, denoted by l_0, that can be modelled with strain-softening behaviour is determined from equation 5.2:

$$l_0 \leq \frac{2EG_f}{\sigma_t^2}$$

For typical dam concrete properties of E = 30 000 MPa, G_f = 0.2 N/mm, and σ_t = 2.0MPa, the limiting value is $l_0 \leq$ 3.0m. This limit on maximum dimension, which is much higher than the material characteristic dimension, w_c, of Bazant and Oh (1983), also has often been considered stringent for large scale finite element analysis at reasonable cost.

Figure 5.5: Nonlinear fracture mechanics in smeared crack propagation model

To circumvent this limit on the size of finite elements, and at the same time respect the principle of conservation of energy, one proposition is to reduce the fracture initiation stress, σ_0, with increasing finite element size and assume an elasto-brittle failure criterion for element sizes greater than l_0 (Figure5.5-a). This is the so-called size reduced strength (SRS) criterion proposed by Bazant (1984) and Bazant and Cedolin (1979, 1983). This size reduced strength criterion (or in other words the elastic fracture criterion) can be criticized for two reasons: (i) the size independent critical COD value, δ_f, of no tensile resistance, implied by the conservation of fracture energy in the nonlinear fracture model, is violated (Figure5.5-b), and (ii) when applied with a strength based crack initiation criterion, the principle of fracture energy conservation is likely to be violated in the interior element as well as in the exterior element (figure5.5-c). An important numerical side effect of the elasto-brittle SRS failure criterion is the generation of spurious shock waves in the finite element model. El-Aidi and Hall (1989a) encountered such numerical difficulties in the nonlinear seismic analysis of concrete gravity dams. The alternate proposition of Bazant (1985) is to take the softening modulus, E_t, as a material property and reduce the fracture initiation stress with increasing size of element (Figure5.5-d) for conserving the fracture energy. This approach may allow numerically stable algorithm as opposed to the elasto-brittle model, but it seems to be based on a weaker theoretical consideration, and the questions raised for the elasto-brittle criterion are still present. Moreover, taking E_t, as a material property has not been justified from experimental investigations. The limit on the maximum size of finite elements thus appears to be a requirement to ensure a reliable application of the nonlinear fracture mechanics criteria in smeared crack propagation analysis.

Several other models with some variations of the crack band model have also been proposed in the literature. Gajer and Dux (1990) decomposed the finite element strain increment in the following form:

$$\Delta\varepsilon = \Delta\varepsilon_e + \alpha\Delta\varepsilon_{cr} \tag{5.3}$$

where the incremental strains $\Delta\varepsilon_e$ and $\Delta\varepsilon_{cr}$ correspond to the uncracked concrete and the crack band respectively, and α is the averaging factor defined as the ratio between the crack band area and the gross element area. For decomposition of strain in the fracturing direction, equation 5.3 essentially represents the nonlinear smeared fracture model described earlier. Gajer

and Dux (1990) apparently ignored the directional property of cracking by applying the scalar factor, α, in the global finite element direction. An enhanced form of the crack band model is the so-called nonlocal cracking model (Bazant and Lin 1988). In that approach, the crack strain at an integration point is smeared over the neighboring points of the finite element mesh. A crude form of the nonlocal model can be considered to be the nonlinear smeared fracture model, described earlier, where the crack strain is averaged over a characteristic dimension of single element.

Figure 5.6: Closing and reopening of partially formed cracks

Application of nonlinear fracture mechanics models in dynamic analysis requires the definition of unloading and reloading behaviours during the fracture process. Very few studies have been reported in the literature in this respect. Bazant and Gambarova (1984) proposed a hypothetical nonlinear

stress-strain relationship for closing and reopening behaviours of partially open cracks as depicted in Figure 5.6-a. Numerical simulation of such nonlinear model is very complex. de Borst and Nauta (1985) applied the linear tangent softening modulus (line 1-2 in Figure5.6-b) to characterize the FPZ behaviour of increasing strain with decreasing stress and a secant formulation (line 2-0 in Figure5.6-b) to represent the closing of partially open cracks. Gambarova and Valente (1990) have applied an assumption of sudden stress release when the closing of partially open cracks is detected at any instant of the fracture process (Figure5.6-c). Dahlblom and Ottosen (1990) proposed the following relationship for closing and reopening behaviours of partially fractured concrete:

$$\varepsilon = [\lambda + (1 - \lambda)\frac{\sigma}{\sigma_{\max}}]\varepsilon_{\max} \tag{5.4}$$

where λ is the ratio between the residual strain upon closing of cracks and the strain of open cracks (Figure5.6-d). It appears that the techniques applied by de Borst and Nauta (1985) and Gambarova and Valente (1990) are subsets of this generalized model with $\lambda = 0.0$ and 1.0 respectively. The physical phenomenon of crack closing and reopening taking place before the complete fracture of the material is, however, yet to be investigated rationally.

5.3.3 Shear resistance of fractured concrete

After the initiation of fracture process on a plane perpendicular to the direction of major principal tensile stress, it is not unlikely to expect the rotation of principal stress directions under varying deformation modes. Hence, shear deformation may take place on the partially formed rough fracture plane. The definition of shear stress-strain behaviour of concrete during the fracture process seems to be difficult. Bazant and Oh (1983) ignored the shear deformation on the fracture plane, and the material stiffness matrix was derived for normal strains only. This formulation is not compatible with the linear isotropic stiffness matrix of initial state. In another proposition, Bazant and Gambarova (1984) proposed a nonlinear mathematical model, named the crack band microplane model, to account for shear in the partially formed crack, propagating as a blunt front of micro-cracks. Gambarova and Valente (1990) retained the initial shear modulus unchanged until the complete fracture had taken place and then applied an aggregate interlock model. de Borst and Nauta (1985) and Gajer and Dux (1990) applied the concept of

simple shear retention factor, β, proposed by Suidan and Schnobrich (1973), to derive the tangent shear modulus of the fracture plane. The simplified approach of applying a shear retention factor ignores the shear dilation and the dependence of crack shear stiffness on the crack opening displacement (COD). Dahlblom and Ottosen (1990) assumed a linear relationship between shear resistance and COD. The models proposed by Bazant and Gambarova (1980), Chen and Schnobrich (1981) Reinhardt and Wairaven (1982), Riggs and Powell (1986), and Wairaven (1981) represent the shear resistance and dilation on crack open surfaces of concrete. The models are very often computationally inconvenient because of the nonsymmetric stiffness matrix. A comparative study on different rough crack models is available in Feenstra et al. (1991a, 1991b). A special numerical problem associated with the shear retention in smeared crack finite element model is the spurious tension stiffness in the direction across the fracture plane (El-Aidi and Hall 1989a). This happens due to the application of continuous shape functions in deriving the finite element stiffness matrix. Discontinuous shape functions proposed by Ortiz et al. (1986) for localized failure analysis may be a solution to this problem.

Investigate on the Shear resistance of fractured concrete.

5.4 Post-fracture behaviour of concrete

The fracture direction is generally fixed based on the principal stress direction that initiates the first crack. An additional crack plane is allowed to form only when the stress reaches the tensile strength on the plane orthogonal to the first fracture plane. This type of model is stated as fixed or stationary crack model . In the "rotating crack" model, proposed by Cope et al. (1980), the orthotropic material reference axis system is rotated when the principal stress direction deviates by a certain amount from the direction that initiated the fracture process. The rotation of physical crack direction does not seem to be acceptable from common perception. After early opposition to the rotating crack model, Bazant et al. (Bazant 1983; Bazant and Lin 1988) adopted the concept based on the argument that the cracks of one direction may close and lock in shear while cracks of another direction may form. A special numerical technique to represent non-orthogonal multiple crack formation has been perfected by de Borst et al. (de Borst 1987; de Borst and Nauta 1985).

A very special post-fracture problem, associated with dynamic analysis, is the modelling of contact-impact phenomenon occurring upon closing and reopening of the cracks. Special numerical techniques to simulate the impact behaviour in discrete crack models have been proposed in the literature (Ayari and Saouma 199 1; Pekau et al. 199 1). El-Aidi and Hall (1989a) presented a discussion on numerical difficulties arising from high velocity closing and reopening of cracks in smeared crack analysis No rigorous procedure has been reported in the literature to deal with shock wave generated by the sudden change in stiffness resulting from the closing and reopening of the smeared cracks. And the consequences of the shock-wave phenomenon in smeared crack analysis are not conclusively known yet.

5.5 Material parameters for fracture propagation analysis

The present development of mathematical models is far ahead of the current knowledge of material behaviour, specially under transient conditions. Material parameter data determined from reliable experimental studies is limited in the literature for dam concrete. Recent experimental investigations, such as the one by Briihwiler (1990) and Briihwiler and Wittmann (1990) are revealing significant differences in the mechanical properties of structural concrete and mass concrete. Ideally, the selection of material properties for safety analysis of concrete dams should be dealt with on a case-to-case basis, because the material properties are widely varying from dam to dam. However, a review of literature is presented here to establish a reasonable limit of parametric values.

Poisson's ratio, ν, and elastic modulus, E, are applied to represent the elastic behaviour of concrete in all analyses irrespective of constitutive models selected for propagation of cracks. Jansen (1988) suggested the Poisson's ratio for 1-year old dam concrete between 0.17 and 0.28. A value of 0.20 has been applied almost universally in the past studies. Briihwiler (1990) observed the reduction of Poisson's ratio with increasing compressive strain rate applied to the concrete cylinder. However, the influences of rate sensitive ν may be insignificant in comparison to the influences of other material parameters. The static modulus for 1 -year old dam concrete was suggested by Jansen (1988) in the range of $28000 - 48000$ MPa. A significant feature of

concrete constitutive behaviour is the dynamic magnification of the elastic modulus under rapidly varying loading condition. A review of this phenomenon along with the tensile strength property of concrete is presented in the following section. Separate reviews are presented for commonly used material parameters in three major crack propagation criteria strength of material, linear elastic fracture mechanics, and nonlinear fracture mechanics. The shear resistance parameter of fractured concrete is also discussed.

5.5.1 Strength-of-material parameters

The governing material parameter in SOM-based fracture propagation models is either critical stress or strain. From a rigorous study with some 12 000 published test results, Raphael (1984) proposed the following relationship between tensile and compressive strengths of concrete under static loading:

$$\sigma_t' = 0.324 f_c'^{2/3} \tag{5.5}$$

where f_c' and σ_t are respectively static compression and tensile strengths of concrete in MPa. In absence of experimentally determined values, the above equation can be applied as an approximation to the expected static tensile strength of concrete.

Tensile strength of concrete increases significantly with increasing rate of applied loading, but the failure strain remains more or less unchanged under varying load rate. In the limited dynamic tests performed on mass concrete, the dynamic load rate effect has been observed to be higher than that in usual structural concrete. The selection of dynamic magnification of the concrete tensile strength is not very evident from the literature. Raphael (1984), from his study with the published data, proposed a dynamic magnification factor of 1.50 resulting in the dynamic tensile strength of concrete:

$$\sigma_t = 0.48 f_c'^{2/3} \tag{5.6}$$

Briihwiler and Wittmann (1990) observed a dynamic magnification of up to 80% for the investigated strain rates between 10^{-5} and 10^{-2} per second, and this magnification decreased significantly due to compression preloading on the tested specimens. There is a controversy as to whether the static tensile strength or the dynamic strength should be used in seismic response analysis of concrete dams. Under alternating tensile and compressive loadings, substantial micro- level damage may take place in the material, resulting in

reduced dynamic tensile strength. Nevertheless, 50% dynamic magnification proposed by Raphael (1984) seems to have received wide recognition (Chopra 1988; Kollgaard 1987; NRC 1990).

Figure 5.7: Strength-of-material-based failure criterion

A confusion, however, exists about the interpretation of tensile stresses computed from finite element analysis. Since the pre-peak stress-strain relationship is assumed to be linear elastic in most analyses, some investigators have suggested to compare the predicted tensile stresses with the apparent strength of the material (Figure**??**-a). Experimental evidences seem to support an apparent static tensile strength, σ_a, about 30% higher than the value given by equation 5.5. Under dynamic loading, the near-peak stress-strain nonlinearity decreases substantially (Briihwiler 1990; Hatano 1960). Recognizing the fact that the initial tangent modulus does not increase at

the same rate as the tensile strength under dynamic loading, the Canadian Electrical Association (1990) report on safety assessment of concrete dams recommended the following relationship between E_i' and E_i, the dynamic and static initial tangent moduli respectively:

$$E_i' = 1.25E_i \tag{5.7}$$

Assuming that the failure strain remains the same under static and dynamic loadings, above relation gives the apparent dynamic tensile strength, σ_a', to be 25% higher than the apparent static strength, σ_a. Thus,

$$\sigma_a' = 1.25(1.3 \times 0.324) f_c'^{2/3} = 0.526 f_c'^{2/3} \tag{5.8}$$

Comparing equation 5.6 and equation 5.7, the apparent dynamic tensile strength is only about 80% higher than the actual dynamic strength, instead of 30% as proposed by Raphael (1984). Equation 5.8 respects the experimental evidences of rate insensitive failure strain, ε_t, and reduced near-peak $\sigma - \varepsilon$ nonlinearity under dynamic loading. The apparent tensile strength, however, may have to be lowered by about $10\% o - 20\%$ due to the existence of relatively weak construction lift joints in dams, if such joints are not modelled explicitly (NRC 1990).

Apparently, no empirical formula is readily available in the literature for dam concrete to select the initial static tangent modulus,E_i, from the static compressive strength, $f_c'$of concrete. Many more experimental investigations are required to establish an acceptable mathematical model for the effects of pre-compression load and the fatigue behaviour under cyclic loading. In the experimental study by Mlakar et al. (1985), the tensile strength of concrete under tension- compression loading was observed to increase with increasing rate of loading; the failure strain showed the general tendency of rate insensitivity. The behaviour under biaxial loading can be expressed using the standard failure envelopes in principal stress space (Figure**??**-b).

5.5.2 Linear elastic fracture mechanics parameters

The principal parameter applied in the linear elastic fracture mechanics crack propagation models is the fracture toughness, K_{1c}, of concrete. No definite relationship is readily available in the literature of dam concrete to determine the fracture toughness from standard material parameters such as strength, elastic modulus, and aggregate size. And only a handful of experimentally

determined results has been reported so far. Saouma et al. (1989) found a K_{1c} value of 1.1 MPa-m$^{1/2}$. Linsbauer (1990) reported K_{1c}, values in the range of $2.0 - 3.5$ MPa-m$^{1/2}$. The following guideline has been proposed by Saouma et al. (1990) to select K_{1c}: a zero value as a first approximation; should the response be unacceptable, a value of $K_{1c} = 1.0$ MPa - m $^{1/2}$ is used; and if this value still results in unacceptable crack lengths, laboratory experiments could be performed on recovered core specimens. Due to multiaxial confining stresses in the field conditions, the in situ values for fracture toughness, K_{1c}, were determined as three times the unconfined laboratory test values (Saouma et al. 1989, 1991b). The fracture toughness can also be estimated from the following well-known relationship (Irwin 1957):

$$K_{1c} = \sqrt{G_f E}$$

where E is the elastic modulus and G_f the fracture energy. The strain rate sensitivity of K_{1c} for mass concrete is not well addressed in the literature. In the seismic analysis of Koyna Dam (India), Ayari and Saouma (1990) assumed an arbitrary dynamic magnification factor of 60 for K_{1c}, which seems too high for concrete. Briihwiler (1990) predicted the rate sensitivity of K_{1c} to be lower than that of concrete tensile strength.

5.5.3 Nonlinear fracture mechanics parameters

Fracture energy, G_f, is the key parameter that is combined with elastic modulus, E, and tensile strength, σ_t, to define the entire constitutive behaviour of concrete in the nonlinear fracture mechanics models. Usually, the tensile strength, σ_t, beyond which a strain softening process is assumed to take place, is determined from uniaxial or split cylinder tests and the fracture energy, G_f, from wedge splitting tests (Briihwiler and Wittmann 1990). Values for σ_t and E can be selected according to the guidelines used for strength-of-material failure criterion. Empirical relationships have been proposed to determine the fracture energy from standard material parameters (Bazant and Oh 1983; Oh and Kim 1989). Those relationships were derived from the results of laboratory experiments performed with small size aggregates specific of structural concrete behaviour. Extrapolation of the test results from structural concrete does not seem to be realistic to establish the behaviour of mass concrete that has distinct features of much larger and weaker aggregates.

Limited results have been reported from experimental investigations on concrete collected from dam construction sites (Briihwiler 1990; Briihwiler and Wittmann 1990). The G_f value under static loading condition was determined to be in the range of 0.175and 0.310 N/mm; meaning that the G_f of dam concrete is two to three times larger than that of structural concrete. Fracture energy values for the specimens subjected to compressive pre-loading were found considerably low. The G_f parameter determined under simulated seismic loading rates showed substantial strain rate sensitivity, and a maximum of 80% dynamic magnification over the pseudo-static value was observed. Briihwiler and Wittmann (1990) attributed the rate sensitivity of G_f mainly to the rate sensitivity of σ_t. That means, the dynamic magnification criterion selected for tensile strength can be applied to the fracture energy of the nonlinear fracture mechanics model. More complex relationships can also be established, including the rate sensitivity of critical crack opening displacement, δ_f (Briihwiler 1990).

Experiments performed by Saouma et al. (1990, 1991a) have shown that the fracture properties are not affected by the specimen or aggregate sizes used. In contrary to this finding, a study performed by H.N. Linsbauer (Dungar et al. 1991) reported larger G_f values for larger specimen sizes, and another study by H. Mihashi (Dungar et al. 1991) reported the increase of fracture energy with increasing aggregate size. The test results reported in the literature are thus sketchy at the present time, and they are often in contradiction to one another.

Laboratory tests performed at the University of Colorado (Briihwiler and Saouma 1991) showed significant reduction of the fracture properties of concrete with increased water pressure along the crack. The effect of multiple cracks on fracture energy dissipation phenomenon is not known precisely. Biaxial and triaxial stress-strain effects on fracture energy dissipation characteristic of concrete are also required to be investigated (Kreuzer et al. I 99 1).

5.5.4 Shear resistance of fractured concrete

The fractured concrete derives shear resistance from interlocking of aggregates protruding out of the fracture plane. Numerous investigations have been conducted to determine the phenomenon of aggregate interlock in structural concrete where the aggregates are usually very strong. The physical characteristic of fractured dam concrete, where the aggregate strength is

substantially low, is not known clearly. The recent fracture investigation of dam concrete, performed by Briihwiler and Wittmann (1990), have shown that the crack does not travel around the aggregates; it goes straight through them. The roughness on resulting fracture plane, thus, would be mild with low shear resistance. No specific information is currently available to establish a shear resistance model. Rigorous parametric analyses are required to study the sensitivity of nonlinear seismic response of concrete dams to the,selected shear resistance model.

5.6 NONLINEAR MODELLING OF CONCRETE DAMS USING DAMAGE MECHANICS

Micro cracking in concrete is believed to occur at relatively low levels of loading. Therefore, cracking progresses in a heterogeneous medium because of an increase in micro cracking, and because of the linking of various micro cracked zones. Experiments performed on cement paste as well as concrete show that micro cracking has an arbitrary orientation. When the load is increased, macroscopic cracks develop and the crack orientations follow the principal stress directions in the material.

Proper understanding and mechanical modeling of the damage process of concrete, brought about by the internal defects, is of vital importance in discussing the mechanical effects of the material deterioration on macroscopic behavior. Modeling of this phenomenon has triggered intensive research activities over the past 20 years or so.

The main concept of this theory is to represent the damage state of material by an internal variable, which directly characterizes the distribution of micro cracks formed during the loading process. Each damage model established mechanical equations to describe the evolution of the internal variables and the mechanical behavior of damaged material. The damage mechanic model can be divided into isotropic and anisotropic damage models. The isotropic damage mechanics model uses a single scalar parameter and is based on Lenlaitre's hypothesis of strain equivalence. It was used with some success to describe the damage of concrete. Yet, few practical applications to real structures were conducted using this approach. However, it was experimentally observed that crack growth in concrete structures significantly

depends on the direction of the applied stress and strain. Hence, the damage process in concrete is essentially orthotropic, the isotropic description is a mere simplification.

Compared with the fracture mechanics theory used in the context of discrete cracks the continuum models with fixed mesh have the advantage of avoiding remeshing when finite elements are adopted. However, when compared with the smeared crack approach there seems to be a small advantage. Researchers have proved that different mechanical phenomena can be formulated within the same framework of damage mechanics. The swelling problem is investigated in concrete dams using this concept. Finally, damage mechanics permits the easy implementation of any initial damage due to thermal stresses or any other phenomena, such as alkali-aggregate reactions, acting on an existing dam.

5.6.1 NUMERICAL PROBLEMS RELATED TO STRAIN SOFTENING

Damage process is associated with strain softening, which is usually accompanied by sudden transition from a smoothly varying deformation field into a localized band. The treatment of strain softening and localization by finite elements could lead to serious difficulties, as reported by Simo (1989), Bazant and Belytschko (1985), and Wu and Freund (1984).

Some of these difficulties are:

(1) cracks tend to localize in a band that is generally the size of the element used in the discretization;

(2) the fracture energy dissipated decreases as the mesh is refined, in the limit it tends towards zero;

(3) the solution obtained is extremely dependent on mesh size and orientation.

To overcome these difficulties, the following solutions were proposed:

1 . The strain softening is related to the element size (Pietruszczak and Mroz 1981). which leads to the mesh-dependent hardening modulus technique (Bazant and Oh 1983. Pramono and Wiliam 1989; Simo 1989).

2. Nonlocal damage is formulated as proposed by Bazant and Pijaudier-Cabot (1988), Mazars et at. (1991), Saouridis and Mazars (1992).

3. Introduction of viscoplasticity as suggested by Needleman (1988), Loret and Prevost (1991), Sluys and de Borst (1992).

4. The use of the second gradient theory in the definition of the strain tensor (sluys et al. 1993).

5. Cosserat continuum approach (de Borst 1991; Vardoulakis 1989).

From a purely mathematical viewpoint Simo (1989) showed that the first three solutions can be interpreted as regularization procedures of the dissipation function. Pijaudier-Cabot et al. (1988) performed a comparative study of these techniques for the propagation of waves in a longitudinal bar.

5.6.2 FUNDAMENTAL EQUATIONS OF DAMAGE MECHANICS

The concept of the damage mechanics model is based on the dissipation of energy by means of cracking and loss of rigidity of the material. Any induced plastic behavior is ignored.

Equilibrium of the system is defined by the thermodynamic potential, which is considered here as the strain energy $W(\varepsilon, d)$ and is a function of the strain vector $\{\varepsilon\}$ and the damage variable d. Thus, $W(\varepsilon, d)$ can form the basis to formulate the following expressions:

$$\sigma_i = \frac{\partial W}{\partial \varepsilon_i} \qquad and \qquad Y = -\frac{\partial W}{\partial d}$$

where σ_i is the component of the stress vector in engineering notation; and Y is the thermodynamic force associated with d, interpreted as a damage energy release rate. The time derivative of the specific energy yields

$$\dot{W} = \{\sigma\}^T\{\dot{\varepsilon}\} - Y\ \dot{d}$$

The Clausius Duhem inequality gives a condition on the energy dissipated W_d by the damage process, which can be written as:

$$\dot{W_d} = Y\ \dot{d} = \{\sigma\}^T\{\dot{\varepsilon}\} - \dot{W} \geq 0 \tag{5.9}$$

The formulation of a damage model first requires the definition of threshold of damage. which is the conditions that initiates the propagation of damage. Secondly, the evolution of the damage with loading must also be defined, and it is a function of a measure of strains, stresses or energy.

5.6.3 ISOTROPIC DAMAGE MODEL FOR CONCRETE

To establish the damage constitutive equation, it is necessary to relate the damage variable d to the other internal variables by some physical hypothesis. Here we try to briefly describe an isotropic damage mechanics model. The hypothesis of strain equivalence of Lemaitre and Chaboche (1978) is empirical in nature. It states that any constitutive equation for a damaged material can be derived from the same potentials as that for a virgin material by for a damaged material by replacing the stresses by effective stresses. The effective stresses are defined as:

$$\{\bar{\sigma}\} = [M(d)]\{\sigma\} \tag{5.10}$$

where$[M(d)]$ is in general a symmetric matrix of rank four. For isotropic damage model equation 5.10 is valid when the strains in the damaged material are assumed to be equivalent to strains in the virgin material, but possess a reduced modulus by a factor $(1-d)$. Figure 5.8C;D shows the basis of this assumption. In equation 5.10, $[M]$ is a diagonal matrix equal to$\frac{1}{1-d}I$; and I is identity matrix.$[M]$ represents the damage matrix. Thus, in the context of strain equivalence, equation 5.10 reduces to:

$$\{\bar{\sigma}\} = \frac{1}{1-d}\{\sigma\} \tag{5.11}$$

The strain energy for a damaged material is $W = 1/2\{\varepsilon\}^T[C(d)]\{\varepsilon\}$, where $[C(d)]$ is a second order matrix of material properties. In such a case, the evolution of damage decreases the material stiffness and the following expression can be written

$$[C(d)] = (1-d)[C_0] \tag{5.12}$$

where $[C_0]$ is initial matrix of undamaged material properties. The stress vector and the rate of energy dissipation can be easily obtained:

$$\{\sigma\} = (1-d)[C_0]\{\varepsilon\}$$

and

$$Y = \frac{1}{2}\{\varepsilon\}^T[C_0]\{\varepsilon\} = -\frac{\partial W}{\partial d}$$

Since Y is a quadratic function of strain, it is positive and, thus, d is always increasing as shown in equation 5.9. This is a characterization of the irreversibility of damage.

Different hypothesis have been proposed for isotropic damage model. The basic assumption in behaviour of the damaged and equivalent undamaged element will results in different model. Among several models, special attention will be given to the two models. They are mainly based on two concepts of the modelling. In the first model, Energy-Based Damage Model, a single damage variable independent of directions of stresses describes the behavior of concrete. The damage evolution is defined as a function of the elastic strain energy of an undamaged equivalent material. To ensure mesh objectivity of the finite- element solution, the softening parameters are made mesh-dependent using the energy equivalence concept. This technique leads to reasonable mesh size and the model is suitable for the analysis of large concrete structures. While in the second concept, Strain-Based Damage Model, the damage is described by coupling the compression and tension effects to define a single damage variable d. This variable is calculated based on a certain measure of the material's strain field. The objectivity of the finite-element solution is ensured by introducing the nonlocal description of this measure by averaging it within an influence area in the finite-element mesh. The size of the influence area is of the order of three times the aggregate size. In this case an extremely refined mesh is required. If the aggregate size varies between 100 and 300 mm, it becomes impractical to model real dams with a reasonable size mesh since at least three elements are required within the influence area of about 300-900 mm.

5.6.4 ANISOTROPIC DAMAGE MODEL FOR CONCRETE

A G_f-type anisotropic damage model is described in this part for different reasons: when roller compacted concrete is used in dams, the material itself is initially orthotropic. Therefore, the development of an anisotropic damage model is essential. In addition, orthotropic damage models allow the modeling of joints in the dam and at the dam-foundation interface, even though these problems are not addressed in this paper. It will be shown that by developing an orthotropic damage model, the isotropic model becomes a special case (Chow and Wang 1987; Ju 1989; Chow and Lu 1991).

Figure 5.8: Material model in the damage mechanics concept; A)effective areas for isotropic and anisotropic damages; B)characteristic length; C)strain equivalence hypothesis; D)stress-strain curve for equivaalence hypothesis; E)closing-opening criterion; F)initial damage formulation

When isotropic damage is considered, the effective stress $\{\bar{\sigma}\}$ (Lemaitre and Chaboche 1978) and the elastic stress $\{\sigma\}$ are related by 5.11. If damage is no longer isotropic, because of cracking, material anisotropy introduces different terms on the diagonal of $[M(d)]$. If the concept of net area is still considered, the definition for d_i becomes:

$$d_i = \frac{\Omega_i - \Omega_i^*}{\Omega_i}$$

where Ω_i is tributary area of the surface in direction i; and Ω_i^* is lost area resulting from damage, as shown in Figure 5.8-A. The index $i(1,2,3)$ corresponds with the Cartesian axes x,y and z. In this case the ratio of the net area over the geometrical area may be different for each direction.

The relation between the effective stresses $\{\overset{*}{\sigma}\}$ and the elastic equivalent stresses $\{\sigma\}$ becomes:

$$\begin{bmatrix} \overset{*}{\sigma}_1 \\ \overset{*}{\sigma}_2 \\ \overset{*}{\sigma}_{12} \\ \overset{*}{\sigma}_{21} \end{bmatrix} = \begin{bmatrix} \frac{1}{1-d_1} & 0 & 0 \\ 0 & \frac{1}{1-d_2} & 0 \\ 0 & 0 & \frac{1}{1-d_2} \\ 0 & 0 & \frac{1}{1-d_1} \end{bmatrix} \begin{bmatrix} \sigma_1 \\ \sigma_2 \\ \sigma_{12} \end{bmatrix}$$

In this case the effective stress tensor is no longer symmetric and an anisotropic damage model, *based on equivalent strains*, results in a nonsymmetric effective stress vector. Various attempts to restore symmetry were proposed by, Chow and Lu (1991) and Valliappan et al. (1990). They are based on the principle of elastic energy equivalence. This principle postulated that the elastic energy in the damaged material is equal to the energy of an equivalent undamaged material except that the stresses are replaced by effective stresses.

If the symmetrized effective stress vector is defined as:

$$\{\bar{\sigma}\} = \{\bar{\sigma}_1 \bar{\sigma}_2 \bar{\sigma}_{12}\} = \{\overset{*}{\sigma}_1 \overset{*}{\sigma}_2 \sqrt{\frac{\overset{*}{\sigma}_{12}^2 + \overset{*}{\sigma}_{21}^2}{2}}\}$$

It can be related to the real stresses by:

$$\begin{bmatrix} \bar{\sigma}_1 \\ \bar{\sigma}_2 \\ \bar{\sigma}_{12} \end{bmatrix} = \begin{bmatrix} \frac{1}{1-d_1} & 0 & 0 \\ 0 & \frac{1}{1-d_2} & 0 \\ 0 & 0 & \sqrt{\frac{1}{2}\left(\frac{1}{(1-d_1)^2} + \frac{1}{(1-d_2)^2}\right)} \end{bmatrix} \begin{bmatrix} \sigma_1 \\ \sigma_2 \\ \sigma_{12} \end{bmatrix} \qquad (5.13)$$

This equation can be written as $\{\bar{\sigma}\} = [M]\{\sigma\}$. where$[M]$ is damage matrix.

The elastic strain energy stored in the damaged material is equal to:

$$W_d^e = \frac{1}{2}\{\sigma\}^T[C_d]^{-1}\{\sigma\} \tag{5.14}$$

The elastic strain energy for the equivalent undamaged material is given by:

$$(W_0^e)^{equivalent} = \frac{1}{2}\{\bar{\sigma}\}^T[C_0]^{-1}\{\bar{\sigma}\} \tag{5.15}$$

Equating equations 5.14 and 5.15 and substituting for $\{\bar{\sigma}\}$ from equation 5.13 yields:

$$[C_d]^{-1} = [M]^T[C_0]^{-1}[M]$$

which results in the following expression for the effective plane stress material matrix:

$$[C_d] = \begin{bmatrix} \frac{E}{1-\nu^2}(1-d_1)^2 & \frac{E\nu}{1-\nu^2}(1-d_1)(1-d_2) & 0 \\ \frac{E\nu}{1-\nu^2}(1-d_1)(1-d_2) & \frac{E}{1-\nu^2}(1-d_2)^2 & 0 \\ 0 & 0 & \frac{2G(1-d_1)^2(1-d_2)^2}{(1-d_1)^2+(1-d_2)^2} \end{bmatrix} \tag{5.16}$$

The term $C_d(3,3)$ in equation 5.16 represents the shear resistance of the damaged material. It can be written in a manner similar to that of the smeared crack approach, i.e., $C_d(3,3) = \beta G$ in which β is the shear retention factor that is given here as a function of damage scalars d_1 and d_2.

$$\beta = \frac{2(1-d_1)^2(1-d_2)^2}{(1-d_1)^2 + (1-d_2)^2}$$

If d_2 is neglected as it assumed in the smeared crack approach, β can be expressed as a function of strain in the principal direction.

The constitutive law can be written as:

$$\{\sigma\} = [C_d]\{\varepsilon\}$$

where the principal directions of damage are assumed to coincide with the principal stresses. Transforming to the global axes, the constitutive relation can be written as:

$$[C_d]_G = [R]^T[C_d][R]$$

Where$[C_d]_G$ is material matrix in the global axes; and $[R]$ is transformation matrix defined by:

$$[R] = \begin{bmatrix} \cos^2\beta & \sin^2\beta & \sin\beta\cos\beta \\ \sin^2\beta & \cos^2\beta & -\sin\beta\cos\beta \\ -2\sin\beta\cos\beta & 2\sin\beta\cos\beta & \cos^2\beta - \sin^2\beta \end{bmatrix}$$

and β is angle of principal strain direction. If $d_1 = d_2 = d$, the following relation is obtained:

$$[C_d] = (1-d)^2[C_0]$$

which represents the damaged isotropic model. This model differs from equation 5.12 by a square factor because of the energy equivalence.

5.6.5 EVALUATION OF DAMAGE VARIABLE

Now we try to relate the damage variable to the state of an element using uniaxial behaviour of a concrete specimen.. Consider the elastic brittle uniaxial behavior as shown in Figure 5.9. If a point A_t on the stress strain curve (σ, ε) moves to A_2, because of damage, a certain amount of energy is dissipated (dW_d). Under conditions of infinitesimal deformation and negligible thermal effects, the first law of thermodynamics requires:

$$dW = dW_e + dW_d$$

where dW_e is elastic energy variation; and dW_d is energy dissipated by damage. It can be seen that after damage the strain will reach to its original strain at zero. The total dissipated energy is calculated as:

$$W_d = \int dW_d = Area(OA_1A_2O)$$

The upper bound of W_d is total available energy of the material g_t given by:

Figure 5.9: Stress-strain curve for energy dissipation due to fracture

$$g_t = \int_0^x \sigma d\varepsilon \tag{5.17}$$

The fracture energy per unit surface G_f is defined by:

$$G_f = l_{ch} g_t \tag{5.18}$$

and l_{ch} characteristic length of the element of volume representing the material's average behavior.

For uniaxial loading, the relation between the strain energy stored in the damaged material W_d^e, and the elastic energy in the virgin material W_0^e is:

$$W_d^e = (1-d)^2 W_0^e = (W_0^e)^{equivalent} \tag{5.19}$$

Therefore, the effective material modulus is:

$$\bar{E} = (1-d)^2 E_0$$

5.6.6 Damage evolution for concrete subjected to tensile strain

An element of volume of the material which can be representative of the global behaviour is now considered. This volume will be characterized by its length which provides a measure of the region over which the damage is smeared so that the global response is reproduced by this volume. This length, l_{ch}, is called characteristic length and it should be measured in the direction normal to a potential crack plane (Figure 5.8-B).

To define the damage evolution of concrete, The principal strains are measured for an element to determine the state of the system. The initial threshold is the strain beyond which damage can occur and is given by:

$$\varepsilon_0 = \frac{f_t'}{E_0}$$

Using equation 5.19, a possible expression for damage is:

$$d = 1 - \sqrt{\frac{W_d^e}{W_0^e}} \tag{5.20}$$

where W_d^e is recoverable elastic energy of the damaged material. When the deformations are less than the initial threshold (ε_0) the material is elastic and all the energy is recoverable, which implies that $W_d^e = W_0^e$, and therefore $d = 0$. In the limit of damage, $W_d^e \to 0$, which implies $d = 1$. A simple way to evaluate d is to adopt a postpeak stress function. According to Rotls (1991), the strain-softening curve of concrete must be concave. By considering an exponential function as proposed by Lubliner et al. (1989):

$$\sigma(\varepsilon) = f_t^{'}[2\exp(-b(\varepsilon - \varepsilon_0)) - \exp(-2b(\varepsilon - \varepsilon_0))] \tag{5.21}$$

The constant b can be evaluated using equations 5.17, 5.18, and 5.21, which leads to:

$$b = \frac{3}{\varepsilon_0(\frac{2G_f E}{l_{ch} f_t^{'}} - 1)} \geq 0 \tag{5.22}$$

Using 5.20 and 5.21, the evolutionary model for damage can be expressed as:

$$d = 1 - \sqrt{\frac{\varepsilon_0}{\varepsilon}[2\exp(-b(\varepsilon - \varepsilon_0)) - \exp(-2b(\varepsilon - \varepsilon_0))]} \tag{5.23}$$

If a simple linear softening curve is assumed, Figure 5.8-D can show that:

$$d = 1 - \sqrt{\frac{\varepsilon_0}{\varepsilon} - \left(\frac{\varepsilon - \varepsilon_0}{\varepsilon_f - \varepsilon_0}\right)\left(\frac{\varepsilon_0}{\varepsilon}\right)}$$

The fundamental issue of this approach lies in the introduction of a geometrical factor, l_{ch}, in the constitutive model. When the finite element method is used, a so-called mesh-dependent hardening modulus is obtained. This technique was proposed by Pietruszcak and Mroz and was employed by a number of authors. Using equation 5.18 ensures conservation of the energy dissipated by the material. Amongst many strategies used to ensure mesh objectivity, the mesh-dependent hardening technique is the most practical for mass structures such as dams. Condition in equation 5.22 should be interpreted as a localization limiter on the characteristic length of the volume representing the global behaviour of the material. In other words, if $l_{ch} \geq \frac{2EG_f}{f_t'^2}$, it is not possible to develop strain softening in the volume. For mass concrete, using average values for $E = 30000$ MPa, $G_f = 200$ N/m and $f_t^{'} = 2$MPa yields a limit for $l_{ch} = 3$ m. This leads therefore to a reasonable

mesh size for dam models. The introduction of such parameter is not for numerical convenience. The characteristic length can be related to the Fracture Process Zone (FPZ) commonly used in fictitious crack model for concrete.

5.6.7 Opening and closing of the crack and initial damage

When the strain is increasing, damage will also increase. During cyclic loading the strains are reversed and unloading will occur. Experimental cyclic loading of concrete in tension shows evidence of permanent strain after unloading. Under compression the material recovers its stiffness. The classical split of the total strain in a recoverable elastic part ε^e and an inelastic strain ε^{in} gives:

$$\varepsilon = \varepsilon^e + \varepsilon^{in} = \varepsilon^e + \lambda\varepsilon_{\max}$$

where $\varepsilon_{\max}$ is the maximum principal strain reached by the material and λ is a calibration factor varying from 0 to1. Figure 5.8-E illustrates this criterion. The value $\lambda = 0.2$ is selected; the unloading-reloading stiffness becomes :

$$E_{unl} = E_0\frac{(1-d)^2}{(1-\lambda)} \tag{5.24}$$

When the principal strain is less than ε^{in} the crack is considered closed. Alternatively, the crack will open when the principal strain is greater than $\lambda\varepsilon_{\max}$.

The damage model presented here is based on three parameters: the elastic modulus E, the initial strain threshold ε_0 and the fracture energyG_f. If the element of volume is initially damaged ($d = do$), the secant modulus and the fracture energy are reduced by $(1 - do)$ so the effective values are (Figure 5.8-F):

$$E' = (1-d_0)E \quad G'_f = (1-d_0)G_f$$

5.6.8 ANALYTICAL PROCEDURES IN A FINITE ELEMENT MODEL

In a finite element model, the four-node isoparametric element is preferred in the implementation of the local approach of fracture-based models and has

been used for the implementation of the described constitutive model. The standard local definition of damage is modified such that it refers to the status of the complete element. The average of the strain at the four Gauss points is obtained and the damage is evaluated from the corresponding principal strains of the element. The constitutive matrix $[C_d]$ is updated depending on the opening/closing and the damage state of the element. The stresses at each integration point are then computed using the matrix $[C_d]$ and the individual strains.

The characteristic length of the element is calculated approximately, using the square root of its total area. For an efficient control of the damage propagation in the finite element mesh, some adjustments have to be considered. During the softening regime the stiffness is reduced as a consequence of damage ,equation 5.23. At the unloading stage the secant modulus is calculated using equation 5.24 until closing of the crack. When the crack closes the material recovers its initial properties. In the reloading regime the last damage calculated before unloading is used again.

Finite element implementation of the damage mechanics

1. Compute total displacement $\{u\}_{i+1} = \{u\}_i + \{\Delta u\}$
2. Initialization $Iselect = 0$, $E_{\max} = 0$
3. Loop over elements $e = 1, nel$
   - (a) Compute deformations for each Gauss point : $\{\epsilon\}_e^{gp} = [B]^{gp}\{u\}_e$
   - (b) If the element is already damaged call subroutine UPDATE
   - (c) If not: (selection of element with largest energy density)
   - Compute ε_1, if $\varepsilon_1 \leq \varepsilon_0$ go to (d)
   - Compute $E_e = \frac{1}{2}\{\sigma\}_e\{\varepsilon\}_e$
   - if $E_e \geq E_{\max}$ then $E_{\max} = E_e$, $Iselect = e$
   - (d) $\{\sigma\}_e = [C_d]\{\varepsilon\}_e$
   - (e) Compute the internal force vector $r_e = \int_{A_e}[B]^T\{\sigma\}_e dA$
   - f) Assemble the element contribution $r \leftarrow r_e$
4. If ($Iselect \neq 0$), (New element damaged)
   - (a) Correction of stresses due to damage
   - (b) Update data base of damaged elements

Subroutine UPDATE (Stress and damage update)

1. Set damage parameter $d = d_{old}$
2. Compute the average strains within the element and the corresponding principal strains: ε_1, ε_2 set $\varepsilon = Max(\varepsilon_1, \varepsilon_2)$
3. Check for loading/unloading and closing/opening of crack:
   - (a) if ($\varepsilon \geq \varepsilon_{\max}$) the element is in a loading state

Calculate d from equation 5.23
update if $\epsilon^{in}, \varepsilon_{\max} = \varepsilon$
(b) else if $\varepsilon \geq \varepsilon^{in}$)
$d = d_{old}$
(c) else $d = 0$

4. Compute$[C_d]$ using equation 5.16

5.7 CONSTITUTIVE MODEL FOR SMEARED FRACTURE ANALYSIS

The constitutive model defining (i) the pre-softening material behaviour, (ii) the criterion for softening initiation, (iii) the fracture energy conservation, and (iv) the softening, closing and reopening of cracks, and the finite element implementation of the formulations are presented in the following sections. A linear elastic relationship is assumed between compressive stresses and strains. The tensile stresses and strains are referred to as positive quantities in the presentation.

5.7.1 Pre-fracture behaviour

Stresses $\{\sigma\}$ and strains $\{\varepsilon\}$ in a linear elastic condition are related as:

$$\{\sigma\} = [D]\{\varepsilon\}$$

where $[D]$ is the constitutive relation matrix defined for an isotropic plane stress condition as:

$$[D] = \frac{E}{1-\upsilon^2}\begin{bmatrix} 1 & \nu & 0 \\ \nu & 1 & 0 \\ 0 & 0 & \frac{1-\nu}{2} \end{bmatrix}$$

Here, E is the elastic modulus; and ν is the Poisson's ratio.

5.7.2 Strain softening of concrete and the initiation criterion

The stress-strain relationship for concrete becomes non-linear near the peak strength [Figure 5.10-a]. In the post-peak strain softening phase, coalescence

Figure 5.10: Constitutive modelling for smeared fracture analysis; a)softening initiation criterion; b)fracture energy conservation; e)local axis system; d)closing and re-opening of cracks

of the microcracks causes a gradual reduction of the stress resistance. The area under the uniaxial stress-strain curve up to the peak is taken as the index for softening initiation:

$$U_0 = \int_0^{\varepsilon_1} \sigma d\varepsilon = \frac{\sigma_i \varepsilon_i}{2} = \frac{\sigma_i^2}{2E} = \frac{E\varepsilon_i^2}{2} \qquad \sigma_1 > 0$$

where σ_i is the apparent tensile strength, that may be approximately taken 25-30% higher than the true static strength, σ_t. It is calibrated in such a way that a linear elastic uniaxial stress-strain relationship up to σ_i will preserve the value U_0[Figure 5.10-a].

In finite element analyses, a linear elastic relationship is assumed until the tensile strain energy density, $\frac{1}{2}\sigma_1\varepsilon_1$ (σ_1, and ε_1 are the major principal

stress and strain, respectively), becomes equal to the material parameter, U_0 :

$$U_0 = \frac{1}{2}\sigma_1\varepsilon_1 = \frac{\sigma_i^2}{2E} \qquad \sigma_1 > 0 \tag{5.25}$$

Taking the square roots of both sides, the biaxial effect in the proposed strain softening initiation criterion is expressed as:

$$\frac{\sigma_1}{\sigma_i} = \sqrt{\frac{\sigma_1}{E\varepsilon_1}}$$

The above equation is a representative of a biaxial failure envelope. The principal stress σ_1, and the principal strain, ε_1, at the instance of softening initiation, are designated by σ_0, and ε_0, respectively [Figure 5.10-a].

Under dynamic loads, the pre-peak non-linearity decreases with increasing values for both σ_t and ε_t [Figure 5.10-b]. The strain-rate effect on the material parameter U_0 is considered through a dynamic magnification factor, DMF_e, as follows:

$$U_0' = \frac{\sigma_i'^2}{2E} = (DMF_e)^2\, U_0$$

where the primed quantities correspond to the dynamic constitutive parameters. The increased material resistance due to inertia and viscous effects under dynamically applied loads has been explicitly considered in the dynamic equilibrium equations. Reviewing the literature on the dynamic fracture behaviour of concrete, a 20 percent dynamic magnification of the apparent tensile strength is considered adequate for seismic analyses of concrete dams. Under dynamic loading, the material parameter U_0 in equation 5.25 is replaced by the corresponding dynamic value, U_0'. At the instant of softening initiation under a dynamically applied load, the principal stress, σ_1, and the principal strain, ε_1, are designated by σ_0' and ε_0', respectively, as shown in Figure 5.10-b.

5.7.3 Fracture energy conservation

The tensile resistance of the material is assumed to decrease linearly from the presoftening undamaged state to the fully damaged state of zero tensile resistance [Figure 5.10-b]. The slope of the softening curve is adjusted such that

the energy dissipation for a unit area of crack plane propagation, G_f, is conserved. The strain-rate sensitivity of fracture energy is considered through a dynamic magnification factor, DMF_f, applied to magnify the static fracture energy:

$$G'_f = DMF_f G_f$$

The strain-rate sensitivity of fracture energy can mainly be attributed to that of tensile strength. DMF_f can therefore be assumed to be equal to DMF_e. In finite element analyses, the final strains of no tensile resistance for static and dynamic loading are defined as:

$$\varepsilon_f = \frac{2G_f}{\sigma_0 l_c} \qquad \varepsilon'_f = \frac{2G'_f}{\sigma'_0 l_c}$$

where l_c is the characteristic dimension defined in the previous section.

5.7.4 Constitutive relationships during softening

After the softening initiation, a smeared band of microcracks is assumed to appear in the direction perpendicular to the principal tensile strain. The material reference axis system, referred as the local axis system, is aligned with the principal strain directions at that instant [directions n-p in Figure 5.10-c. The constitutive matrix, relating the local stresses to local strains is defined as:

$$[D]_{np} = \frac{E}{1-\eta\upsilon^2}\begin{bmatrix} \eta & \eta\nu & 0 \\ \eta\nu & 1 & 0 \\ 0 & 0 & \mu\frac{1-\eta\nu}{2(1+\nu)} \end{bmatrix} \qquad \eta = \frac{E_n}{E} \qquad (5.26)$$

where the parameter η ($0 \leq \eta \leq 1$) is the ratio between the softening Young's modulus E_n, [Figure 5.10-d], in the direction normal to a fracture plane and E, is the initial isotropic elastic modulus; and μ is the shear resistance factor. The following options are considered with respect to the orientation of crack bands in finite element analyses.

5.7.5 Coaxial Rotating Crack Model (CRCM)

The local axis system $n-p$ is always kept aligned with the directions of principal strains, ε_1, and ε_2. In this model, the strains ε_n and ε_p are, respectively,

ε_1, and ε_2 at the newly oriented material reference state. Using an implicit definition of the softened shear modulus in cracked elements, the parameter μ is defined for the CRCM as follows:

$$\mu = \frac{1+\nu}{1-\eta\nu^2}\left(\frac{\eta\varepsilon_n - \varepsilon_p}{\varepsilon_n - \varepsilon_p} - \eta\nu\right) \qquad 0 \leq \mu \leq 1 \tag{5.27}$$

Here, ε_n and ε_p is the normal strain components in the directions normal and parallel to the fracture plane, respectively.

5.7.6 Fixed Crack Model With Variable Shear Resistance Factor (FCM-VSRF)

In this model, the local reference axis system is first aligned with the principal strain directions at the instance of softening initiation, and kept nonrotational for the rest of an analysis. The shear resistance factor, μ, is derived using the strain components ε_n and $\varepsilon_p$corresponding to the fixed local axis directions (which are not necessarily coaxial with the principal stress directions). The definition of a variable shear resistance factor according to equation 5.27, that takes account of deformations in both lateral and normal directions to a fracture plane, is different from the usual formulations where only the crack normal strain is often considered as the damage index.

The total stress-strain relationship matrix, defined in equation 5.26, is similar to the formulation presented by BaZant and Oh (1983), except that they have not considered shear deformations in the constitutive relationship. The present formulation, with the degraded shear modulus term, maintains a backward compatibility with the presoftening isotropic elastic formulation when $\eta = 1$ and 2. The local constitutive relationship matrix, $[D]_{np}$, can be transformed to the global coordinate directions as follows:

$$[D]_{xy} = [T]^T [D]_{np} [T]$$

where $[T]$ is strain transformation matrix defined as follows in terms of the inclination of the normal to it crack plane, θ [Figure 5.10-c]:

$$[T] = \begin{bmatrix} \cos^2\theta & \sin^2\theta & \sin\theta\cos\theta \\ \sin^2\theta & \cos^2\theta & -\sin\theta\cos\theta \\ -2\sin\theta\cos\theta & 2\sin\theta\cos\theta & \cos^2\theta - \sin^2\theta \end{bmatrix}$$

With an increasing strain softening, the damaged Young's modulus, E_n, (Figure 5.10-d), and hence the parameters η and μ decrease gradually, and may eventually reach zero values after the complete fracture ($\varepsilon_n > \varepsilon_f$ *or* ε'_f). The constitutive matrix in equation 5.26 is updated as the parameters η and μ change their values. In the CRCM, a change in the global constitutive relationship may also be caused by a rotation of the local axis system, which is always kept aligned with the directions of coaxial principal stresses and strains. During unloading/reloading, when the strain, ε_n, is less than the previously attained maximum value, $\varepsilon_{\max}$ [Figure 5.10-d], the secant modulus, E_n, remains unchanged; the parameter μ, however, may change during that process.

The change in global constitutive relations is also caused by a rotation of the local axis system, which is always kept aligned with the directions of principal strains to keep the principal stresses and strains coaxial. The CRCM is very effective in alleviating the stress locking generally observed in fixed crack models. During unload ing/reloading, when the strain, ε_n, is less than the previously attained maximum value, $\varepsilon_{\max}$[Figure 5.10-f], the secant modulus, E_n, remains unchanged; the parameter μ, however, changes during that process.

5.7.7 Closing and reopening of cracks

Under reversible loading conditions, the tensile strain, ε_n, in an element may alternatively increase and decrease. With the reduction Of ε_n, the shear resistance factor, μ, gradually increases. The softened Young's modulus in the direction n, E_n (which may have reached a zero value), is replaced by the undamaged initial value, E, if the parameter μ is greater than a threshold value μ_c. Parametric analyses have shown that the seismic fracture response of concrete gravity dams is not affected by a value of μ_c between 0.90 and 0.9999. A relatively flexible tolerance, $\mu_c = 0.95$, can be used to minimize spurious stiffness changes during the closing of cracks. When $\varepsilon_n > 0$ in subsequent load steps, the value μ is determined by using the damaged value of η to determine the reopening of cracks. If μ becomes less than μ_c, the element behaviour is determined by either the reloading or the reopening path depending on the final state attained in previous tension cycles. The appropriate value of the damage modulus, E_n, is reused in equation 5.26 at that state. For $\mu_c \approx 1$, the residual strain upon closing of a crack is given by $\varepsilon_n = \nu\varepsilon_s^2$. Figure 5.10-d sshows the closing-reopening behaviour for a special

case when $\varepsilon_n \approx 0$.